EXPERIMENTAL INVESTIGATION OF SUBMERGED, INCOMPRESSIBLE, TURBULENT, IMPINGING JETS

BY

DAVID TZEH-HSIAN LEE

A THESIS

PRESENTED IN PARTIAL FULFILLMENT OF

THE REQUIREMENTS FOR THE DEGREE

OF

MASTER OF SCIENCE IN MECHANICAL ENGINEERING

AT

NEWARK COLLEGE OF ENGINEERING

Newark, New Jersey
1969

ABSTRACT

Measurements concerning various flow parameters of jets impinging on a smooth lucite plate and a heated metal plate have been carried out. In particular, it is shown that the potential core length of a jet is a function of the Reynolds number and of the jet diameter. It has also been demonstrated that impinging jets behave in many important respects like free jets, except in the immediate vicinity of the target plate.

The flow behavior in the wall jet zone was investigated experimentally, and a satisfactory agreement with the results of the previous investigators was found. The maximum velocity decay parameters for a radial wall jet were also investigated analytically, and appear in a good agreement with the experimental results.

APPROVAL OF THESIS

EXPERIMENTAL INVESTIGATION OF SUBMERGED,

INCOMPRESSIBLE, TURBULENT, IMPINGING JETS

BY

DAVID TZEH-HSIAN LEE

FOR

DEPARTMENT OF MECHANICAL ENGINEERING

NEWARK COLLEGE OF ENGINEERING

BY

FACULTY COMMITTEE

APPROVED:_____

_____

_____

NEWARK, NEW JERSEY
1969

ACKNOWLEDGEMENTS

The author wishes to thank his advisor, Dr. Peter Hrycak, for his instruction and encouragement. Grateful acknowledgements are also due to Dr. R. Y. Chen and Mr. Norman Shilling for their very helpful suggestions in the experimental work, and to Mr. Walter Schmiedeskamp for his help in the instrumentation.

The financial support by NASA under Grant NGR-31-009-004 is also acknowledged.

TABLE OF CONTENTS

Page

LIST OF SYMBOLS

a	coefficient in Eq. (14)
b	width of jet
C	defined in Fig. 4.1. or in Eq. (10)
D	nozzle diameter
L	Lip of the nozzle and definition in Fig. 4.1.
m,n, M and N	Defined in Eq. (26) and (27)
P	pressure
P_∞	ambient atmosphere pressure
P_c	static pressure along the jet centerline
P_{max}	maximum pressure
r	radial distance
Re_D	Reynolds number based on nozzle diameter and air properties at nozzle exit
U	velocity in the x and z direction
U_m	maximum axial velocity of the jet
U_{oc}	velocity at center of nozzle exit
V	velocity in the r direction
V_m	maximum velocity along the flat plate
V_{RB}	reference boundary velocity, Eq. (20)
x	distance away from the nozzle, Fig. 1.1.
y	defined in Fig. 1.1.
$y_{\frac{1}{2}}$	y-location where $U = \frac{1}{2} U_m$
z	defined in Fig. 1.1.

$z_{\frac{1}{2}}$ z-location where $V = \frac{1}{2} V_m$

z_n normal distance between target plate and nozzle

α power of r in Eq. (64)

δ boundary layer thickness, wall jet region

μ dynamic viscosity

ζ $(z - \delta) / b$

ρ density

Subscript "o" indicates conditions at the origin (real of virtual).

Barred symbols indicate dimensionless quantities.

Prime indicates differentiation with respect to r.

Roman I indicates Free Jet Zone, II indicates Deflection Zone,

III indicates Wall Jet Zone.

LIST OF FIGURES

CHAPTER I. INTRODUCTION

1.1. Historical Introduction

Since the Prandtl's old theory of free turbulence was published, jets have been intensively investigated, and also, in particular, the circular free jet. Tollmien is the first person to apply the Prandtl's old theory,i.e. Prandtl's mixing length hypothesis, to solve the problem of an axially symmetrical jet issuing from a small orifice[1]*. In 1932, Taylor developed another theory of free turbulence[1]. In 1942, Prandtl published again a new theory based on Newton's law of viscous friction[1]. Using this theory,Görtler obtained the solution for a free circular turbulent jet in a closed form[1]. Many famous investigators, later on, like Reichardt, Abramovich and Schlichting worked on this interesting topic. The theory described by Schlichting[9] on three-dimensional stagnation flow might also be used to describe the jet deflection region for an impinging jet. The flow spreading radially outward along the flat plate, called the "wall jet", has been investigated by Glauert in 1956[4]. Thereafter, Bakke[2] studied the wall jet experimentally, while Poreh and Cermak[8], Tani and Komatsu[11], Brady and Ludwig[3], and Strand[18] also investigated various additional aspects of the wall jet problem theoretically and experimentally.

1.2. Experimental Introduction

Investigation of various phenomena related to impinging jets is of interest today because of many practical engineering applications, such as a vertical take-off or landing air craft, rocket take-off,

---

*The raised numbers refer to References at the end of the thesis.

arc welding, blast drying, paint spraying and various applications for cooling and heating purposes where impinging jets occur naturally.

The experimental investigation presented here is primarily undertaken to investigate the characteristics of the turbulent, circular, submerged air jet normally impinging on a smooth flat plate, with the velocity of the jet not too high, so that the jet flow could still be treated as incompressible. Generally speaking, for this the velocity has to be lower than 300-400 fps.

A number of previous investigators have studied some important related phenomena, but more work has been done so far on free jets than on the impinging jets. In this study , nozzle Reynolds numbers ranging from as low as 600 to as high as 1×10^5 were tested and the normal distance between the exit of the nozzle and plate was varied from two to thirty nozzle diameters ,in order to observe the influences of varying Reynolds number and normal distance on the flow parameters. Some aspects of this work, as will be pointed in detail later, have never been described in detail in the open literature. The other aspects investigated below may represent nothing new. However, it is difficult to proceed with new measurements and to be sure that correct techniques have been used everywhere, unless some ground is covered which has also been treated by other investigators.

The flow field for a circular jet impinging on a flat plate was generally divided into three main regions by the previous investigators, (Fig. 1.1). The free jet zone is a portion of jet extending

from the circular source to approximately eight-tenths of z_n, the normal distance to the plate. If the normal distance between the flat plate and the nozzle exit is smaller than 1.5D to 2D, it has been found in the present investigation that the readings at the nozzle exit are affected by the flat plate, which result is the same as that of Brady and Ludwig[3]. Therefore, in the present experiment whenever the readings are taken in the region where the normal distance, z_n, is greater than 2D, the effect of the target plate is disregarded. This is justifiable by the results shown in Fig. 1.2.

The second region is the deflection zone where the flow changes in direction from vertical to radial. Thereafter, the flow then spreads radially outward along the flat plate. This region is termed "wall jet" zone by Glauert.[4]

Throughout these experiments, various flow parameters studied are shown here to undergo changes caused by varying the Re_D and the normal distance. Essentially, the main stress of this investigation has been to determine if certain secondary flow parameters that have been long accepted as "constants" had not actually been functions of the Reynolds number and of the other independent flow parameters.

CHAPTER II. EXPERIMENTAL APPARATUS AND PROCEDURE

2.1. Experimental Apparatus

2.1.1. Piping System

The sketch of the piping system is shown in Fig. 2.1. The compressed air is supplied by a reciprocating compressor, through a large storage tank to provide a steady flow. The air mass flow rate is controlled by the valves and measured with a pair of rotameters with a calibrated accuracy better than 1%. The inlet pressure at the rotameter inlet was registered by a Bourdon pressure gage. The flow goes through the controlled section, then enters a 1 1/2 in. pipe; further downstream of the piping system and before a plenum chamber, an orifice flow meter is located between two pressure taps which may also be used to calculate the flow rate. Upstream of the plenum chamber, a thermocouple is inserted into the center of the pipe in order to measure the air temperature before it enters the plenum chamber. The plenum chamber is 2 1/2 in. in diameter and 35 in. in length, and is connected to the 1 1/2 in. pipe by a 90^{o} 1 1/2 - 2 1/2 in. reducer. At the end of the plenum chamber where an end plate is welded on, three different nozzles with diameter 1/8 in., 1/4 in., and 3/8 in. may be screwed on to the end plate with a rubber ring to prevent air leakage. The plenum chamber is built vertically and its exact alignment can be adjusted by varying the length of three supporting guide wires.

2.1.2. Manometers

Two large vertical column manometers with water as the fluid and one large vertical column manometer with mercury as fluid were used. For low pressure measurement, a micromanometer using a fluid with specific gravity 0.7970 was available. Readings are obtained by turning the dial which is divided into the smallest subdivisions (one thousandths of an inch - 0.001) and bringing the meniscus back to zero, the vertical scale reads the major divisions.

2.1.3. Impinging plate

A lucite plate 10 inches in diameter, shown in Fig.2.2, was provided with nineteen 1/64" diameter holes for pressure taps to measure the pressure distribution along the plate. The plate was supported by a three-leg frame which can be freely rotated and raised or lowered (Fig. 2.2). In addition to the lucite plate, a metal, heated plate is also employed to find the effect of heat energy. The plate can be heated by steam and electricity.

2.1.4. Traversing carriage

The measuring probes are mounted on the traversing carriage by means of a slide (Fig. 2.3). The carriage is similar to a lathe carriage, and the slide-carriage system combined can be moved three-dimensionally. The slide travel in the z-direction is 2 ft., and the carriage travels in both the x and y directions 6 inches. Besides the pressure pick up probe still could be rotated around the longitudinal axis of the tube, to fit exactly the jet flow patterns.

2.1.5. Pressure measuring probes

Figure 2.4 shows the details of the probes used. Three total pressure probes, one static pressure probe and many micro-tubing pressure taps of 0.016 in. diameter are utilized. The pressure probes are of the design recommended by NASA, as was also the nozzle with a unique lip feature shown in Figure 2.4.

2.1.6. Smoke producer

A short tube with a flange drilled through to provide air flow control could be placed inside the nozzle and a cigarette could be inserted into the short tube shown in Fig. 2.4. Smoke is generated at the nozzle exit when a lighted cigarette is put into the tube.

2.1.7. Thermocouple and potentiometer

These are employed to measure the temperature of the air flow. Copper-Constantan on thermocouples have been used in combination with the K-2 and K-5 Leeds and Northrup potentiometer.

2.2. Experimental Procedure

The purpose of the experimental set up (Figs. 2.1 to 2.4) was to measure the total pressure and static pressure in order to study the velocity and pressure distribution everywhere. The circular, incompressible, turbulent jets emanating from three different diameter nozzles (1/8 in., 1/2 in., and 3/8 in., Fig. 2.4) impinged three-dimensionally on the flat lucite plate. First of all, the nozzle was kept exactly vertical to the target plate and aligned

with the vertical direction of traversing unit. The plate was kept horizontal. The procedure used to assure that the motion of the probes was along the centerline was to align the jet centerline with the actual stagnation point on the plate. Then the line connecting the stagnation point and the center of the nozzle was the centerline of the jet. A drop of dark grease applied at the approximate stagnation point would spread out radially, therefore, the streamlines and stagnation point were very clearly and easily observed. This procedure was recommended by Snedeker[10] to observe the flow pattern on a flat plate. Then the probe could be lowered down from the center of the nozzle to the plate to see if it coincided with the stagnation point. In this experiment, the Reynolds number based on the nozzle diameter varied from 600 to 10^5, and the normal distance between the nozzle exit and plate was changed from $z_n/D = 4$ to 30. The velocity and pressure distribution of the jet were measured with total and static pressure probes (Fig. 2.4.). For each particular measurement, the mean value was taken, and then the probe was rotated according to the angle required to fit exactly the streamlines of the spreading jet, and the error of the location due to the probe's rotation was corrected. This was possible because of the arrangements shown in some detail in Fig. 2.3.

In the free jet zone, the velocity and pressure distribution and velocity decay along the centerline were measured to investigate the effect of the Reynolds number on the length of the potential core. In the wall jet zone, the velocity profile and the maximum velocity decay along the plate were studied. The pressure distri-

bution in the deflection zone and wall jet zone was detected by a series of 1/64 in. tubes inserted on the plate as the pressure taps. The velocity profile was investigated at different z_n/D values and at several locations away from the stagnation point. The growth of the jets in free jet zone and wall jet zone were measured based on half-valued velocity ($Z_{1/2}$ where $V = 1/2\ V_m$). The coordinate system and flow pattern are shown in Fig. 1.1.

In order to compare the difference of the boundary layer between a smooth lucite plate and a heated metal plate, an invar plate was heated to the temperature between $100^{o}F$ to $200^{o}F$ on the surface, and then exposed to impinging jets as a deflector.

CHAPTER III. THEORETICAL ANALYSIS

3.1. Free Jet Zone

The free jet zone was determined as eight-tenths of the normal distance between the target and nozzle exit, Z_n shown in Fig.1.1 by previous investigators as Poreh and Cermak[8] and verified by Tani and Komatsu[11] and the present experiment, in which the flow properties remain the same as in a free jet. The free jet zone can be theoretically divided into the potential core region where the center line velocity still remains constant and the fully-developed region where the flow velocity begins to decay according to a certain equation given later and develops a typical velocity profile. The theoretical analysis of a free jet is based on Prandtl's theory. The very famous Prandtl's mixing length theory, i.e. Prandtl's old theory is written as,

$$\tau = \rho l^2 \left|\frac{\partial u}{\partial y}\right| \frac{\partial u}{\partial y} \tag{1}$$

and

$$\tau = \rho l^2 \frac{\partial u}{\partial y} \sqrt{\left(\frac{\partial u^2}{\partial y}\right) + l_1^2 \left(\frac{\partial^2 u}{\partial y^2}\right)^2} \tag{2}$$

where the mixing lengths l and l_1 are purely local functions. Thereafter, Prandtl presented a hypothesis, i.e. Prandtl's new theory as in the form

$$\tau = \rho \varepsilon \frac{\partial u}{\partial y} = \rho K_1 b (U_{max} - U_{min}) \frac{\partial u}{\partial y} \tag{3}$$

where b denotes the width of the mixing zone, K_1 is empirical constant, and ε is the virtual kinematic viscosity, such that

$$\varepsilon = K_1 b \ (U_{max} - U_{min}) \tag{4}$$

and, according to the theory given ny Schlichting[9], the variation of the width of the jet with respect to the distance from jet source, x, is constant.

$$\frac{db}{dx} = \text{const.} \tag{5}$$

or

$$b = \text{const. } x \tag{6}$$

and the momentum of a circular jet can be obtained by conservation of momentum.

$$J = \rho \int u^2 \, dA = \text{const.} = \text{const. } \rho \ U_m^{\ 2} \ b^2 \tag{7}$$

and introducing the relation between b and x

$$U_m = \text{const.} \ \frac{1}{x} \ \frac{J}{\rho} \tag{8}$$

Thus, according to Eq. (8), the velocity in the center of a circular submerged jet is inversely proportional to the distance from the jet source. In this experiment, the flow is assumed incompressible, ρ = const., and it follows,

$$U_m = \frac{\text{const.}}{x} \tag{9}$$

or in a dimensionless form

$$\frac{U_m}{U_{oc}} = \frac{C}{\frac{x}{D}} \tag{10}$$

Eq. (10) governs the maximum velocity decay along the centerline of the jet, and is valid only within the fully developed region.

The coefficient C in Eq. (10) is a number related to the length of the potential core shown in Chapter 4. A conclusion on the coefficient C is given by Abramovich[1]. He analyzed the experiments of Trupel, Zimm, the Gottingen Aerodynamics Institute, Turkus, and Syrkin and shows that the coefficient in Eq. (10) does not depend on the Reynolds number over a very wide range for $2 \times 10^4 < Re <$ to 40×10^5. The results of the present experiments are only slightly different from these conclusions within that range of the Reynolds number shown in Chapter 4.

For incompressible, low speed jet, the static pressure in the submerged free jet is, according to the simplified theory, invariable and equal to the ambient pressure. Actually, the static pressure in the jet of the present experiment was found to vary. If the velocity is high, the static pressure distribution becomes a function of Mach number, according to investigations by Snedeker and Donaldson[10]. Nobody so far has determined a static pressure variation in incompressible, turbulent jets.

The equation of velocity distribution developed by Schlichting[9] is given as

$$U = \frac{3}{8\pi} \frac{K}{\varepsilon_o x} \frac{1}{(1+\frac{1}{4}\eta^2)^2} \tag{11}$$

$$V = \frac{1}{4}\sqrt{\frac{3}{\pi}}\sqrt{\frac{K}{x}}\ \frac{\eta - \frac{1}{4}\eta^2}{(1 + \frac{1}{4}\eta^2)^2} \tag{12}$$

and

$$\eta = \frac{1}{4}\sqrt{\frac{3}{\pi}}\sqrt{\frac{K}{\varepsilon_o}}\ \frac{y}{x} \tag{13}$$

where $K = J/\rho$ is the expression for kinematic momentum.

3.2. Deflection Zone

Schlichting[9] analyzed the problem as the stagnation flow in three dimension where the flow may be assumed to be inviscid, the well-known equations are,

$$V = ar \tag{14}$$

$$U = -2az \tag{15}$$

and

$$P_o - P = \frac{1}{2}\rho\,(V^2 + U^2) = \frac{1}{2}\rho\,a^2\,(r^2 + 4z^2) \tag{16}$$

These three equations describe the velocities in z and r direction and pressure distribution within the region near the stagnation point. Because the deflection zone in the present experiment is not large, and the plate is very smooth, the viscous effect is not important at the stagnation point. The Schlichting's equation is quite satisfactory to describe the flow and is supported by the present experiment. By observation of Eq.(14), the radial velocity incresed linearly from zero at the stagnation point (where r = 0 and z = 0).When the flow reaches some place farther from the stagnation point, the viscous dissipation is predominant, and the flow is no longer governed by Eq.(14). The rate of velocity increase is reduced and finally

reaches zero value. Then velocity starts to decrease. Eq. (15) shows the axially (opposite z-direction) velocity of flow is linearly decresed to zero at the stagnation point on the flat plate. The pressure varies parabolically along the flat plate and jet centerline as given by Eq. (16).

If in the case of viscous flow, the equations for the velocities and pressure distribution are

$$V = rf'(z) \tag{17}$$

$$U = -2f(z) \tag{18}$$

and

$$P_o - P = \frac{1}{2}\rho a^2 [\, r^2 + F(z) \,] \tag{19}$$

A solution of those equations in the form of a power series was firstly given by F.Homann. The other analyses were given by Schach[17], Strand[18] and Tani and Komatsu[11].

3.3. Radial Wall Jet Zone

Farther out from the stagnation point, where the effect of viscous friction predominates, there begins the region of radial wall jet. Poreh and Cermak[8] assumed that the effect of the wall on the wall jet would be confined to the boundary layer near the wall and found it is useful to define in the wall jet region a reference boundary velocity, V_{RB}, which can be extrapolated from the velocity profile near the plate as

$$V_{RB} = 2\varepsilon_1 \frac{\alpha^2}{r} = \frac{\text{const.}}{r} \tag{20}$$

whereas the velocity distribution in dimensionless form is given by

$$\frac{V}{V_{RB}} = 1 - \tanh^2 \alpha\eta \qquad \eta = \frac{z}{r} \tag{21}$$

According to the result, the reference boundary velocity is expected to decay inversely proportional to r, and the velocity distribution is expected to follow Eq. (21), which was obtained from the integration of the momentum equation according to Prandtl's second hypotheses. This equation is similar to the one valid for a plane free jet.

A similar result was also obtained by Abramovich[1]. He used the Schlichting formula $U/U_m = (1 - \xi^{1.5})^2$ together with db/dr = 0.22 and energy equation to solve a problem of a fan jet and to get the equation

$$\frac{V_m}{V_o} \simeq \frac{3.8\ b_o}{r}\sqrt{\frac{r_o}{b_o}} \tag{22}$$

or

$$V_m = \frac{\text{const.}}{r} \tag{23}$$

This equation is similar to Eq. (20); the radial wall jet can be handled as half of the fan jet except for a thin layer near the wall.

Poreh, Tsuei, and Cermak[7] who developed a theory for the radial wall jet, used the conservation of mean momentum in the radial and vertical direction and the continuity equation to establish a relation between the skin friction τ_w and the velocity field as,

$$\frac{\tau_w}{\rho} = \frac{1}{r}\frac{\partial}{\partial r}\left[r \int_o^\infty V^2\, dz\right] \tag{24}$$

and further assumed that except for a very thin layer near the wall, the velocity of the wall jet is similar and can be described as,

$$V = V_m f(\zeta) \tag{25}$$

where $\zeta = Z/Z_{\frac{1}{2}}$, V_m are functions of r only, and can be written as

$$V_m = Mr^m \tag{26}$$

and

$$Z_{\frac{1}{2}} = Nr^n \tag{27}$$

thereafter, they conclude that,

$$\frac{\tau_w}{\rho} = - M^2 N (2m+n+1) \int_0^\infty f^2 d\zeta \cdot r^{2m+n-1} \tag{28}$$

In the case of a wall jet, τ_ω is always positive. Since N must also be positive, it follows

$$2m+n+1<0 \tag{29}$$

To make V_m, $Z_{\frac{1}{2}}$ and τ_w/ρ dimensionless, three functions have to be defined as functions of $\sqrt{K}/\nu$ and r/Z_n and written as

$$V_m Z_n/\sqrt{K} = F_m (\sqrt{K}/\nu) (r/Z_n)^m \tag{30}$$

$$Z_{\frac{1}{2}}/Z_n = F_n (\sqrt{K}/\nu) (r/Z_n)^{n-1} \tag{31}$$

and

$$\tau_w Z_n^2/\rho K = F_\tau (\sqrt{K}/\nu) (r/Z_n)^{2m+n-1} \tag{32}$$

where K is the kinematic momentum flux of the circular jet leaving the orifice. Finally, Eq. (28) becomes

$$F_\tau = - F_m^2 F_n (2m+n+1) \int_o^\infty f^2 \, d\zeta \tag{33}$$

The experimental results they obtained are m = - 1.1 and n = 0.9 and Eq. (30) and Eq. (31) in the forms as

$$V_m Z_n / K = 1.32 (r/Z_n)^{-1.1} \tag{34}$$

and

$$Z_{\frac{1}{2}}/Z_n = 0.098 (r/Z_n)^{0.9} \tag{35}$$

Eq. (29) is satisfied by the values of m and n in Eq. (34) and Eq. (35)

$$2m+n+1 = 2 (-1.1) + 0.9 + 1 < 0$$

The expression for the friction coefficient becomes

$$T_w/\rho V_m^2 = 0.06 (V_m \delta/\nu)^{-0.3} (r/Z_n)^{-0.16} , \tag{36}$$

which is different from the Blasius relation.

Ludwig and Bradt[14] also gave the equations to describe the maximum velocity and thickness of boundary of wall jet as

$$V_m/\bar{V}_m = C_v (r/R)^a \tag{37}$$

and

$$Z_{\frac{1}{2}}/R = C_z (r/R)^b \tag{38}$$

where C_v and C_z are two constants which may be functions of Z_n/D. Their experimental results of a and b are -1.143 and 1.028. Eq. (37) and (38) are similar to Eq. (30) and (31) derived by Poreh, Tsuie and

Cermak[7]. The a and b are correspondent to m and n and also satisfy Eq. (29) as

$$2(-1.143) + 1.028 + 1<0$$

Furthermore, an equation for the actual maximum velocity decay for the radial wall jet is derived herein. We proceed to analyze it in a way similar to that used for analysis of two-dimensional wall jets by Abramovich[1]. In order to set up the momentum balance equation, a control volume with cross-section ABCD in Fig. 3.1 is set up. Writing the equation of conservation of momentum for the control volume ABCD.

$$\left(\begin{array}{l}\text{momentum in}\\ \text{thru the surface AB}\end{array}\right) - \left(\begin{array}{l}\text{momentum out}\\ \text{thru the surface AD}\end{array}\right)$$

$$+ \left(\begin{array}{l}\text{momentum in}\\ \text{thru the surface BC}\end{array}\right) - \left(\begin{array}{l}\text{momentum out}\\ \text{thru the surface DC}\end{array}\right)$$

$$= \left(\begin{array}{l}\text{momentum accumulation}\\ \text{in control volume ABCD}\end{array}\right) \qquad (39)$$

This equation is true only if $\tau \propto \frac{dv}{dz} = 0^*$ at $V = V_m$. Moreover, assume ρ is constant, the ambient fluid is stationery, and flow is in the steady state; then the third term on the left hand side and the term on the right hand side vanish and reduce the equation to

$$2\pi r_o b_o \rho V_o^2 - \int_{r_o}^{r} \rho V_m \frac{\partial}{\partial r} \left(\int_o^{\delta} V.2\pi r dz\right)dr = \int_{\delta}^{b+\delta} \rho V^2.2\pi r dz \qquad (40)$$

Because ρ = constant, for the flow that is incompressible, one has

$$V_o^2 b_o r_o - \int_{r_o}^{r} V_m \frac{\partial}{\partial r} \left(\int_o^{\delta} V r dz\right)dr = \int_{\delta}^{b+\delta} r V^2 dz \qquad (41)$$

---

* For turbulent flow, this assumption is in agreement with the older Prandtl theory which produced in several well-known cases quite satisfactory results. Newer measurements (Poreh, Tsuei and Cermak, for example) indicate that $\tau \neq 0$ at $V = V_m$.

Differentiate Eq. (41) with respect to r,

$$V_m(V_m r)\delta' + V_m \int_o^{\delta} \frac{\partial(rV)}{\partial r}\, dz - (rV_m^2)\,\delta' + \int_o^{b+\delta} \frac{\partial(rV^2)}{\partial r}\, dz = 0$$

$$V_m \int_o^{\delta} \frac{\partial(rV)}{\partial r}\, dz + \int_{\delta}^{b+\delta} \frac{\partial(rV^2)}{\partial r}\, dz = 0 \tag{42}$$

and make the parameters dimensionless, letting

$$\bar{V} = \frac{V}{V_o},\ \bar{V}_m = \frac{V_m}{V_o},\ \bar{z} = \frac{z}{\delta}\ ,\quad \zeta = \frac{z-\delta}{b}$$

and

$$d\bar{z} = \frac{1}{\delta}\, dz\ ,\quad d\zeta = \frac{1}{b}\, dz$$

On introducing the dimensionless parameters into Eq. (42), there follows,

$$\bar{V}_m \delta \int_o^1 \frac{\partial(r\bar{V})}{\partial r}\, d\bar{z} + b \int_o^1 \frac{\partial(r\bar{V}^2)}{\partial r}\, d\zeta = 0 \tag{43}$$

and

$$\bar{V}_m \delta \int_o^1 r \frac{\partial \bar{V}}{\partial r}\, d\bar{z} + \bar{V}_m \int_o^1 r'\bar{V} d\bar{z} + 2b \int_o^1 r\bar{V} \frac{\partial \bar{V}}{\partial r}\, d\zeta$$

$$+ b \int_o^1 r'\bar{V}^2\, d\zeta = 0 \tag{44}$$

Then, the dimensionless velocity distribution for the turbulent boundary layer near the wall can be described by the well-known power law [9]

$$\bar{V} = \bar{V}_m\, (\bar{z})^{\frac{1}{n}} \tag{45}$$

valid for the region that z from 0 to δ or $\bar{z}$ from 0 to 1, and n, a positive number, is a function of the Reynolds number, n varies from 7 to 15 as predicted by previous investigators [13]. For the dimensionless velocity distribution beyond the boundary layer one can use

the relation

$$\bar{V} = \bar{V}_m \quad (1 - \zeta^{\frac{3}{2}})^2 \tag{46}$$

originally proposed by Schlichting[9] and valid for the region where z varies from δ to $\delta+b$ or $\bar{z}$ from 0 to 1. The use of Eq. (46) is satisfactory by observation of Poreh and Cermak's experimental results[8], and also in accordance with the present experimental results. The approximate relations for the thickness of the radial wall jet and for the thickness of the boundary layer are taken as*

$$b = 0.22 \ (r - r_o) \tag{47}$$

and

$$\delta \approx 0.1 \ b \tag{48}$$

on differentiation of Eq. (45), (46) and (47) with respect to r, one gets

$$\frac{\partial \bar{V}}{\partial r} = \bar{z} \ \frac{1}{n} \ (\bar{V}_m' - \frac{V_m}{n} \frac{\delta'}{\delta}) \tag{49}$$

for $0 < \bar{z} < 1$,

$$\frac{\partial \bar{V}}{\partial r} = \bar{V}_m' \ (1 - \zeta^{\frac{3}{2}})^2 + \frac{3\bar{V}_m}{b} \delta' \ \zeta^{\frac{1}{2}}(1 - \zeta^{\frac{3}{2}})$$

$$+ \frac{3\bar{V}_m}{b} b' \ \zeta^{\frac{3}{2}} \ (1 - \zeta^{\frac{3}{2}}) \tag{50}$$

for $0 < \zeta < 1$,

---

*The assumption of the relationship $b = K \ (r-r_o)^a$ is more appropriate here and leads to a certain improvement of the value of α in Table I.

while expression for b' appears as

$$\frac{db}{dr} = 0.22 \tag{51}$$

Therefore, using Eqs. (45), (46), (49) and (50)

$$\bar{V}_m\delta \left[\int_o^1 r \frac{\partial \bar{V}}{\partial r} d\bar{z} + \int_o^1 r' \bar{V} d\bar{z} \right]$$

$$= \bar{V}_m\delta \left\{ \int_o^1 r \left[\bar{z}^{\frac{1}{n}} \left(\bar{V}_m' - \frac{\bar{V}_m}{n} \frac{\delta'}{\delta}\right)\right] d\bar{z} + \int_o^1 r' \bar{V}_m (\bar{z}^{\frac{1}{n}}) d\bar{z} \right\}$$

$$= \bar{V}_m\delta \left[\frac{n}{n+1} r \left(\bar{V}_m' - \frac{\bar{V}_m}{n} \frac{\delta'}{\delta}\right) + \frac{n}{n+1} r' \bar{V}_m \right] \tag{52}$$

and

$$b \left\{ 2 \int_o^1 r\bar{V} \frac{\partial \bar{V}}{\partial r} d\zeta + \int_o^1 r' \bar{V}^2 d\zeta \right\}$$

$$= b \left\{ 2r \int_o^1 \left[\bar{V}_m \bar{V}_m' (1 - \zeta^{\frac{3}{2}})^4 + \frac{3\bar{V}_m^2}{b} \delta' \zeta^{\frac{1}{2}} (1 - \zeta^{\frac{3}{2}})^3 \right.\right.$$

$$\left.\left. + \frac{3\bar{V}_m^2}{b} b' \zeta^{\frac{3}{2}} (1 - \zeta^{\frac{3}{2}})^3 \right] d\zeta + \int_o^1 \bar{V}_m^2 r' (1 - \zeta^{\frac{3}{2}})^4 d\zeta \right\}$$

$$= 0.6312 \bar{V}_m' \bar{V}_m rb + \bar{V}_m^2 \delta' r + 0.31559 \bar{V}_m^2 rb' + 0.31559 \bar{V}_m^2 r'b \tag{53}$$

and, on substituting of Eqs.(52)and (53) into (44), one has

$$\frac{n}{n+1} \left[\bar{V}_m' r\delta + \bar{V}_m r\delta' + \bar{V}_m r'\delta \right] + 0.6312 \bar{V}_m' rb$$

$$+0.31559 \bar{V}_m rb' + 0.31559 \bar{V}_m r'b = 0 \tag{54}$$

Then, on introducing Eq. (47), (48), (51) into (54), one has

$$\frac{n}{n+1}\left[\bar{V}'_m \cdot 0.1\, b \cdot \left(\frac{b}{0.22} + r_o\right) + \bar{V}_m \cdot 0.1\, b' \left(\frac{b}{0.22} + r_o\right)\right.$$

$$\left. + \bar{V}_m \cdot 0.1\, b \cdot \frac{b'}{0.22}\right] + 0.6312\, \bar{V}'_m\, b \cdot \left(\frac{b}{0.22} + r_o\right)$$

$$+ 0.31559 \left(\frac{b}{0.22} + r_o\right) \bar{V}_m b' + 0.31559\, \bar{V}_m b \cdot \frac{b'}{0.22} = 0 \qquad (55)$$

which becomes after a few simple transformations

$$\left[\left(\frac{0.1n}{n+1} + 0.6312\right) r_o\right] \bar{V}'_m b + \left[\left(\frac{0.1n}{n+1} + 0.31559\right) r_o\right] \bar{V}_m b'$$

$$+ \left(\frac{0.909n}{n+1} + 2.869\right) \bar{V}'_m b\, b' + \left(\frac{0.4545n}{n+1} + 2.869\right) \bar{V}'_m b^2 = 0 \qquad (56)$$

Now, one lets also

$$\left(\frac{0.1n}{n+1} + 0.6312\right) r_o = K$$

$$\left(\frac{0.1n}{n+1} + 0.31559\right) r_o = L$$

$$\frac{0.909n}{n+1} + 2.869 = M$$

$$\frac{0.4545n}{n+1} + 2.869 = N \qquad (57)$$

and Eq. (56) is reduced to

$$K \bar{V}_m b + L \bar{V}_m b' + M \bar{V}_m b\, b' + N \bar{V}'_m b^2 = 0 \tag{58}$$

a differential equation where variables can be separated, with the solution

$$\log \bar{V}_m + \log \left[(K + Nb)^{\frac{M}{N}} \left(\frac{Nb}{K+Nb}\right)^{\frac{L}{K}}\right] = C_1 \tag{59}$$

so that

$$\bar{V}_m = \frac{C_1}{(K+Nb)^{\frac{M}{N}} \left(\frac{Nb}{K+Nb}\right)^{\frac{L}{K}}} \tag{60}$$

But, since

$$\frac{Nb}{K+Nb} = 1 - \frac{r_o}{r}\ , \text{ and} \tag{61}$$

$$K + Nb = \left(\frac{0.1n}{n+1} + 0.632\right) r, \tag{62}$$

on letting $N/N = \alpha$, and $L/K = \frac{\alpha}{2}$, Eq. (60) becomes

$$\bar{V}_m = \frac{C_2}{r^{\alpha}\left(1- \frac{r_o}{r}\right)^{\frac{\alpha}{2}}} \tag{63}$$

On Eq. (63), α varies with n, where n is a function of the Reynolds number, which has been found by the previous investigators to vary from seven to fifteen [13]. Then the corresponding values of α become (Table I):

Table I

n	7	9	11	13	15
α	1.1217	1.1247	1.1268	1.1283	1.1294

Thus, α is shown to be but a weak function of the Reynolds number. Furthermore, far from the virtual source, where $r >> r_o$, eq. (63) reduces to a simple form

$$V_m = \frac{C_2}{r^{\alpha}} \tag{64}$$

is very well suited to an experimental verification. Here the above derivation shows that the maximum velocity decay in a radial wall jet is inversely proportional to r^{α}. An alternate analysis of the similar phenomena related to wall jets was given by Glauert[4], who obtained useful results likewise assuming $\tau = 0$ at $V = V_m$.

The present result gives a new relationship among several experimental facts. It shows how the local energy dissipation in the wall jet boundary layer formation, velocity profiles and (through the variation of n) to the original nozzle Reynolds number.

In order to derive the equation for the viscous shear force on the wall (Fig. 3.1), ADE is taken as the control volume, and write the momentum equation as,

$$\int_{r_o}^{r} \rho V_m \frac{\partial}{\partial r} \left(\int_o^{\delta} V.2\pi r dz\right) dr - \int_o^{\delta} \rho V^2.2\pi r dz = \int_{r_o}^{r} \tau_w.2\pi r dr \tag{65}$$

on assumption of ρ = constant,

$$\rho \left[\int_{r_o}^{r} V_m \frac{\partial}{\partial r} \left(\int_o^{\delta} Vrdz\right) dr - \int_o^{\delta} V^2 rdz\right] = \int_{r_o}^{r} \tau_w \, rdr \qquad (66)$$

on differentiation with respect to r in the same way as mentioned before,

$$\rho\left[V_m \int_o^{\delta} \frac{\partial (rV)}{\partial r} dz - \int_o^{\delta} \frac{\partial (rV^2)}{\partial r} dz\right] = \tau_w r \qquad (67)$$

Introducing the dimensionless relations,

$$\bar{V} = \frac{V}{U_{oc}}, \quad \bar{V}_m = \frac{V_m}{U_{oc}}, \text{ and } \bar{z} = \frac{z}{\delta}$$

one has

$$\frac{\tau_w r}{\rho U_{oc}^2} = \bar{V}_m \delta \int_o^1 \frac{\partial (r\bar{V})}{\partial r} d\bar{z} - \delta \int_o^1 \frac{\partial (r\bar{V}^2)}{\partial r} d\bar{z} \qquad (68)$$

Within the boundary layer, the velocity distribution is assumed in the form

$$\bar{V} = \bar{V}_m (\bar{z})^{\frac{1}{n}}$$

Substituting this equation into Eq. (68), leads to

$$\bar{V}_m \delta \int_o^1 \frac{\partial (r\bar{V})}{\partial r} dz = \bar{V}_m \delta \left[\frac{n}{n+1} r \left(\bar{V}_m' - \frac{\bar{V}_m}{n} \frac{\delta'}{\delta}\right) + \frac{n}{n+1} \bar{V}_m\right] \qquad (69)$$

and

$$\delta \int_o^1 \frac{\partial (r\bar{V}^2)}{\partial r} dz = \frac{n}{n+2} \bar{V}_m^2 \delta + \frac{n}{n+2} \left(2\delta r \bar{V}_m \bar{V}_m' - 2r \frac{\bar{V}_m^2}{n} \delta'\right) \qquad (70)$$

so that Eq. (68) becomes,

$$\frac{\tau_w r}{\rho U_{oc}^2} = \frac{n}{n+1}\left[\bar{V}_m \delta r \left(\bar{V}_m' - \frac{\bar{V}_m}{n}\frac{\delta'}{\delta}\right) + \bar{V}_m^2 \delta\right]$$

$$- \frac{n}{n+2}\left[\bar{V}_m^2 \delta + \left(2\delta r \bar{V}_m \bar{V}_m' - 2r \frac{\bar{V}_m^2}{n}\delta'\right)\right] \tag{71}$$

and

$$\frac{\tau_w}{\rho U_{oc}^2} = -\frac{n^2}{(n+1)(n+2)}\delta \bar{V}_m \bar{V}_m' + \frac{n}{(n+1)(n+2)}\delta' \bar{V}_m^2$$

$$+ \frac{n}{(n+1)(n+2)} \frac{V_m^2 \delta}{r} \tag{72}$$

Assuming $\bar{V}_m$ and δ are in the following forms,

$$\bar{V}_m = A\bar{r}^{+\alpha} \tag{73}$$

$$\bar{\delta} = B\bar{r}^{a} \tag{74}$$

where $\bar{r} = \frac{r}{D}$ and $\bar{\delta} = \frac{\delta}{D}$

and

$$\bar{V}_m' = -\frac{\alpha A}{D}\bar{r}^{-(\alpha+1)} \tag{75}$$

On substituting these relations into Eq. (72), the result is

$$\frac{\tau_w}{\rho U_{oc}^2} = \frac{A^2 B\, n}{(n+1)(n+2)}(\alpha n + a + 1)\,\bar{r}^{-2\alpha+a-1} \tag{77}$$

Let $F = \frac{A^2 B\, n}{(n+1)(n+2)}(\alpha n + a + 1)$, one has

$$\frac{\tau_w}{\rho U_{oc}^2} = F \bar{r}^{-2\alpha + a - 1} \tag{78}$$

Clearly, F is a function of n, and n is a function of Reynolds number. Poreh, Tsuei and Cermak[7] gave the equation with the same power of r as,

$$\frac{\tau_w z_n^2}{K} = F_\tau \left(\frac{r}{z}\right)_n^{-2\alpha + a - 1}$$

where $F_\tau = 0.3(K/\nu)^{-0.3}$ can be determined by experiment.

In the present experiment, A = 1.4 and B = 0.0175 a = 0.95

For n = 7 α = 1.1217 F = 0.03269

For n = 15 α = 1.1294 F = 0.0.3589

The boundary layer thickness near the stagnation point on the wall can be calculated for three-dimensional flow according to Schlichting[9] as follows,

$$\delta = \frac{3.25}{\sqrt{\frac{V_m r}{r^2 \nu}}} = \frac{3.25\ r^{\frac{1}{2}}}{\sqrt{\frac{V_m}{\nu}}} \tag{79}$$

where $z = \delta$ at $V/V_m = 1.00$

Since $V_m = ar$

and $$\delta = \frac{3.25}{\sqrt{\frac{a}{\nu}}} \tag{80}$$

Also, V_m can be written in dimensionless form

$$\frac{V_m}{U_{oc}} = a^* \frac{r}{D}$$

Therefore $$a = \frac{a^* U_{oc}}{D}$$

and Eq. (80) becomes

$$\delta = \frac{3.25}{\sqrt{\frac{a^* U_{oc}}{D \nu}}} \tag{81}$$

or

$$\frac{\delta}{D} = \frac{3.25}{\sqrt{a^*}\sqrt{Re_D}} \tag{82}$$

Since, however, a^* is a function of Zn/D, δ is a function of Zn/D and Re_D. For larger a^* or smaller Zn/D and larger Re_D, the boundary layer will be thinner. In the present experiments, a^* had been found, and δ/D can be calculated and shown in Fig. 4.48 to 4.51.

CHAPTER IV. ANALYSIS OF THE EXPERIMENTAL RESULTS

4.1. Free Jet Zone

4.1.1. The Length of the Potential Core in the Free Jet Zone

a. Theoretical dimensionless length of the potential core:

At first, a definition is given for the "theoretical dimensionless length of the potential core" labeled C. C is the dimensionless length x/D at point A as shown in the Fig. 4.1. A_1 is the intersection of the tangent from the plot of the centerline velocity decay in the fully developed region, i.e. $\frac{U_m}{U_{oc}} = C/\frac{x}{D}$, with the line $U_m/U_{oc}=1$ which describes the condition that the centerline velocity remains constant. That is to suppose that the Figure 4.1 shows that centerline velocity of the jet remains constant within C x D and then begins to decay. Actually, the centerline velocity begins to decrease at a distance somewhat closer to the nozzle opening than the location of the intercept, A_1.

To find the effect of Reynolds number on C is one of the primary purposes of these experiments. By way of the experimental investigation, it is also found that C is not only dependent on the Reynolds number but also upon the nozzle size (Figs.4.2 and 4.3). Figs.4.2 and 4.3 are a summary of the Figs. 4.4 to 4.9.

The variation of C as a function of the Re_D is clearly shown in Fig. 4.2. Generally, for three nozzles investigated, C is very large around Re_D = 1000, and abruptly decreases to a minimum between the value of Re_D = 3500 and 5500. C then gradually increases to a value between 6.5 to 6.8 at about Re_D = 10,000. With Reynolds numbers

larger than 10,000, C decreases slightly. The highest Re_D in this experiment was 10^5. The lowest value of C occuring for D=0.375 in. was 4.8 at Re_D = 3500; for D = 0.250 in. it was 5.3 at Re_D = 4000, and for D=0.125 in. it was 5.5 at Re_D = 5500. They increase respectively to the maximum of 6.8, 6.75 and 6.5 around Re_D = 10,000. With Re_D as high as 10^5, C decreases to 6.4. The result shows that the variation of C is a function of the nozzle diameter used in this experiment, but C is not, in general, a monotonic function of the Reynolds number. The recorded variation of C observed by previous investigators is from 5.2 (Tani and Komatsu[11]) to 7.7 (Poreh and Cermak[8]) and the mean value of C is taken as 7 by Trentacoste and Sforza[12].

b. Actual Dimensionless Length of Potential Core

It is defined that the actual dimensionless length,L, (Fig.4.1) is to extend over that axial dimensionless length where the centerline velocity of the jet remains constant, i.e. U_m/U_{oc} near 1 (0.97 - 0.99). It is found that L is also dependent on the Reynolds number (Fig. 4.4 to 4.9). With Reynolds number around 1000, L or the actual value of the dimensionless length of the potential core is between 8 to 11, and then rapidly decreases to a value of 3 for the Reynolds number range from 3500 to 5500. Finally, as the Reynolds number further increases, it reaches x/D = 4 and no longer exhibits large variation. In other words, at the center of the free jet, the velocity remains constant for a certain distance (L x D) and then decays according to the curve shown in Fig. 4.1.

4.1.2. Observation of the Flow Pattern in the Upstream Portion of the Free Jet.

The flow patterns were observed by means of smoke at low Reynolds numbers. Beginning with Re_D = 1000, the flow is laminar up to a distance about x/D = 4 from the nozzle exit. Downstream of this location, some small turbulence occured only on the free jet's boundary with the quiscent surroundings. When the Reynolds number is increased, the length of laminar flow is reduced and more turbulence exists. Finally, at a Reynolds number around 4000, the jet is fully turbulent. This observation helps explain why a relatively long length of the potential core exists at a Reynolds number around 1000 and becomes shorter nad shorter when the Reynolds number is increased to the value of about 4000.

In the literature review on the "Heat Transfer from the Impinging Jets" by Hrycak[13], it is pointed out that Vickers suggested Re_D=1000 to be the critical Reynolds number, which finding was supported by McNaughton and Sinclair[16], who found the flow fully laminar in $300 < Re_D < 1000$ and semi-turbulent in $1000 < Re_D < 3000$ and fully turbulent in $Re_D > 3000$. The above results are confirmed by Cederwall. Our present experimental results seem to be in agreement with those mentioned above.

4.1.3. The Velocity Profile of Free Jet Zone

The velocity profile of a free jet has been studied by many previous investigators like, for example,Schlichting[9],Abramovich[1], and Trentacoste and Sforza[12]. Fig. 4.10 shows the typical dimensionless velocity

profile in the main zone of free jets in comparison with the theories developed by Schlichting[9] and Tollmien.

As shown in the figure, the present experimental results are in agreement with the Schlichting equation 24, 46 (ref.9) for the upper one third of the profile, while the rest of the profile is close to Tollmien's profile. Figure 3.11 shows a comparison of velocity profiles for different locations farther away from the nozzle exit in the region of fully developed flow.

4.1.4. The Pressure Variation along the Jet Centerline and on the Cross Section in the Free Jet Zone

The static pressure should be theoretically identical to that of the ambient quiescent surroundings according to the simplified boundary layer theory. However, it is actually lower than the surrounding pressure and varies with the axial distance from the nozzle. The variation of the gage static pressure P_c along the centerline is shown in Fig. 4.12. P_c is a function of x/D for a fixed nozzle size. By observation of the figure, the variation is steeper and larger for larger diameter of the nozzle and it is supposed to be nearly zero by the figure when the diameter is very small,i.e. a point source. The static pressure reaches a minimum at about x_n/D=6 to 8 and then increases to the ambient pressure at the farther position along the jet centerline.

The pressure variation for varied x_n/D, i.e. for different cross sections of the jet, was measured and shown in Fig.4.13. In the main region of the jet, the minimum pressure is in the center and approaches the ambient pressure at the outer portion of the jet. This pressure variation was investigated by Miller and Comings[6] and Snedeker[10].

Miller and Comings[6] found that the variation of dimensionless static pressure along the centerplane is similar to that presented in Fig. 4.13, but Miller's profile is straighter for two dimensional jets. Snedeker found that the static pressure distribution is a function of Mach number. In the present case, the static pressure distribution for subsonic flow is also approximately similar to his results.

4.1.5. The Spread of the Jet in the Free Jet Zone

Since the growth of the jet width is proportional to the axial distance certified by many previous experiments, the jet is spreading linearly in the main region. The variation of the free jet width and half-valued width (where $U = 0.5\ U_m$) are shown in Fig. 4.14. The equation of the variation of the jet is found by experiment as

$$b/D = 0.271\ x/D \tag{83}$$

and the variation of the half-valued width is

$$Y_{\frac{1}{2}}/D = 0.0926\ x/D \tag{84}$$

for Re_D between 14000 and 67000. This is similar to the coefficient in $Y_{\frac{1}{2}} = 0.097x$ indicated by Abramovich[7]. This equation is valid only in the main region of the free jet zone; when x is bigger than $0.8\ z_n$, then flow characteristics begin to be modified by flow impingement, and the spread is no longer governed by the equations above*.

* The virtual distance is here x/D= -0.2 which in the main region of free jet zone can be disregarded with an error less than 2%.

4.2. Deflection Zone

4.2.1. The Pressure Distribution and Velocity Variation along the Flat Plate in the Deflection Zone

Fig. 4.15 shows a comparison of the dimensionless pressure $(P - P_\infty)/ 1/2\ \rho\ U_{oc}^2$ distribution along the flat plate, where P_∞ is the ambient pressure. The surplus pressure $P - P_\infty$ decreases from the maximum at the stagnation point ($r/D = 0$) to about zero at r/D larger than 4, however, the static pressure can be neglected at the locations farther than 2.5 D. This figure also shows that the pressure distribution is steeper and higher for small z_n/D values. The static pressure distribution in the region $r/D < 1$ can be generally described by the equation.

$$\frac{P - P_\infty}{1/2\ P\ U_{oc}^2} = A - B\ (\frac{r}{D})^2 \qquad (85)$$

which is a parabolic function where constants A and B can be determined by experiment. By observation of Fig. 4.16 to Fig. 4.22, it can be found that the dimensionless pressure distribution is approximately similar for the same value z_n/D but different diameters and initial velocities, i.e. different diameter Reynolds numbers. In Fig. 4.23, the pressure variation with respect to r/z_n is presented for $z_n/D = 4, 7, 10, 20$. Figures 4.24 and 4.25 show another form to make $P - P_\infty$ dimensionless by dividing them by $P_{max} - P_\infty$ and plotting them with respect to r/D and r/z_n. It is an interesting result that the dimensionless pressure distribution is steeper for large z_n/D with r/z_n as a dimensionless parameter but flatter if r/D is used.

The velocity variation along the flat plate in the deflection zone is presented in Fig. 4.26. The radial velocity V in this zone is increasing from zero to a maximum. The maximum velocity V_m is linearly increasing in the region where r/D is smaller than 0.8. Beyond this region, the velocity begins to decay by energy dissipation. It can be observed that in a region fromrr/D = 0 up to r/D = 0.6 to 1.4, depending on z_n/D, the maximum velocity variation is coincident with that derived from pressure distribution, in other words, the viscous dissipation in this small region is negligibly small.

Poreh and Cermak[8] described the additional pressure head by the equation

$$\frac{h}{M}/rz_n^2 = A - B \left(\frac{r}{z_n}\right)^2 \qquad (86)$$

which is similar to the result presented above. The maximum velocity increase and the pressure distribution in the deflection zone have also been presented by Tani and Komatsu[11] and Ludwig and Brady[3] who show similar results.

4.3. Wall Jet Zone

4.3.1. The Similarity of the Dimensionless Velocity Profile of the Wall Jet.

The profiles of dimensionless velocity V/V_m plotted with respect to $z/z_{1/2}$ ($z_{1/2}$ being the z - direction location where $V = 1/2\ V_m$) (Fig. 4.27) within the fully developed wall jet are similar for different locations measured from the stagnation point and for different z_n/D. It can be seen in Fig. 4.28 - 4.32*. The effect of varying Reynolds number was observed only in the portion of the boundary layer

*Dashed line in Figures 4.28 - 4.32 expresses data spread due to the changes of velocity profile as a function of the Reynolds number within boundary layer region.

near the wall.

In particular, the experimental evidence shows that for higher Reynolds numbers, the dimensionless velocity profile near the plate becomes slightly flattened as shown in Fig. 4.28 - 4.32.

The experimental dimensionless velocity profile obtained here is quite similar to that obtained in Bakke's[2] experiment shown in Fig. 4.27, but slightly different from Glauert's[4] velocity profile as shown in Fig. 4.27 at the outer portion of the free turbulent boundary. The profile presented here is lower than Glauert's velocity profile. Except for the profile in the boundary layer near the plate, the characteristics of the velocity profile similarity are like those of the turbulent free jet investigated by many previous investigators. Poreh, Tsuei, and Cermak[7] obtained also a similar dimensionless velocity profile.

Figures 4.28 - 4.32 show that there exists an approximate similarity in the wall jet flow regardless of the distance between the jet nozzle and the target plate; with the particular method used of making the velocity profile dimensionless, it becomes also relatively independent of the Reynolds number influence, except in the boundary layer immediately at the wall. Only a very cursory examination of this layer was possible with the probes available for the present investigation (Fig. 2.4).

Figure 4.33 shows a comparison between the outer portion of the wall jet and Schlichting's formula, among all the governing equations for velocity distribution shown in Fig. 34, Schlichting's formula is the closest to the present experimental results. This leads an additional

support to the derivation of the maximum velocity decay using Schlichting's formula to describe the outer portion of the wall jet.

Figure 4.35 is to plot the velocity profile near the wall on log-log coordinates, in order to observe that the value of power n of governing equation is affected by Reynolds number and may range from 7.5 to 14.

4.3.2. The Maximum Velocity Decay along the Flat Plate

The maximum velocity is the velocity at the location just beyond the turbulent boundary layer. It is the highest value of the wall jet velocity profile.

Figure 4.36 shows that the maximum velocity decay is governed by the equation

$$\frac{V_m}{U_{oc}} = \frac{1.4}{(\frac{r}{D})^{1.12}} \tag{87}$$

and gives a comparison for different z_n/D.

If V_m/U_{oc} is plotted against r/z_n, a family of lines is presented in Figure 4.37, and the maximum velocity decay is described by the equation

$$\frac{V_m}{U_{oc}} = \frac{1.4}{(\frac{z_n}{D})^{1.12}\ (\frac{r}{z_n})^{1.12}} \tag{88}$$

for different z_n/D. It may be given in a general form,

$$V_m = \frac{\text{const.}}{r^{1.12}} \tag{89}$$

Various investigators found that different values of the coefficient

of (r/D) represented their experimental data. Thus, the power of r is taken as 1.1 by Poreh[7], 1.14 by Brady[3], and 1.12 by Bakke[2]. The exact power of r seems to be a function of the Reynolds number; however, this variation is too small to be accurately measured.

The power of r is always larger than 1, that is to say the decay of the maximum velocity along the flat plate is faster than that of a free jet, which decays with the power 1 of r.

4.3.3. The Decay of the Reference Boundary Velocity V_{RB}

The V_{RB} was defined by Poreh and Cermak[8]. Fig. 4.38 shows the V_{RB} decay according to the relationship

$$\frac{V_{RB}}{U_{oc}} = \frac{0.62}{\frac{r}{z_n}} \qquad (90)$$

for $z_n/D = 20$ and Re_D between 14000 and 67000. The value of V_{RB} was approximately obtained by extrapolation.

4.3.4. The Growth of the Half-Valued Width of Wall Jet

The growth of the half-valued width of wall jet has been investigated and is shown in Fig. 4.39. It is found to change proportionally to 0.95 power of the radial distance along the flat plate. It can be shown in a general form as

$$z_{1/2}/_D = \text{const.} \left(\frac{r}{D}\right)^{0.95} \qquad (91)$$

where the constant has been determined experimentally as a function of z_n/D, being, for instance, 0.1025 for $z_n/D = 20$, 0.0945 for $z_n/D=10$ and 0.088 for $z_n/D = 2$. The difference between the constants for two

different z_n/D's is proportional to the difference between the two z_n/D's in question.

The observed power of r is 0.9 as obtained by Poreh, Tsui and Cermak[7], 0.94 by Bakke[2], and 1.028 by Brady and Ludwig[3]. Thus, according to the present results, the rate of growth or spread of wall jet is slightly smaller than that of a free jet.

4.3.5. Comparison of Flow Properties between an Unheated Isothermal Plate and a Heated Plate.

The data on the boundary layer and half-valued width taken from a heated plate are similar to that of a plate not heated; at least, there is no observable difference measured by the present instruments. It seems, however, that the growth of both the boundary layer and half-valued thickness are a little faster than that of a smooth lucite plate. That is because the heated plate tested for this part of the experiment consisting of seven ring-like,symmetrically arranged invar sections, filled with silicone rubber for insulation, is not as smooth as the lucite plate.

It is believed, however, that similarities between the results of flow measurements carried out on the segmented heated plate and the smooth lucite plate, are satisfactory to make the heat transfer results obtained on the segmented plate also generally applicable to the other natural flat surfaces, as occurring, for example, in various machined or cast surfaces. The above conclusion applies only for an invar plate 0.564 in. thick, with surface temperatures between $100^{o}F$ - $200^{o}F$. For higher temperature levels there could possibly occur significant differences between their flow patterns and those

applicable to smooth isothermal plates.

Figure4.40 shows an approximate comparison of boundary layer thickness between a heated plate and an unheated plate, however, the accuracy of the present instruments is not sufficient to show any systematic differences.

The results show that there is a tendency for the heated plate to have a thicker boundary layer. Fig. 4.41 and 4.42 show the maximum velocity decay along the heated plate and unheated plate. The governing equation of the lines is

$$\frac{V_m}{U_{oc}} = \frac{\text{const.}}{(\frac{r}{z_n})^a} \qquad (92)$$

where a = 1.13 to 1.14 for a heated plate and 1.12 to 1.13 for an unheated plate. In other words, the maximum velocity decay along a heated plate is slightly faster than for the plate not heated.

The dimensionless velocity profiles are presented in Fig. 4.43 and 4.44. There is no obvious difference between the heated and unheated plates, but the result shows a small difference from the smooth lucite plate which presents a velocity profile that is higher at the outer portion but only very slightly lower at the tip. However, the flow velocity of a heated plate is increased as shown in Fig.4.47.

4.4 Conclusive Data Analysis

4.4.1. Free Jet Zone

The experimental results of the velocity decay along the centerline shown in Fig. 4.4 to 4.9 are quite in agreement to Eq.(10) within the fully developed region. In the actual potential core region,

the velocity is also described by $U_m = U_{oc}$. However, the velocity at the location between actual potential core and fully developed region (transition region) is no longer governed by either Eq. (10) or $U_m = U_{oc}$.

The coefficient C in the Eq. (10) is a number related to the length of potential core. According to Abramovich's conclusion, C is not a function of Reynolds number over the range from 2×10^4 to 40×10^5, but in the present experiment, C is slightly dependent on the Reynolds number in this range but is strongly dependent on Re_D when Re_D is smaller than 1×10^4, and by observation of the results, C is also dependent on the size of the nozzles for $1000 < Re_D < 4000$.

On the analysis of the free jet zone, no variation of the static pressure was assumed. Actually, the static pressure is varied within the free jet zone, however, the variation of static pressure is very small compared to the velocity and might be neglected.

The growth of the jet shown in Fig. 4.14 is similar to Eq. (6) and the velocity distribution compared with Schlichting's Eq. (11) is presented in Fig. 4.10 which shows a satisfactory agreement.

4.4.2. Deflection Zone.

From Fig. 4.15 to Fig. 4.25, the pressure distribution is shown for different z_n/D's and nozzle diameters. In a small region, the pressure distribution can be described by Eq. (16) at z = 0 and the variation of velocity shown in Fig. 4.25 is quite in agreement with Eq. (14) that is linearly increased with r; beyond this region, the effect of viscous dissipation is predominant and Eq. (14) and (16)

are no longer valid. The flow changes over to a radial wall jet.

4.4.3. Wall Jet Zone

The maximum velocity decay is inversely proportional to $r^{1.12}$ shown in Fig.4.36 and Fig. 4.37. The power α of r in Eq. (64) derived above is varied from 1.1217 for n = 7 to 1.1294 for n = 15. However, the variation is very small and can not be accurately measured in the present experiment, and the experimental result of the power 1.12 is between the values in theoretical analysis. The maximum reference boundary velocity, V_{RB}, defined by Poreh[8], obtained by extrapolation is shown in Fig.4.38 and is governed by Eq. (20).

The velocity profiles near the flat plate vary with Reynolds number shown in Fig. 4.28 to 4.32, but the exact profiles cannot be measured in the present experiment. However, an approximate figure is shown in Fig.4.35. The profile beyond the boundary layer is similar to Bakke's experiment and Glauert's profile with $\alpha = 1.3$.* The present data shows lower profile at the outer portion of the wall jet and closer to Schlichting's formula

$$\frac{V}{V_m} = (1 - \xi^{1.5})^2 \qquad (93)$$

which is shown in Fig.4.33 and 4.34. Therefore, to use Schlichting's formula above for velocity profile is quite satisfactory in this work.

The static pressure along the flat plate in the wall jet zone is actually near to zero which is coincident with the assumption in the theory. The width of the jet b is approximately nine or ten times

*This α defined by Glauert[4] is different from the power α of r in this work.

the boundary layer δ, that is $\delta = 0.1$ to 0.11b whereas in our theoretical derivation we made the assumption $\delta = 0.1b$. The growth of the half-valued width of jet is proportional to $r^{0.95}$; however, it varies approximately linearly with r. By the property of profile similarity, to assume b$\propto$r is reasonable. It is also interesting to note that the relation between the coefficients obtained here still satisfies the inequality $2(-1.12) + 0.95 + 1 < 0$, originally discovered by Poreh et al.[7].

4.5. Comparison between Incompressible and Compressible Flow of Air

Because of the property of compressibility of air, it is not true to consider air incompressible at velocity higher than 300-400 fps. which makes, for instance, the approximate Reynolds number is 75000 for D=0.375 in., 50000 for D=0.250 in., and 25000 for D=0.125 in. at the nozzle exit; however, in most of the measurements in the present experiment, it is satisfactory to consider air incompressible. Higher Reynolds numbers are tested in order to compare the results of the incompressible and compressible flow of air based on the following equations[15],

$$P_t - P_s = \frac{1}{2}\rho V^2 \tag{94}$$

for incompressible flow, and

$$P_t - P_s = \frac{1}{2}\rho V^2\left[1 + \frac{M^2}{4} + \left(\frac{2-k}{24}\right)M^4 + \ldots\ldots\right] \tag{95}$$

for compressible flow, where P_t, P_s and M are stagnation pressure, static pressure and Mach number, respectively. It is found that the ratio of the velocities of compressible and incompressible flow at the nozzle exit is 0.965 for D=0.375 in. at $Re_D = 92000$ and 0.95 for D=0.250 in. at $Re_D = 96000$. Fig. 4.45 and 4.46 shows the comparison

between the velocity decays for the incompressible and compressible flow of air at very high Reynolds number. The coefficient C of the governing equation describing the velocity decay is slightly higher for compressible flow. If the correction is made for the coefficient C at higher Reynolds number, the results will show the slightly higher curves as shown in Figure 4.3.

4.6. The Measurement of Boundary Layer Thickness along the Flat Plate

To measure boundary layer in the present experiment is quite difficult; however, the approximate variations of the boundary layer along the flat plate from the stagnation point to a further distance away had been investigated and the results are shown in Fig. 4.48 to 4.52. It can be seen that the boundary layers near the stagnation point are approximately described by Eq. (82), 10 to 40 percent greater than the values calculated by Eq. (82), and are constant as predicted by Eq.(82). The region of this flow prevails approximately within 1D (or r/D = 1) as shown in Figures 4.48 to 4.52; whereas it is indicated in Fig. 4.26 that the region is within 0.7 to 1D.

The boundary layer growth in fully turbulent region can be roughly described by the equation

$$\frac{\delta}{D} = 0.0175 \left(\frac{r}{D}\right)^{0.95} \qquad (96)$$

according to the results shown in Figure 4.52.

Conclusions

The characteristics of fluid flow resulting from impinging jets in all three zones (free jet zone, deflection zone and wall jet zone) have been investigated. It has been shown that the dimensionless length of the potential core is a weak function of the Reynolds number, in turbulent flow, and becomes a strong function of the Reynolds number for Re_D less that 10^4. The potential core is proportional to the Reynolds number in laminar flow. According to our own experimental results, the highest value of the theoretical dimensionless potential core length, C, is 6.8 and the lowest value is 4.8.

The dimensionless velocity profile of the wall jet is similar except in the portion near the flat plate; however, the deviation from similarity is very small. The velocity and pressure distribution in free jet zone, deflection zone and wall jet zone have been fully studied, and the conclusions reached are in agreement with those obtained by previous investigators. The dependence of maximum velocity decay on Reynolds number is very slight and could not be accurately measured in these experiments. The growth of the half-valued width of the free jet and wall jet has been also presented; there is no observable effect here of a varied Reynolds number,

Also, observations have shown that the differences between the heated and isothermal plates are very small for a moderate amount of heating, as far as flow parameter measurements are concerned. Thus, the heat transfer results obtained with a steam-heated segmented plate can, in principle, be analyzed with the help of flow parameters obtained with our present smooth, round plexiglass plate.

Recommendations

1. This experimental result shows that the coefficient C in Eq.(10) and in Fig.4.2 and 4.3 is a function of Reynolds number and nozzle diameter. It is possible to find the accurate effect of diameter D on the coefficient C by using more nozzles of different sizes. The coefficient C may also be investigated for nozzles of different geometry, for instance, using triangular or aquare nozzles.
2. In this experiment, because the nozzles are quite small, it seems to be harder to measure the flow properties, like velocity and pressure, within the deflection zone. It is so recommended to use bigger nozzles to investigatethe flow properties within the deflection zone, especially to measure the boundary layer and velocity profile.
3. Both the boundary layer thickness and the velocity profile are changed by heating the flat plate. Since the variation is small, so it is suggested to use higher temperature flat plates to test the effect of heating on boundary layer development and velocity profiles.

Bibliography

1. Abramovich, G. N., "The Theory of Turbulent Jets", MIT Press, Cambridge, Mass., 1963.
2. Bakke, P., "An Experimental Investigation of a Wall Jet", J. Fluid Mech., Vol. 12, pp. 467-472, 1957.
3. Brady, W. G., and Ludwig, G., "Theoretical and Experimental Studies of Impinging Uniform Jets", Jl. of Am. Helicopter Society, 8:2:1-13, 1963.
4. Glauert, M. B., "The Wall Jet", Jl. of Fluid Mech., Vol. 1, pp. 625-643, 1956.
5. Kaufmann, W., "Fluid Mechanics", McGraw-Hill Book Co., Inc., New York, 1963.
6. Miller, David R., and Comings, Edward W., "Static Pressure Distribution in the Free Turbulent Jet", J. Fluid Mech., Vol. 3, Pt. 1, pp. 1-6, Oct. 1957.
7. Poreh, M., Tsuei, Y. G., and Cermak, J. E., "Investigation of a Turbulent Wall Jet", ASME Paper No. 67-APM-10, 1967.
8. Poreh, M., and Cermak, J. E., "Flow Characteristics of a Circular Submerged Jet Impinging Normally on a Smooth Boundary", Proc. 6th Midw. Conf. on Fluid Mech., 1959.
9. Schlichting, H., "Boundary Layer Theory", 6th ed., McGraw-Hill Book Company, New York, 1968.
10. Snedeker, R. S., and Donaldson, C. du P., "Experiments on Free and Impinging Underexpanded Jets from a Convergent Nozzle", Ad 461622, 1964.

11. Tani, I., and Komatsu, Y., "Impingement of a Round Jet on a Flat Surface", Proc. XI Int. Cong. of Appl. Mech., pp. 672-676, 1964.

12. Trentacoste, N., and Sforza, P. M., "An Experimental Investigation of Three-Dimensional Free Mixing in Incompressible Turbulent, Free Jets", PIBAL Report, No. 17, 1966.

13. Hrycak, Peter, "Heat Transfer from Impinging Jets, A Literature Review". Prepared under Grant NGR-31-009-004, Newark College of Engineering, Newark, New Jersey, August 1968.

14. NASA facsimile reproduction of N65-19287.

15. Binder, R. C.,"Fluid Mechanics," 2nd Edition, Prentice-Hall, Inc., New York, N. Y., 1949.

16. Mc Naughton,K.J., and Sinclair,C.G.," Jets in Cylindrical Flow Vessels", Jl. Fl. Mech., Vol. 25, p.371, 1966.

17. Schach,W.," Deflection of a Circular Fluid Jet by a Flat Plate Perpendicular to the Flow Direction", Ing. Archiv, Vol. 6, pp.51-59, 1935.

18. Strand,T. " On the Theory of Normal Ground Impingement of Axisymmetric Jets in inviscid Incompressible Flow", AIAA Paper 64-424, 1964.

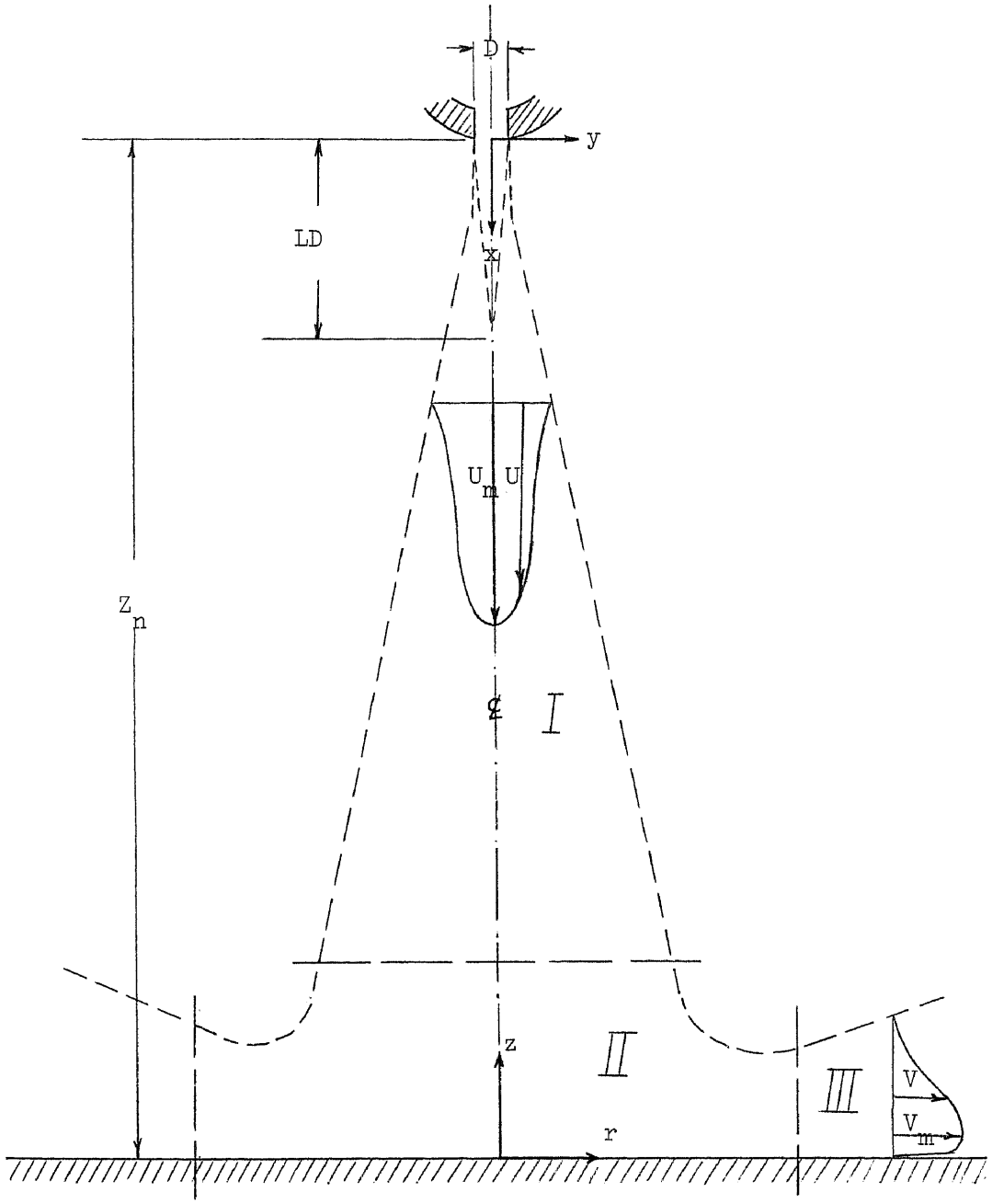

Coordinate System and Flow Pattern

Fig. 1.1

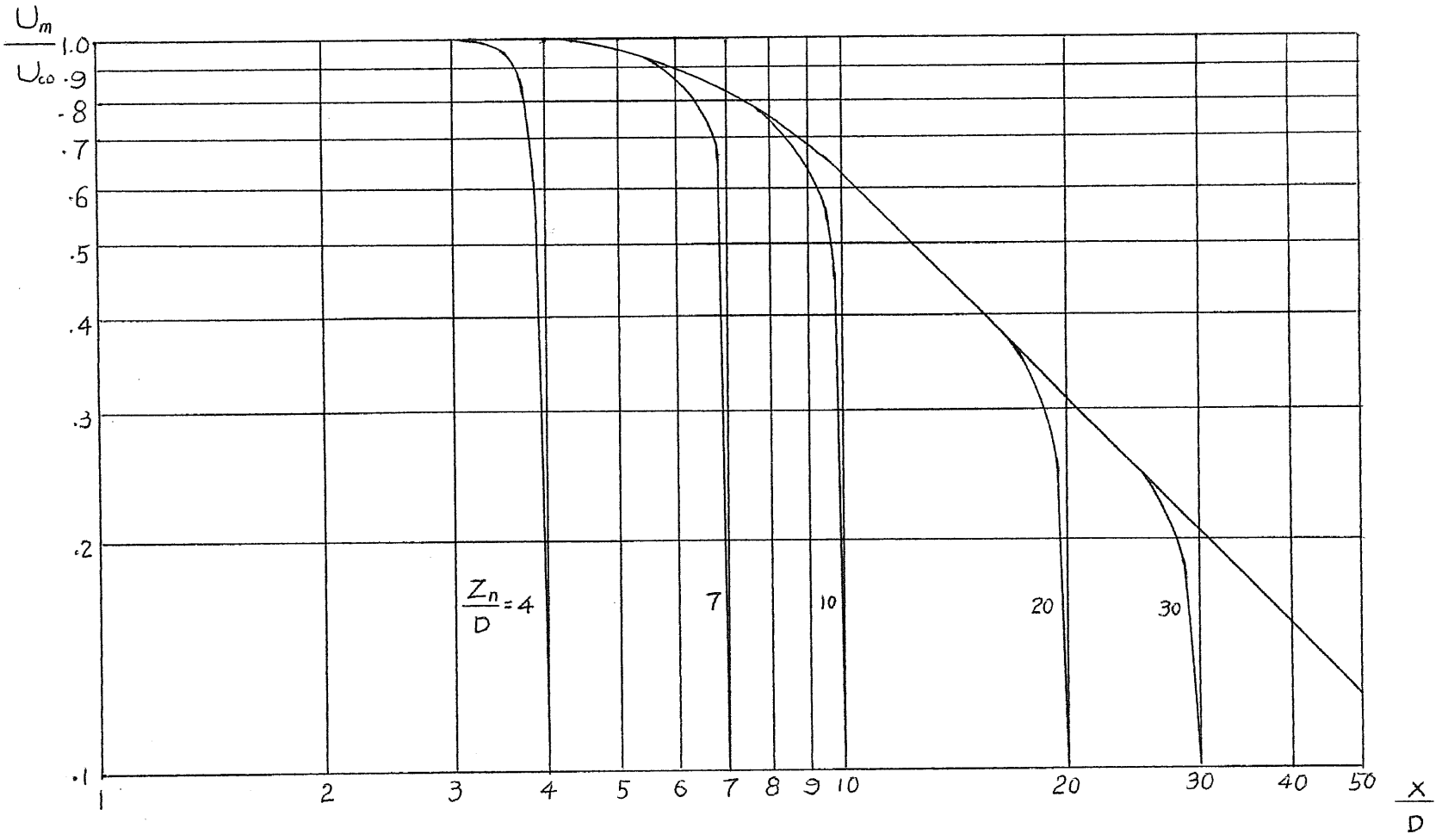

Centerline Velocity Decay with Varied Z_n/D

Fig. 1.2

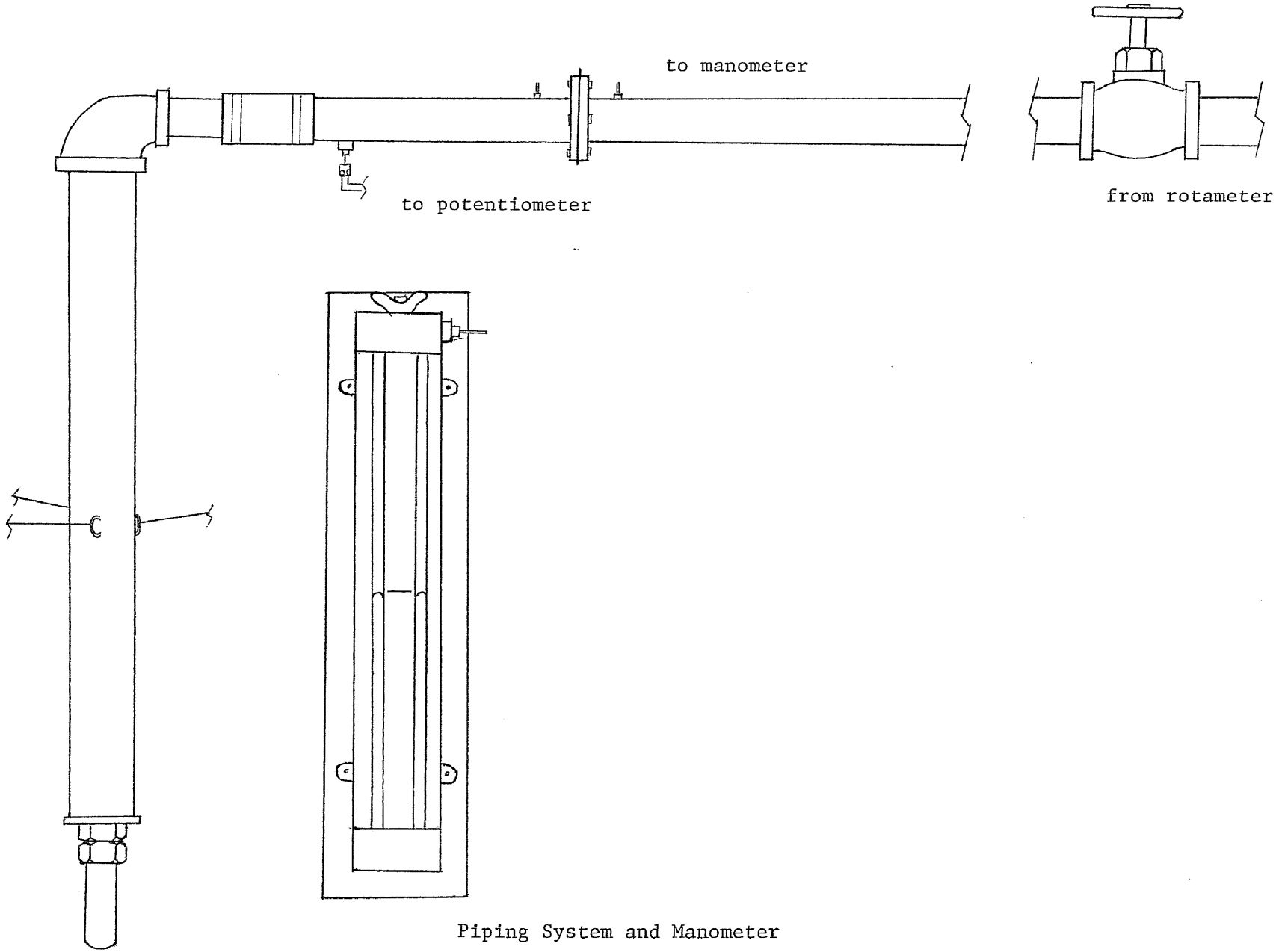

Piping System and Manometer

Fig. 2.1

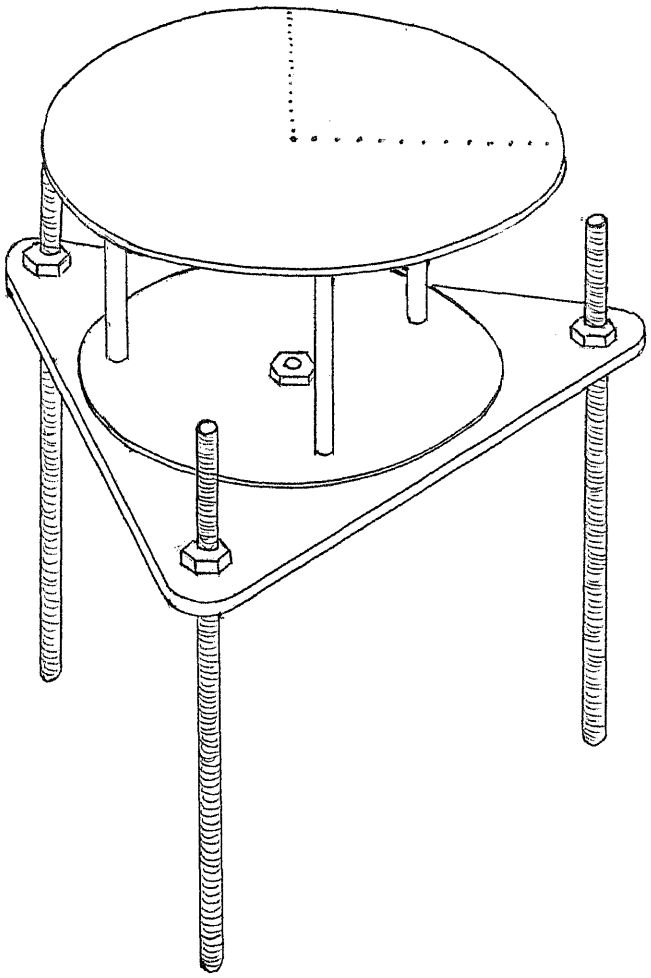

Impinging Plate

Fig. 2.2

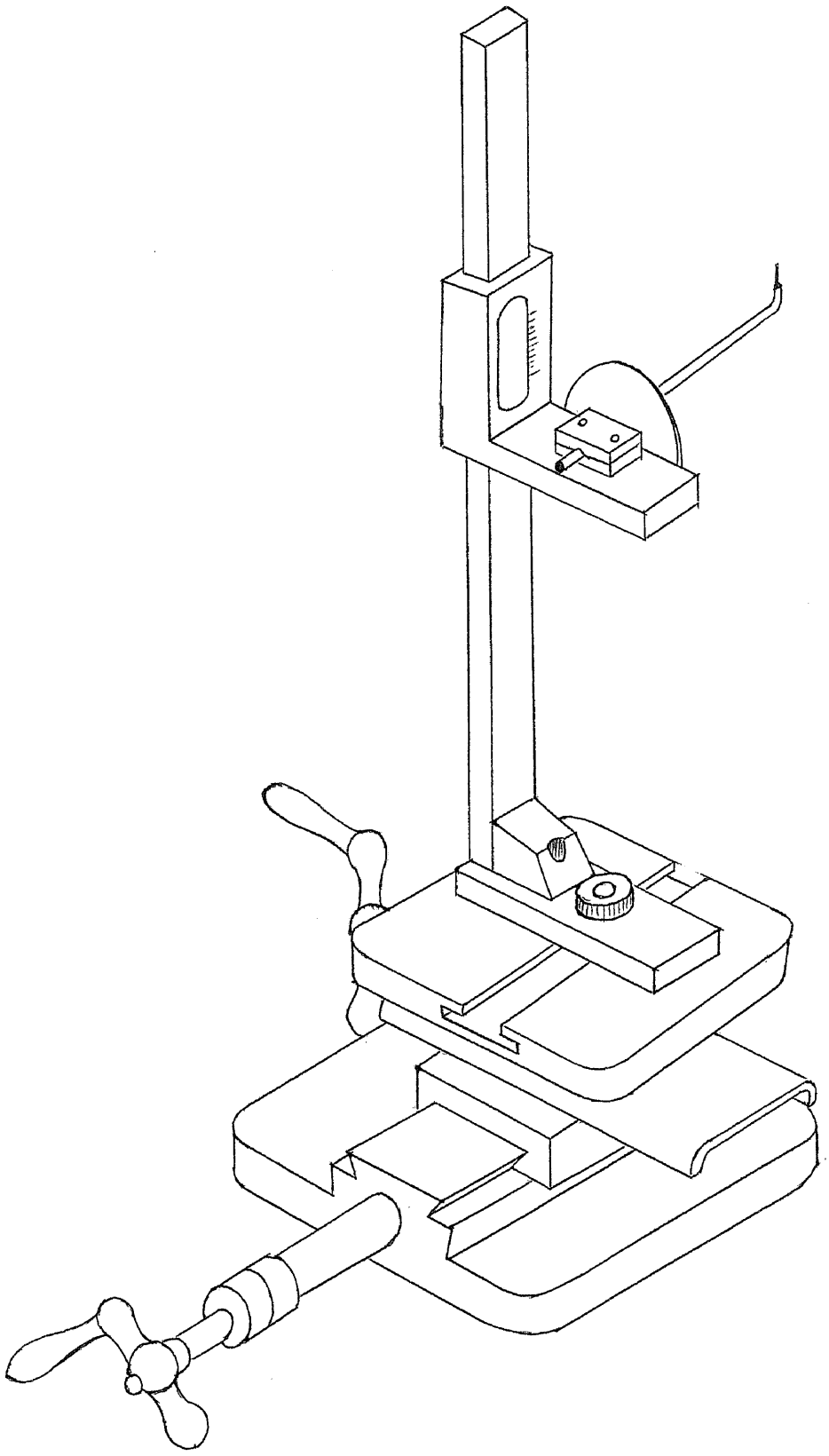

Three Dimensional Carriage

Fig. 2.3

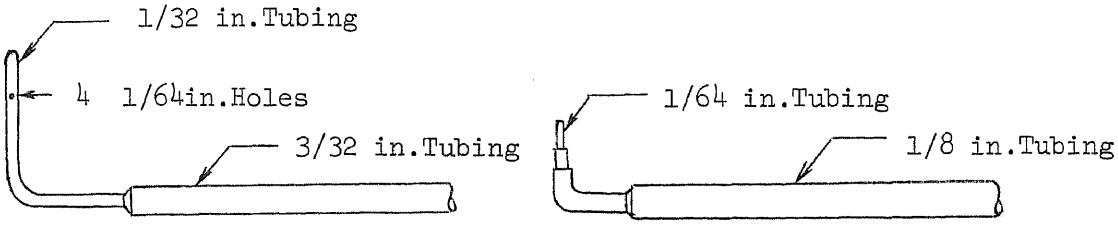

Static Pressure Probe

Total Pressure Probe

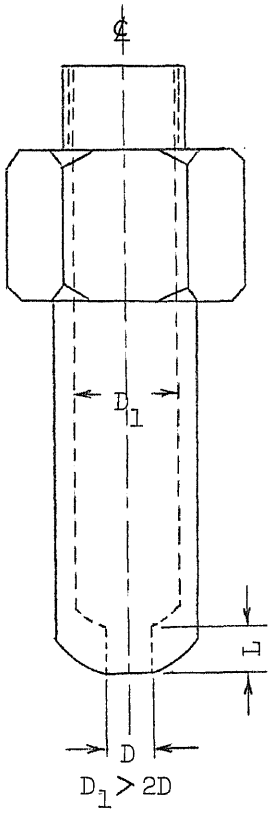

Nozzle

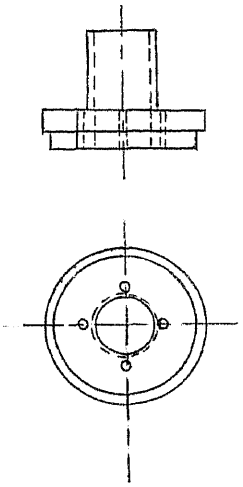

Smoke Producer

Experimental Instruments

Fig. 2.4

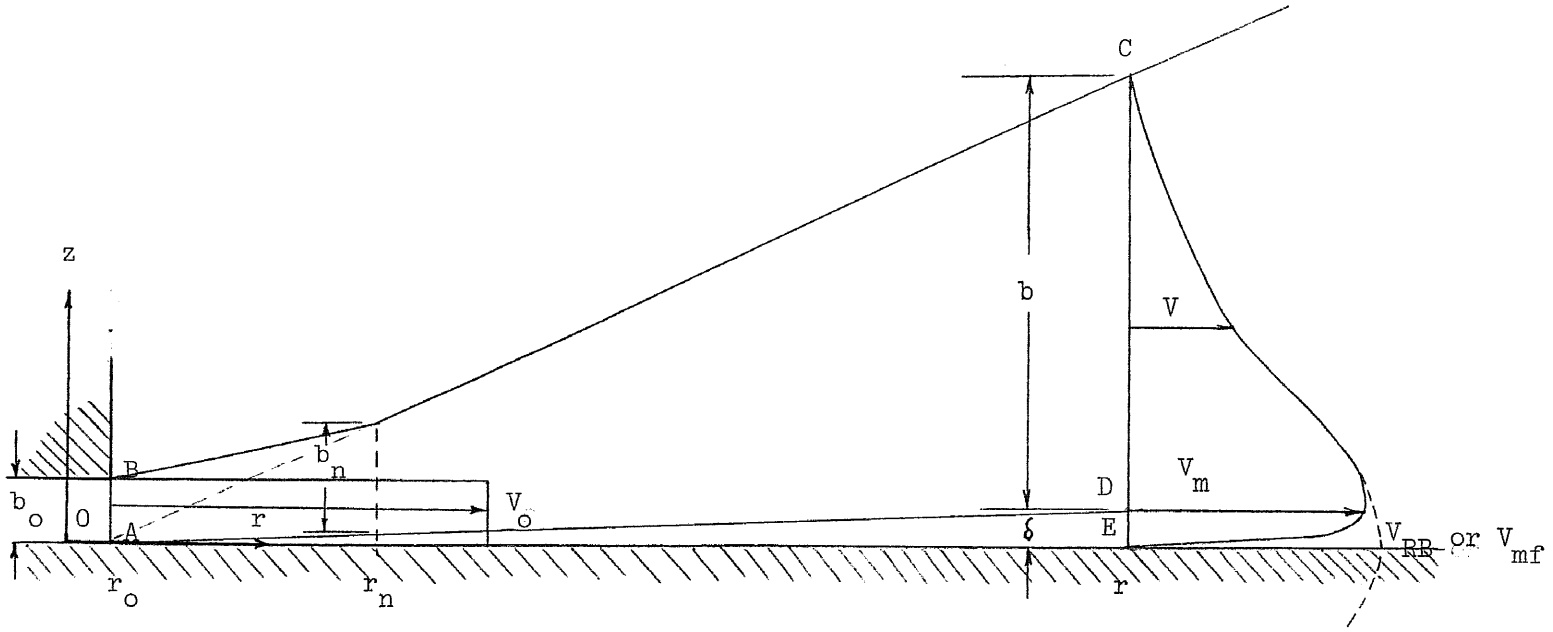

Coordinate System of a Radial Wall Jet

Fig. 3.1

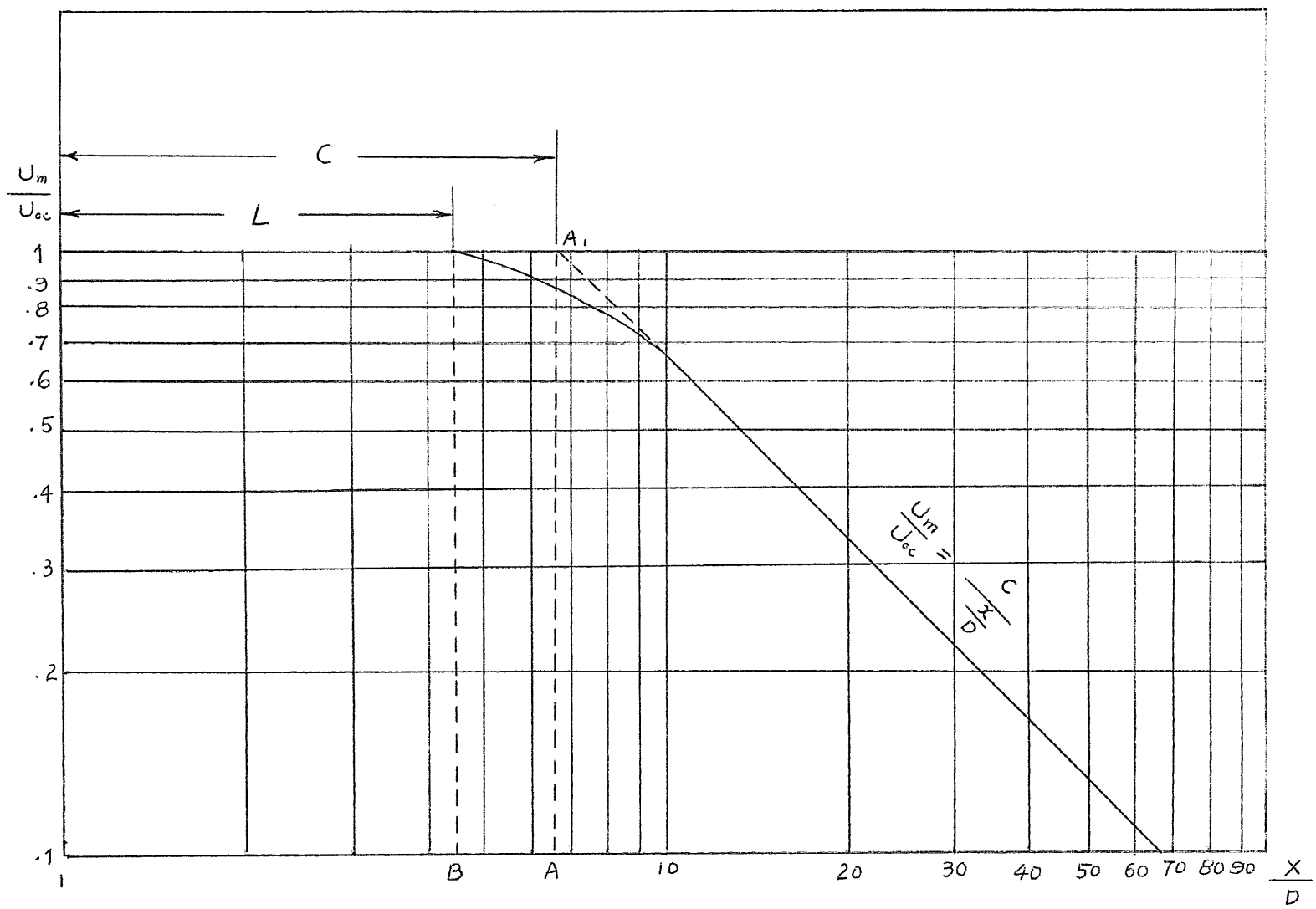

Definition of C and L

Fig. 4.1

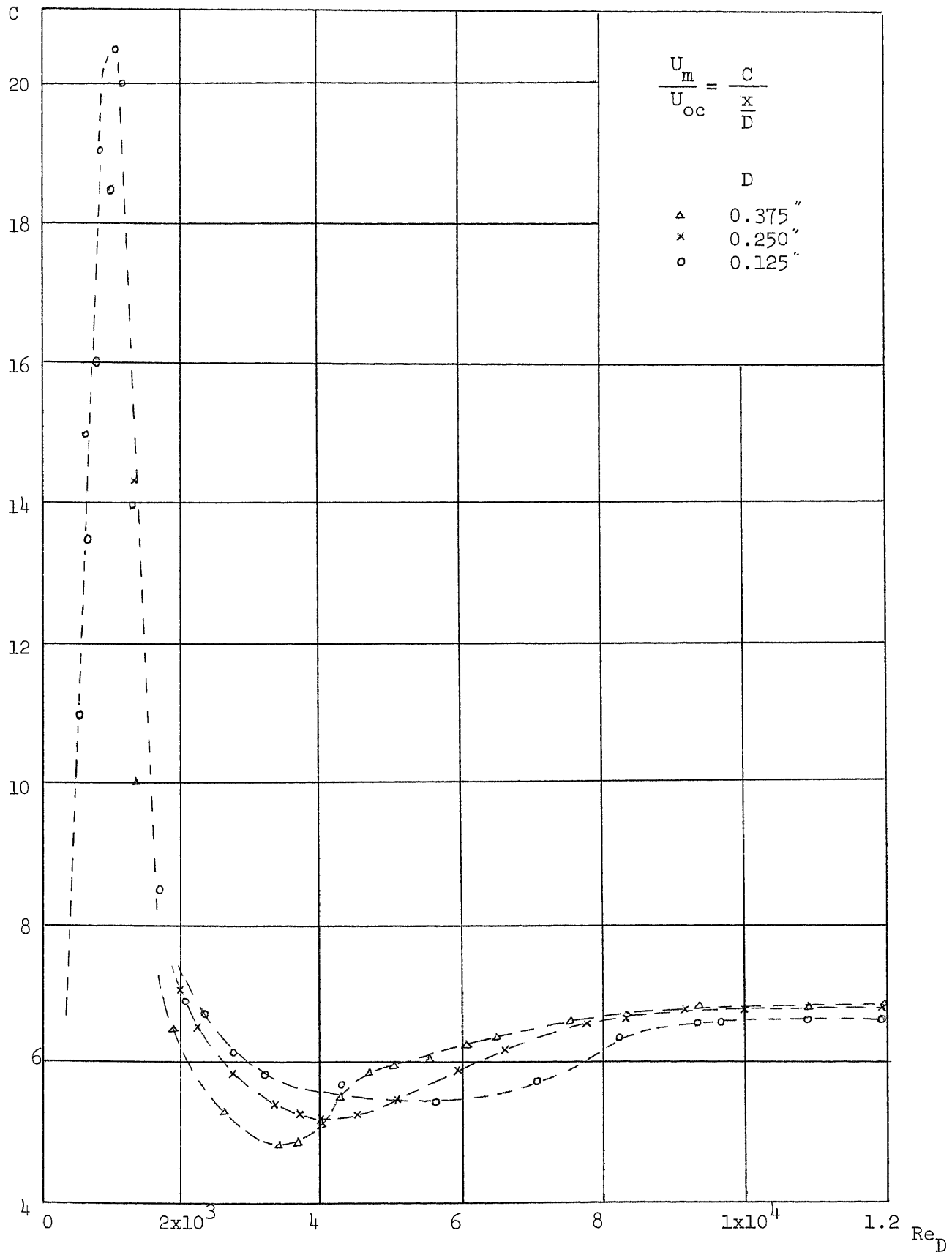

Variation of C

Fig. 4.2

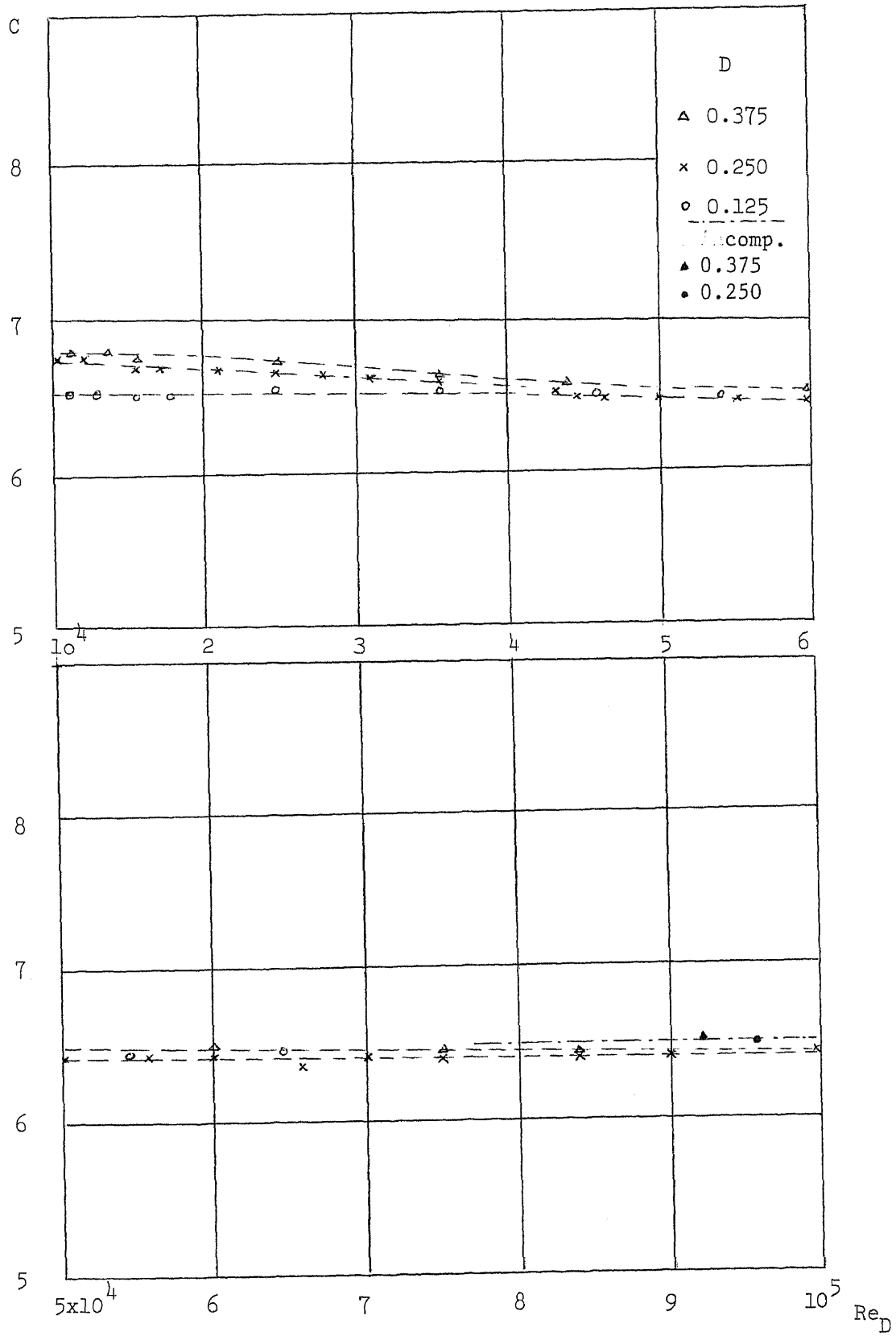

Variation of C

Fig. 4.3

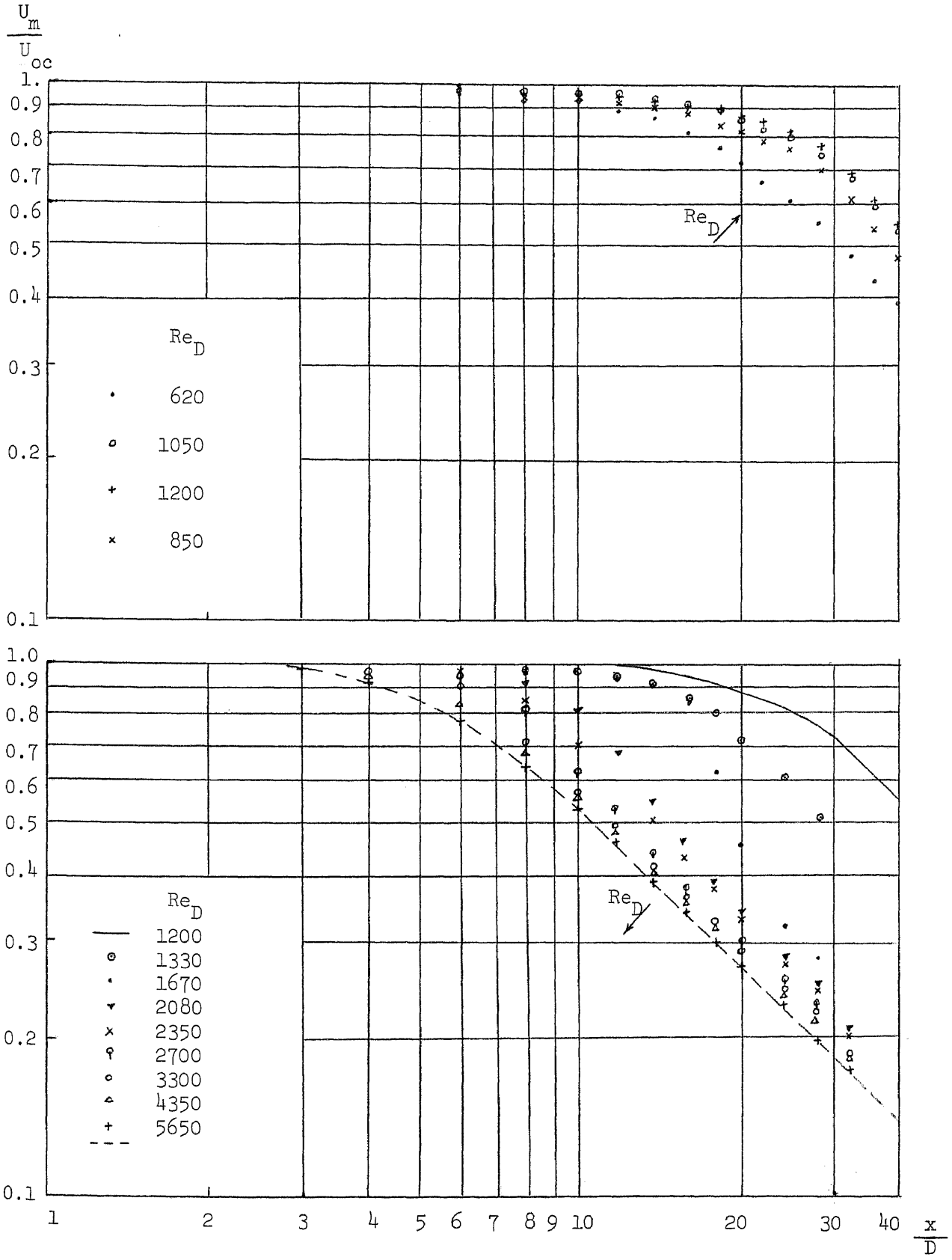

Centerline Velocity Decay with Nozzle Diameter 0.125 in.

Fig. 4.4

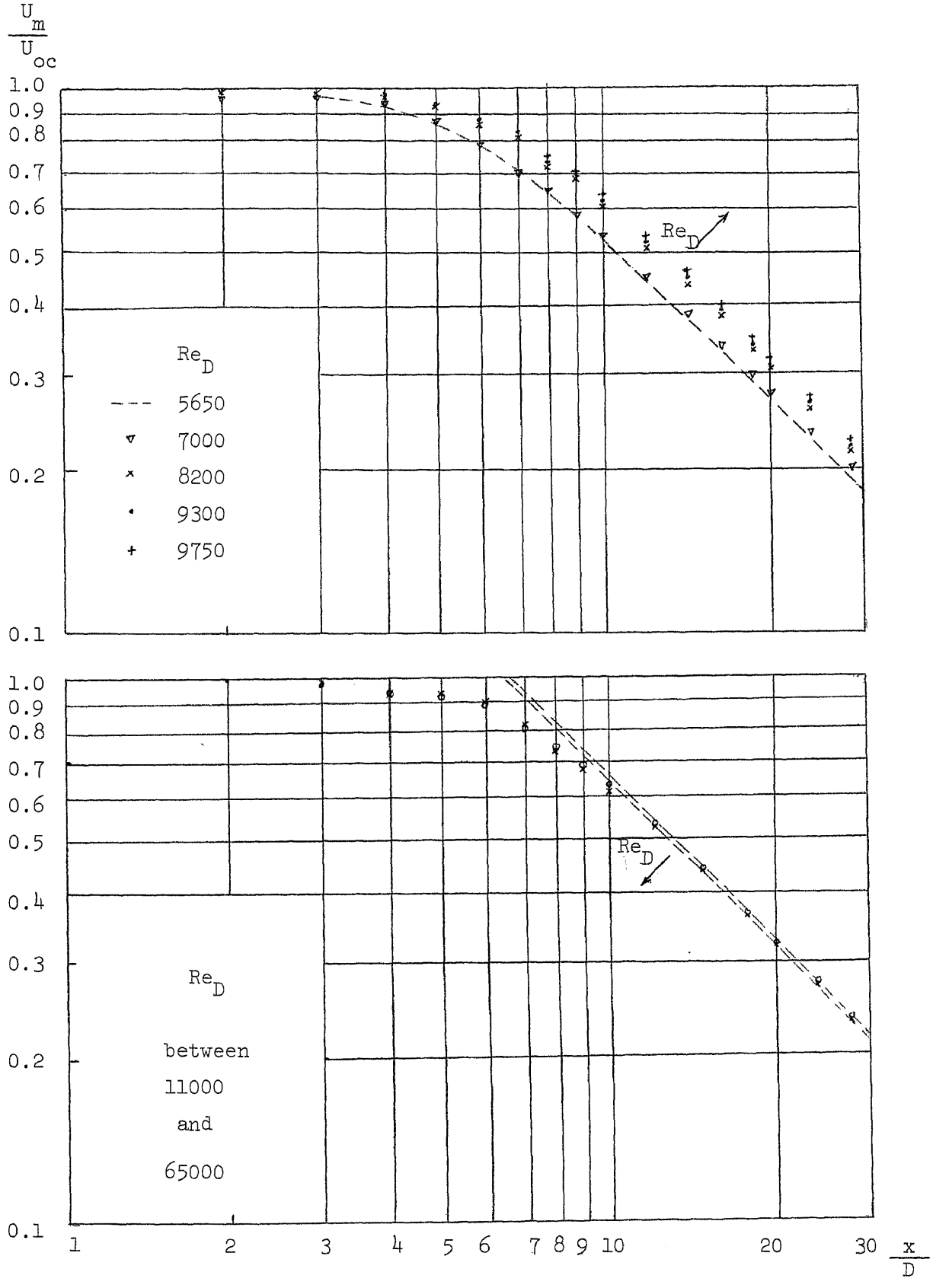

Centerline Velocity Decay of Free Jet with D=.125 and Varied Re_D

Fig. 4.5

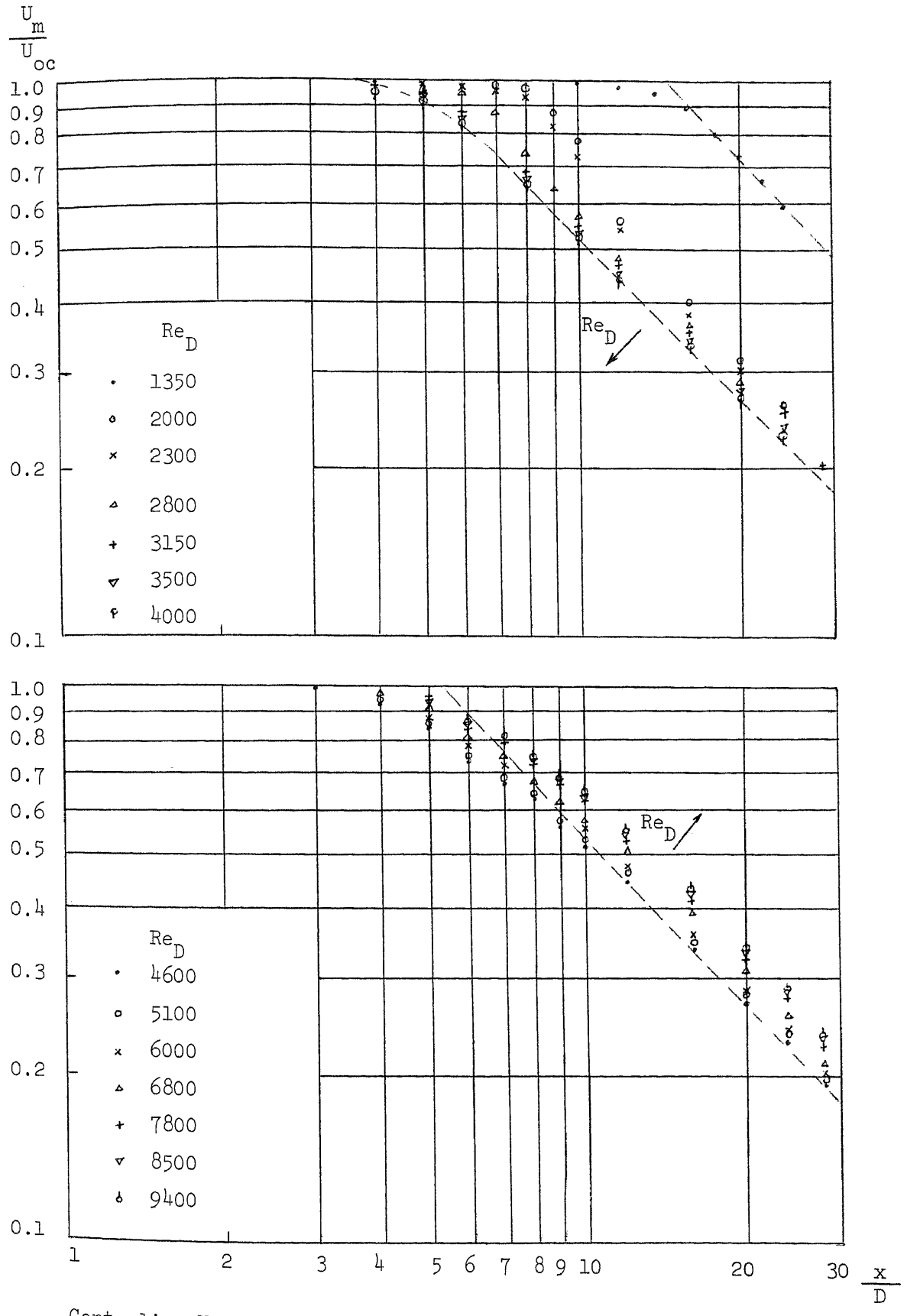

Centerline Velocity Decay of Free Jet with D=.250 and Varied Re_D

Fig. 4.6

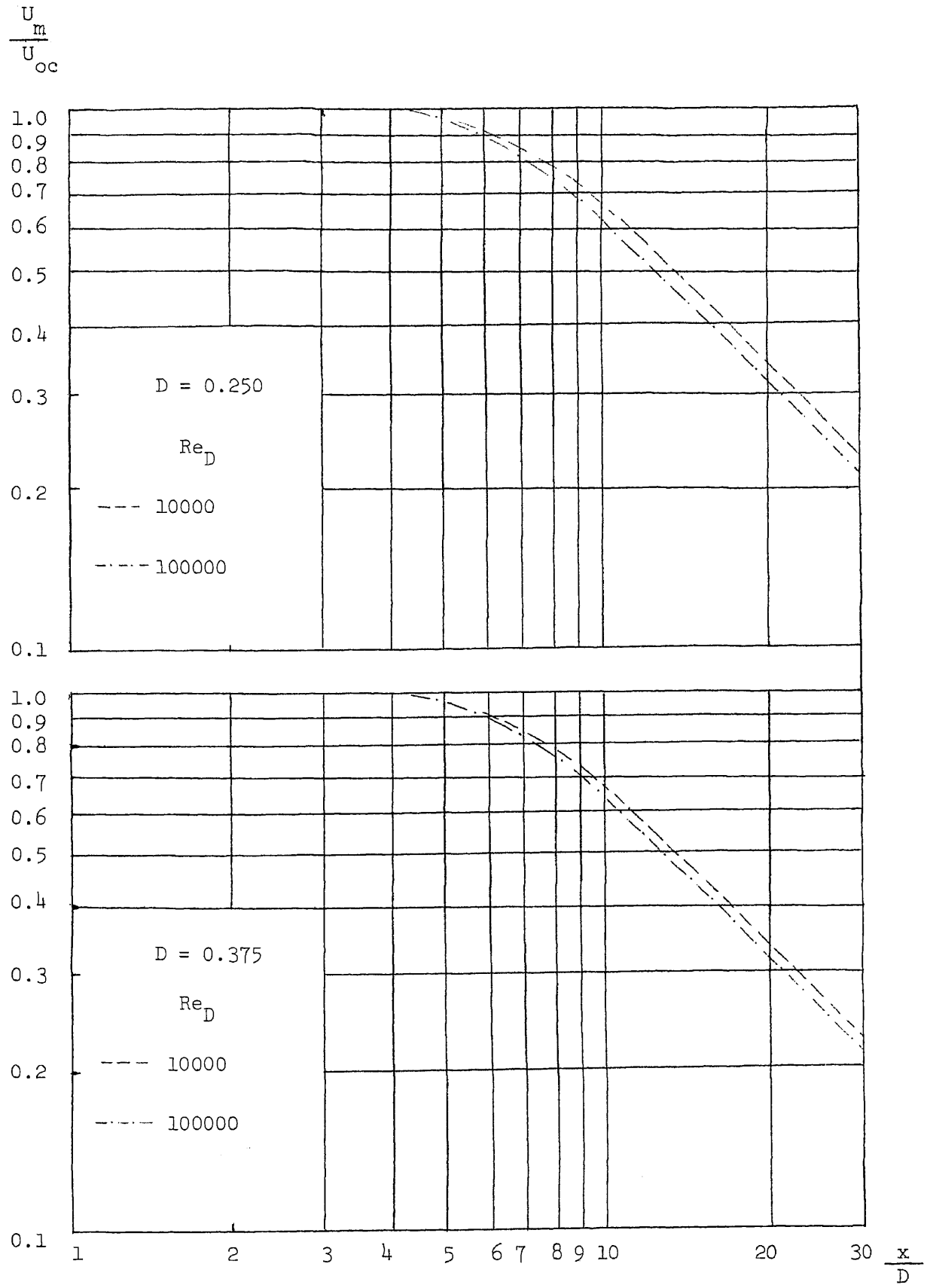

Centerline Velocity Decay for Varied Re_D

Fig. 4.7 & 4.9

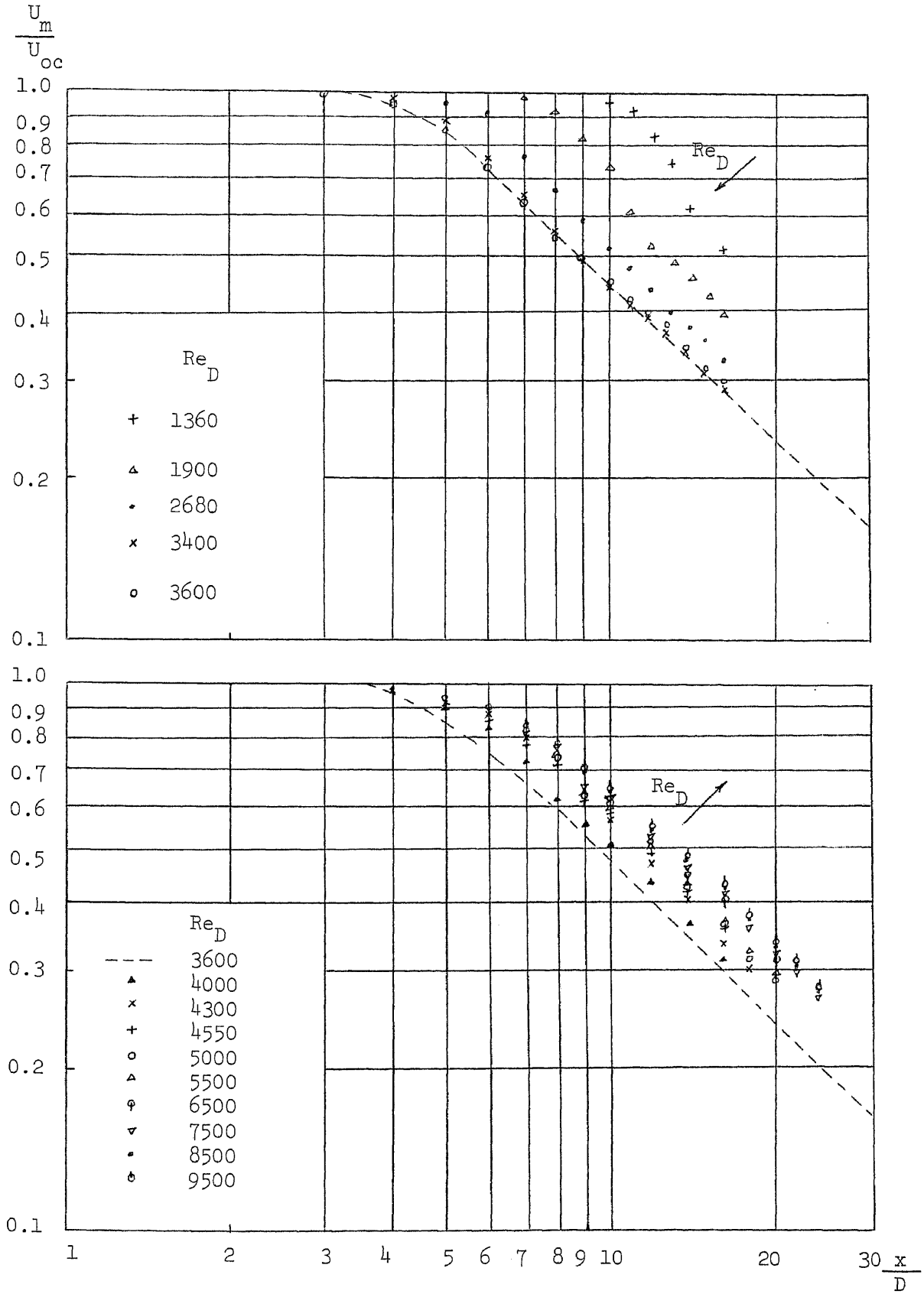

Centerline Velocity Decay with Nozzle Diameter 0.375 in.

Fig. 4.8

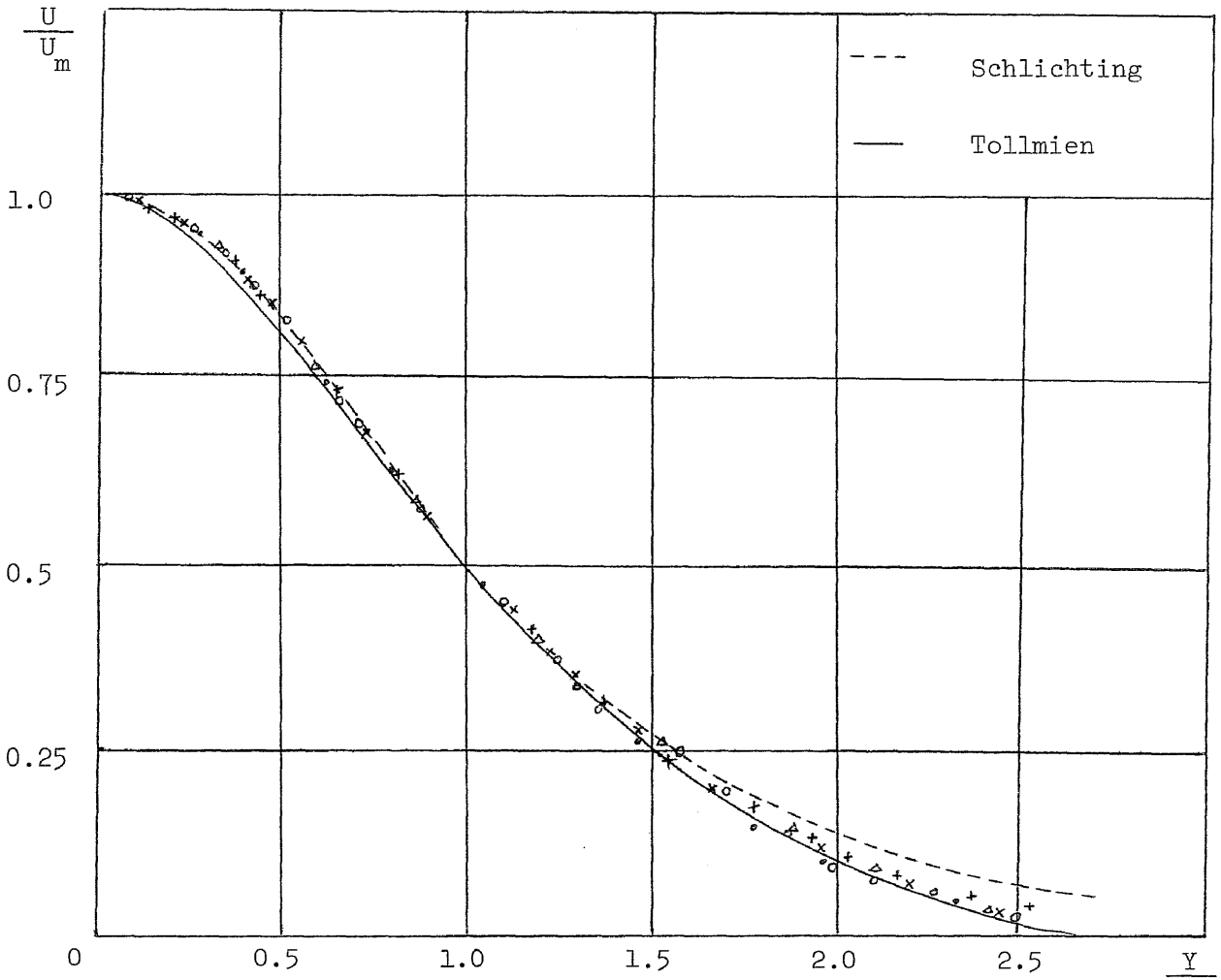

Dimensionless Velocity Distribution of Free Jet with Varied Re_D at Different Station of Main Region

Fig. 4.10

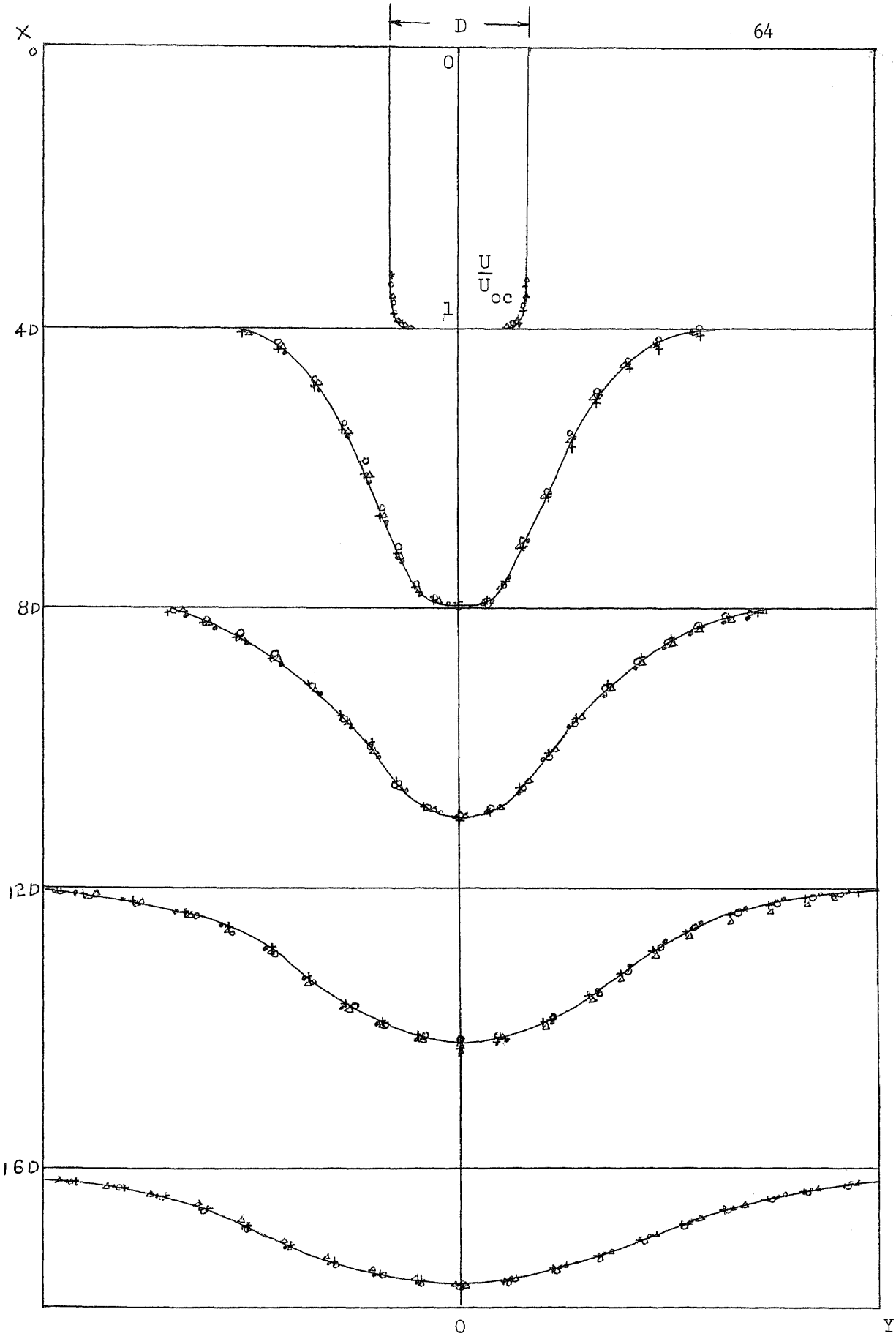

Velocity Distribution at Different Location of Free Jet from Nozzle Exit to Main Region with Varied Re_D

Fig. 4.11

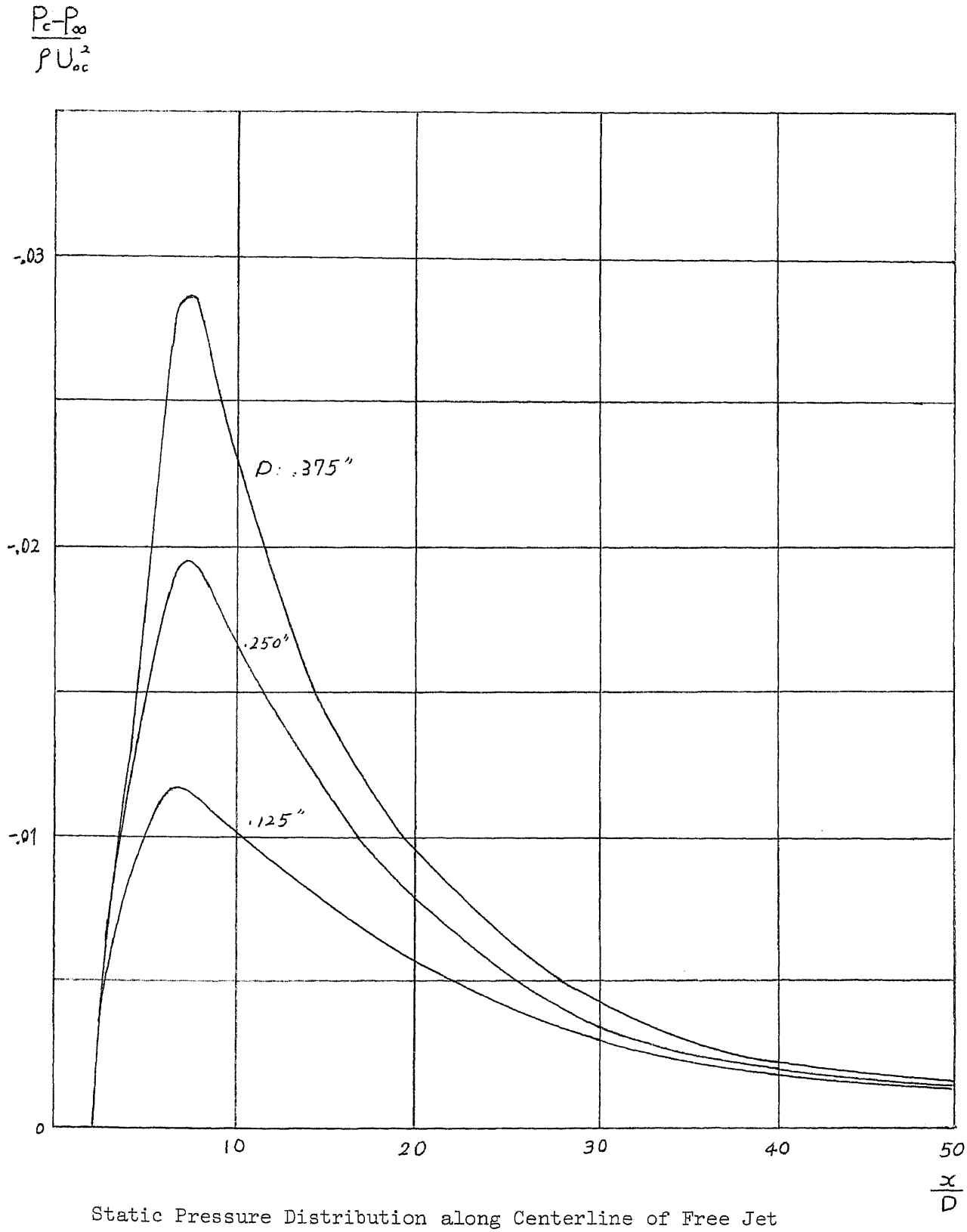

Static Pressure Distribution along Centerline of Free Jet

Fig. 4.12

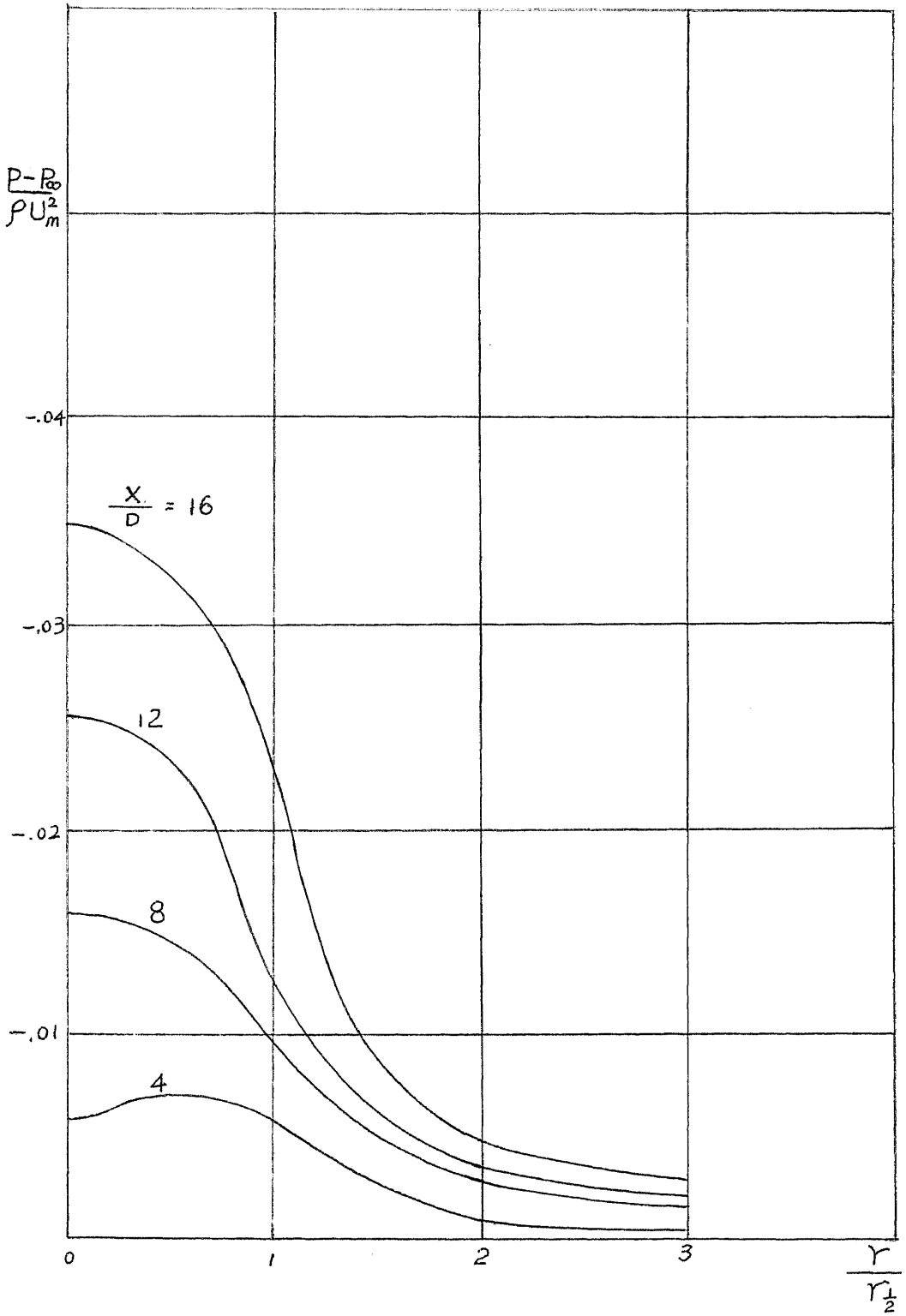

Static Pressure Distribution on the Cross Section of Free Jet

Fig. 4.13

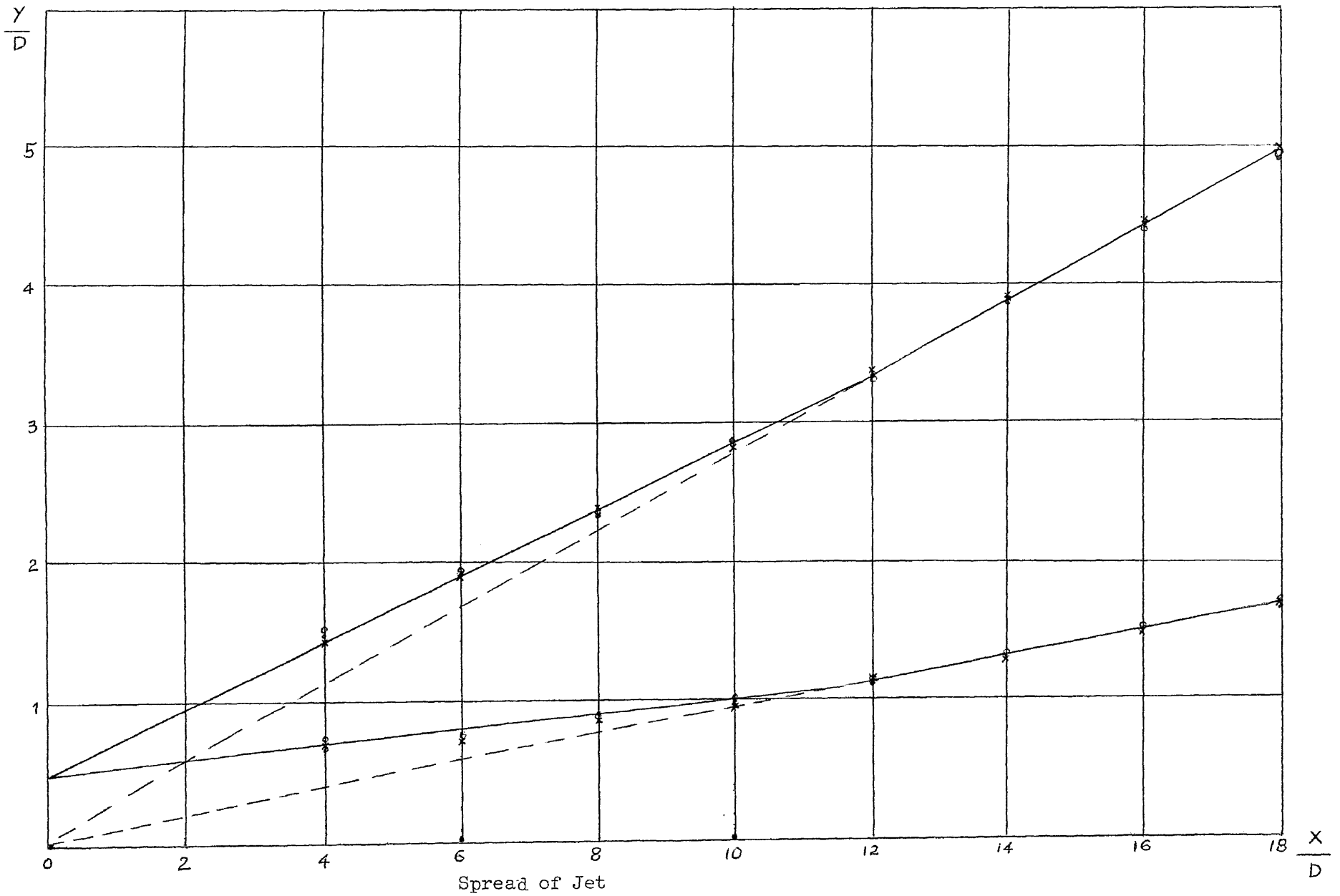

Fig. 4.14

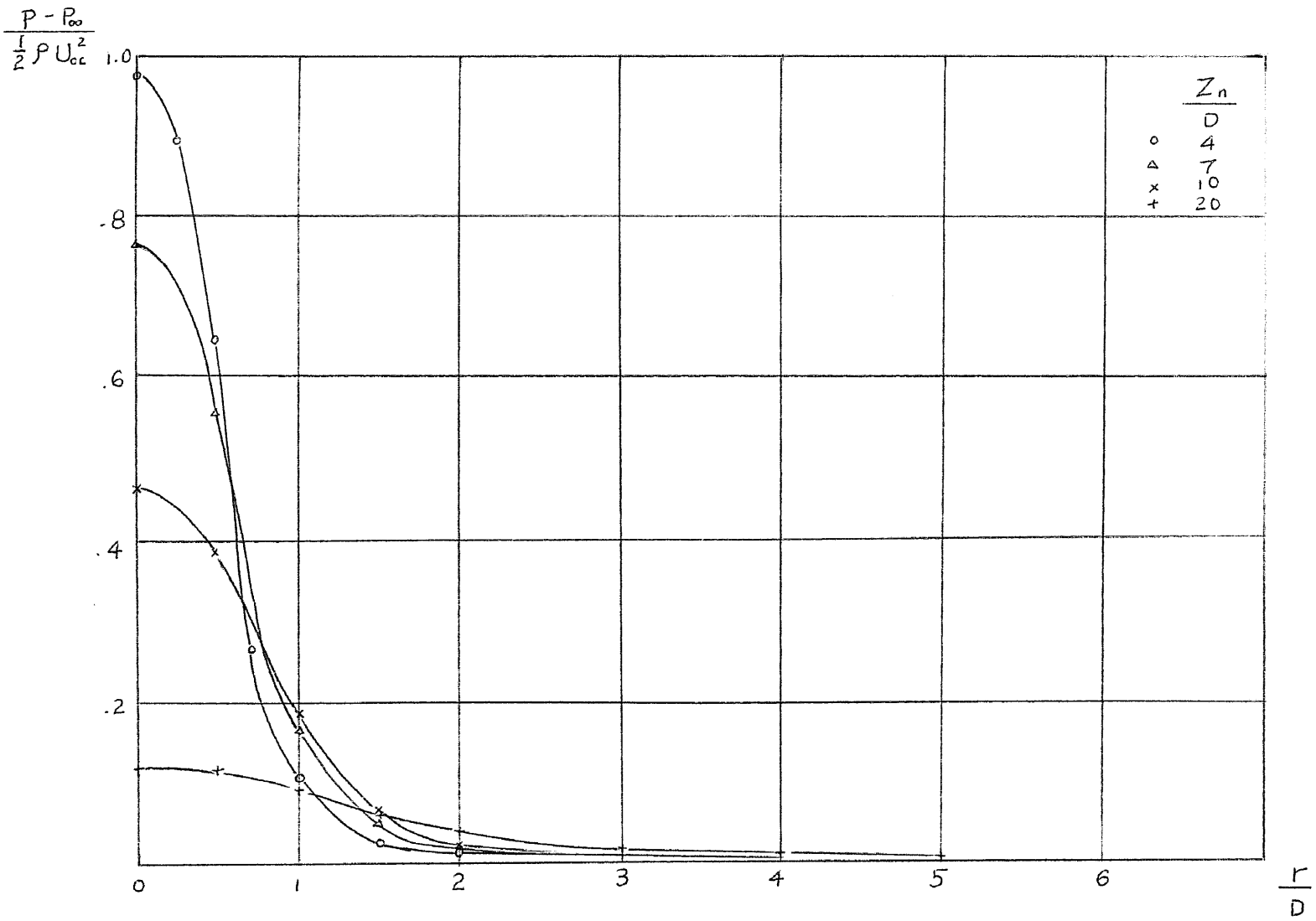

Comparison of Pressure Distribution with Varied Z_n/D =4,7,10,20

Fig. 4.15

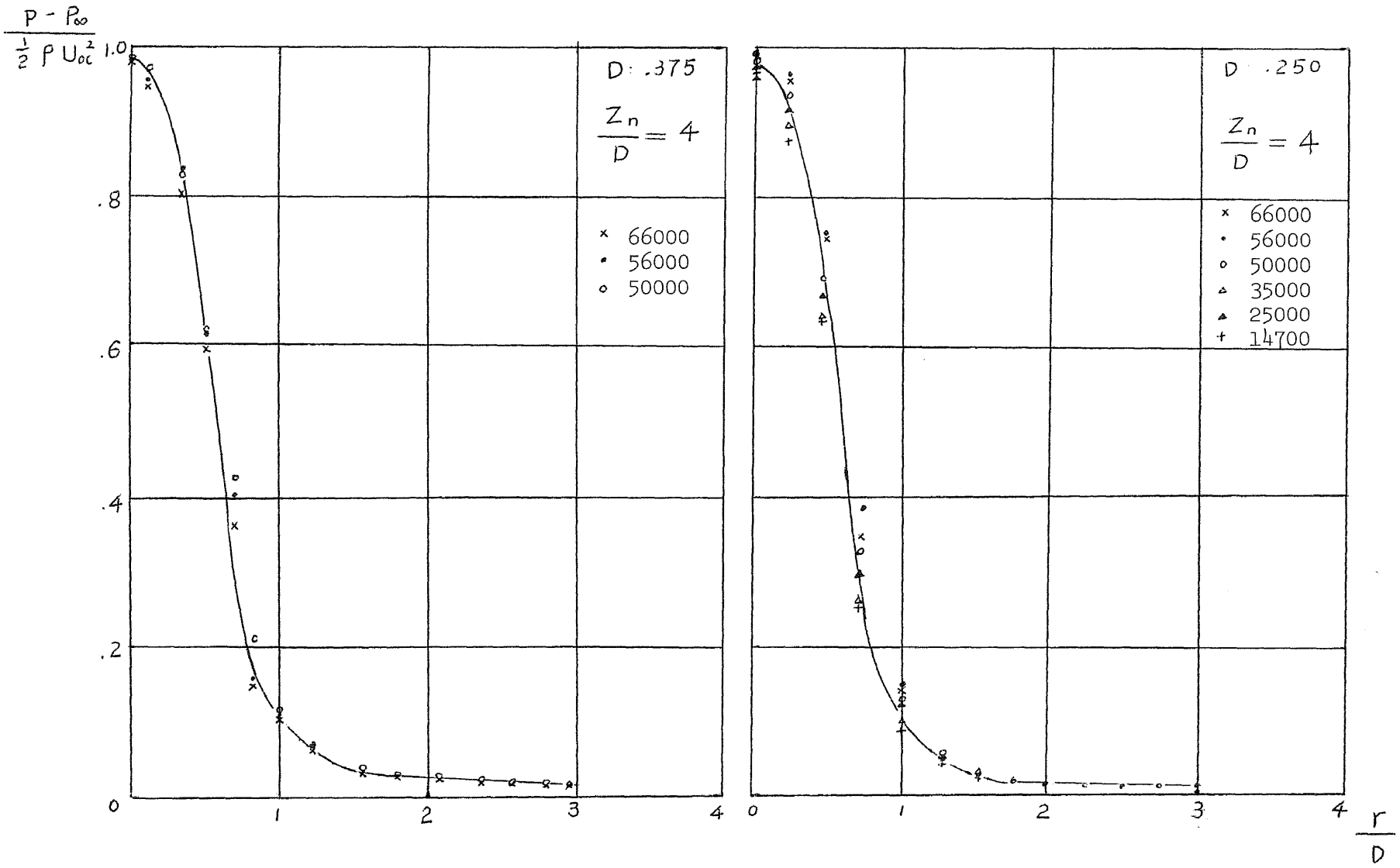

Pressure Distribution along the Flat Plate with $Z_n/D = 4$ and Varied Re_D

Fig. 4.16 & 4.17

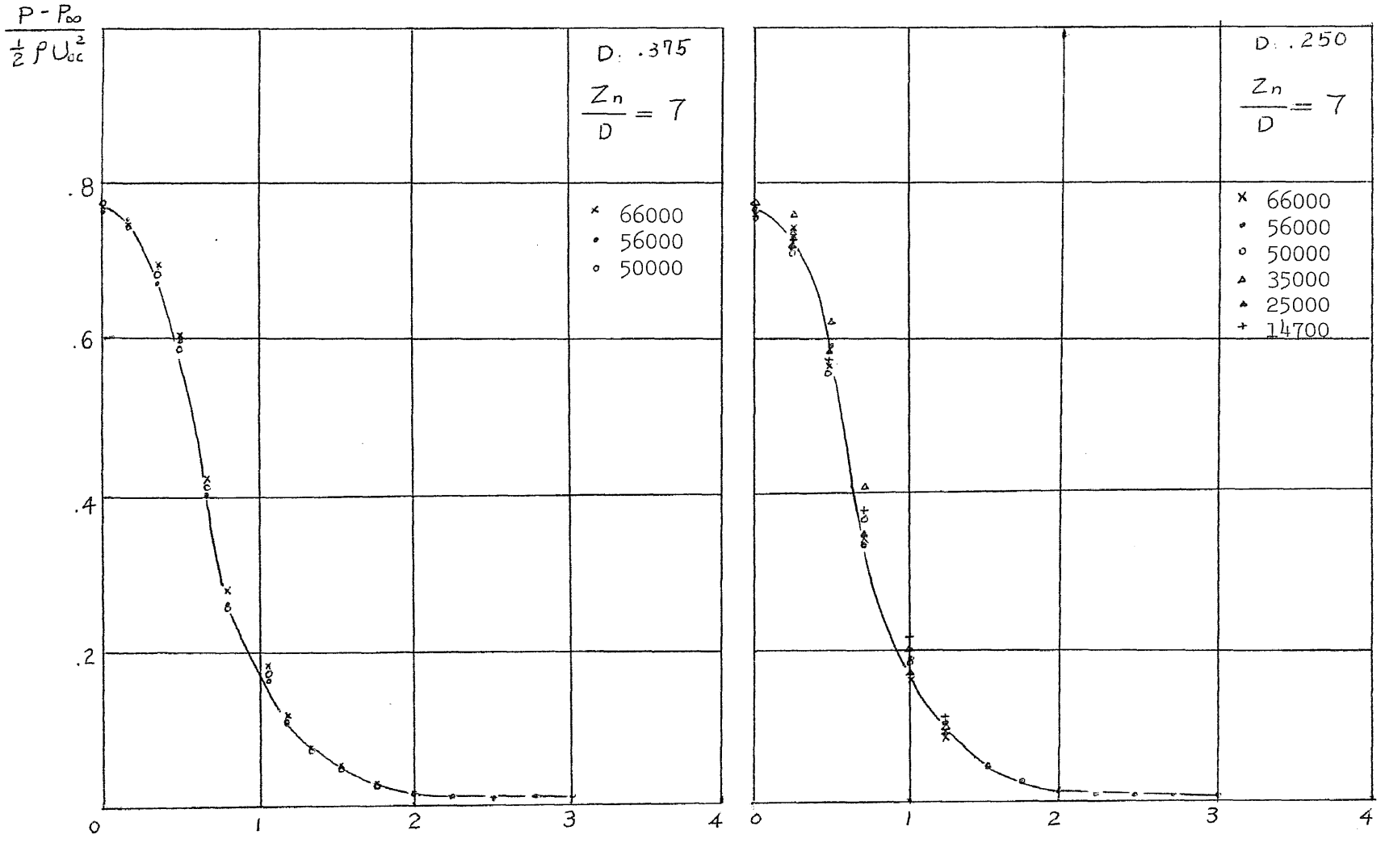

Pressure Distribution along the Flat Plate with $Z_n/D = 7$ and Varied Re_D

Fig. 4.18 & 4.19

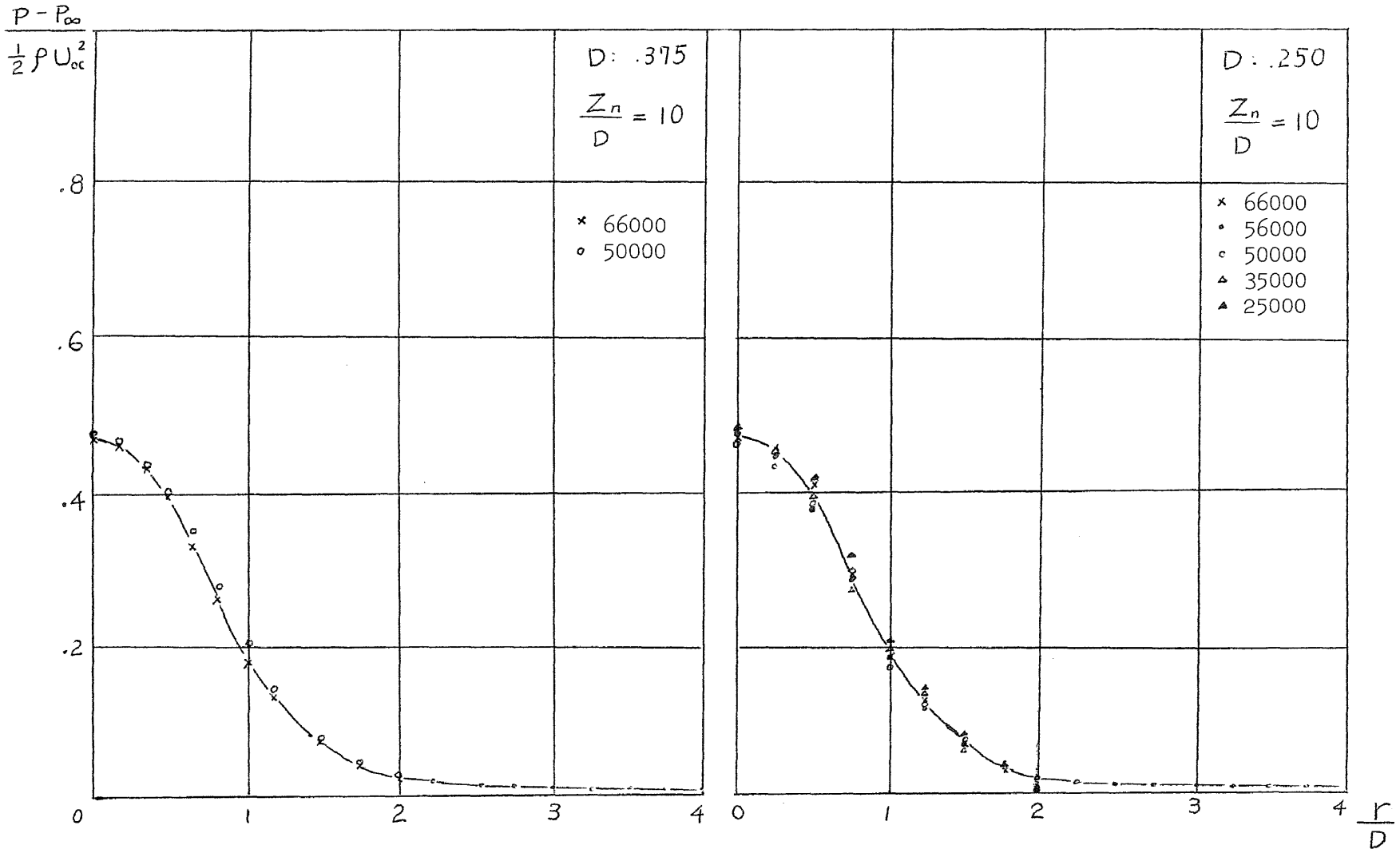

Pressure Distribution along the Flat Plate with Z_n / D = 10 and Varied Re_D

Fig. 4.20 & 4.21

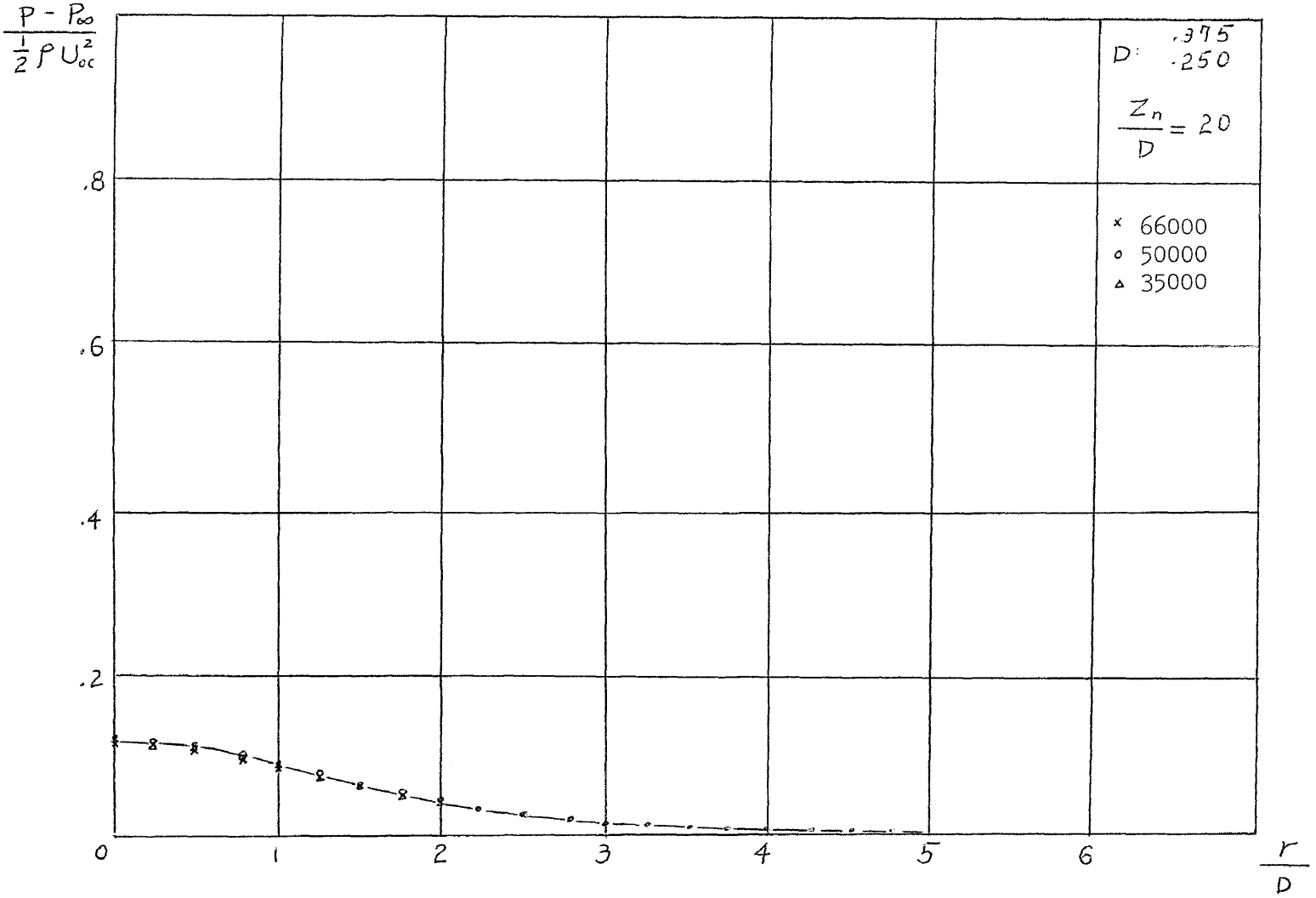

Pressure Distribution along the Flat Plate with $Z_n/D = 20$ and Varied Re_D

Fig. 4.22

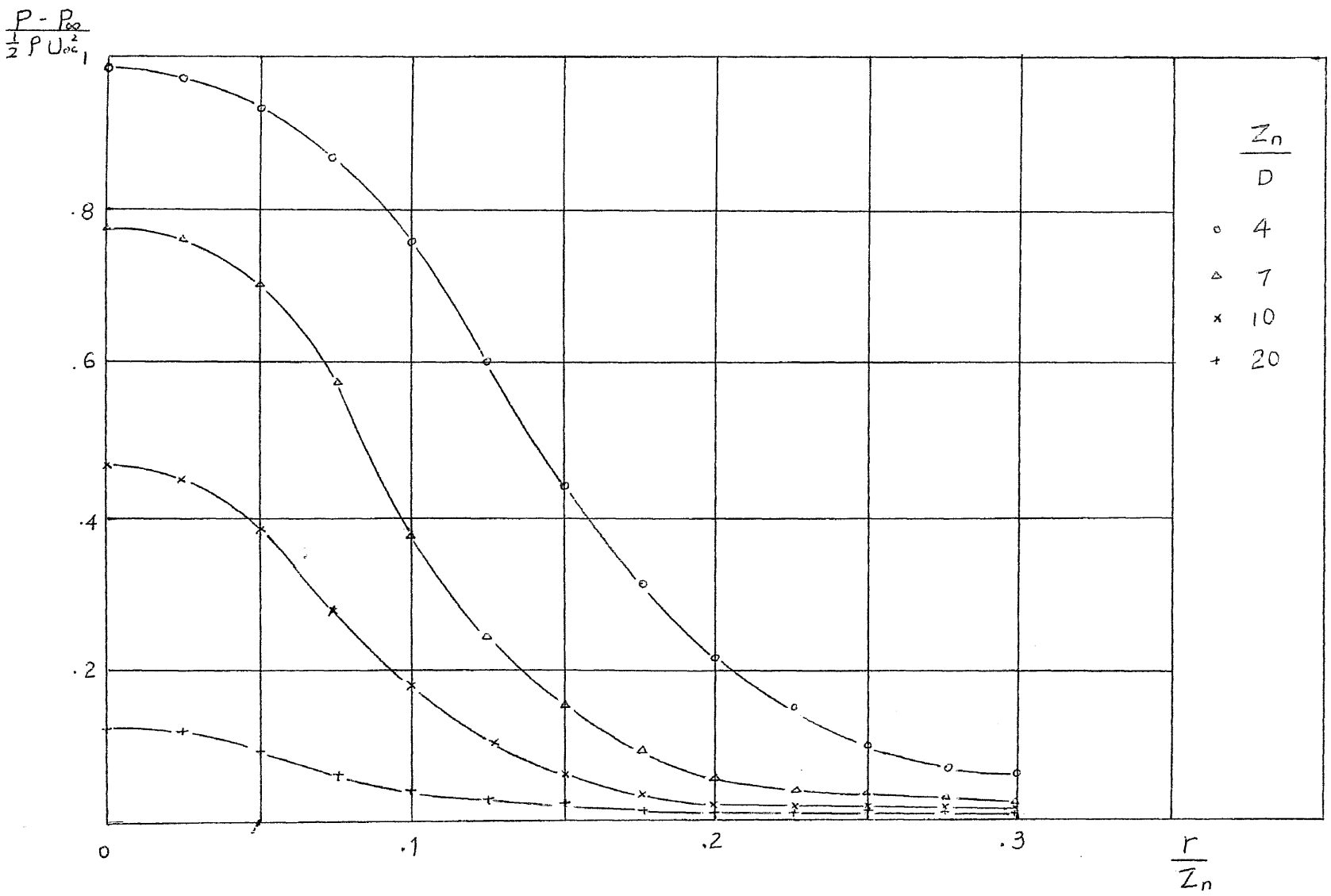

Pressure Distribution along the Flat Plate with Varied Z_n/D

Fig. 4.23

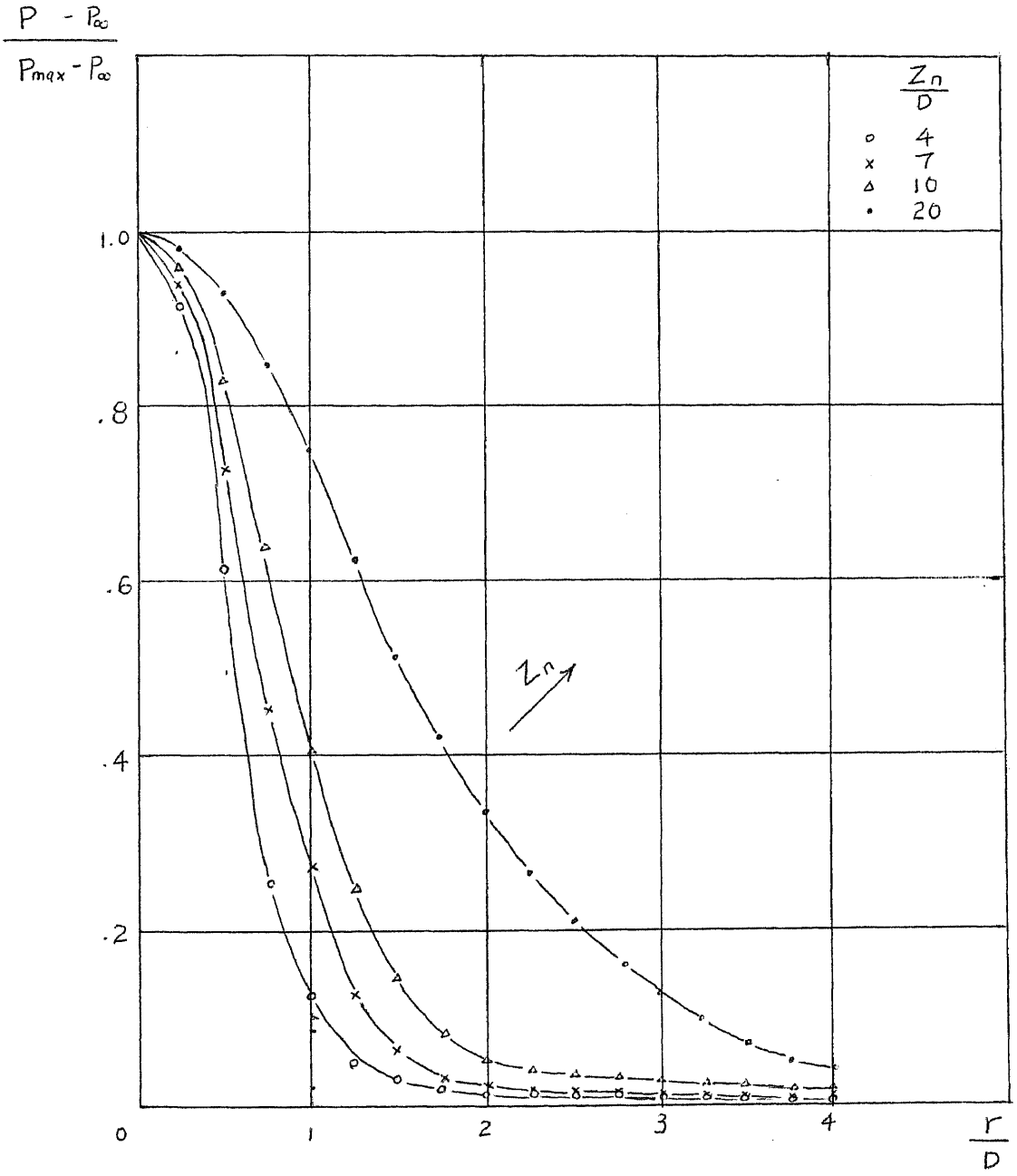

Comparison of Pressure Distribution along the Flat Plate with Varied Z_n/D

Fig. 4.24

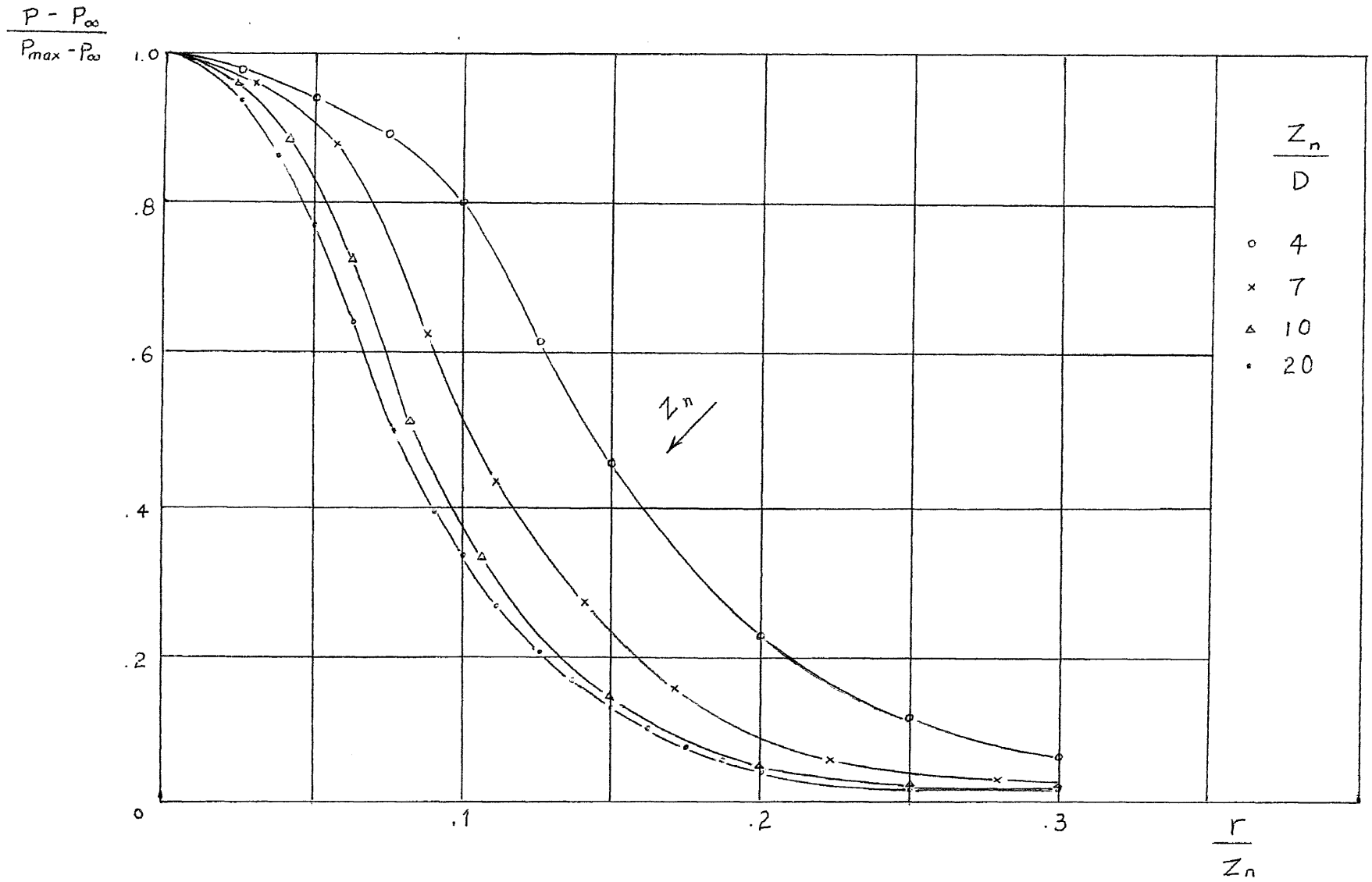

Comparison of Pressure Distribution with Varied Z_n/D

Fig. 4.25

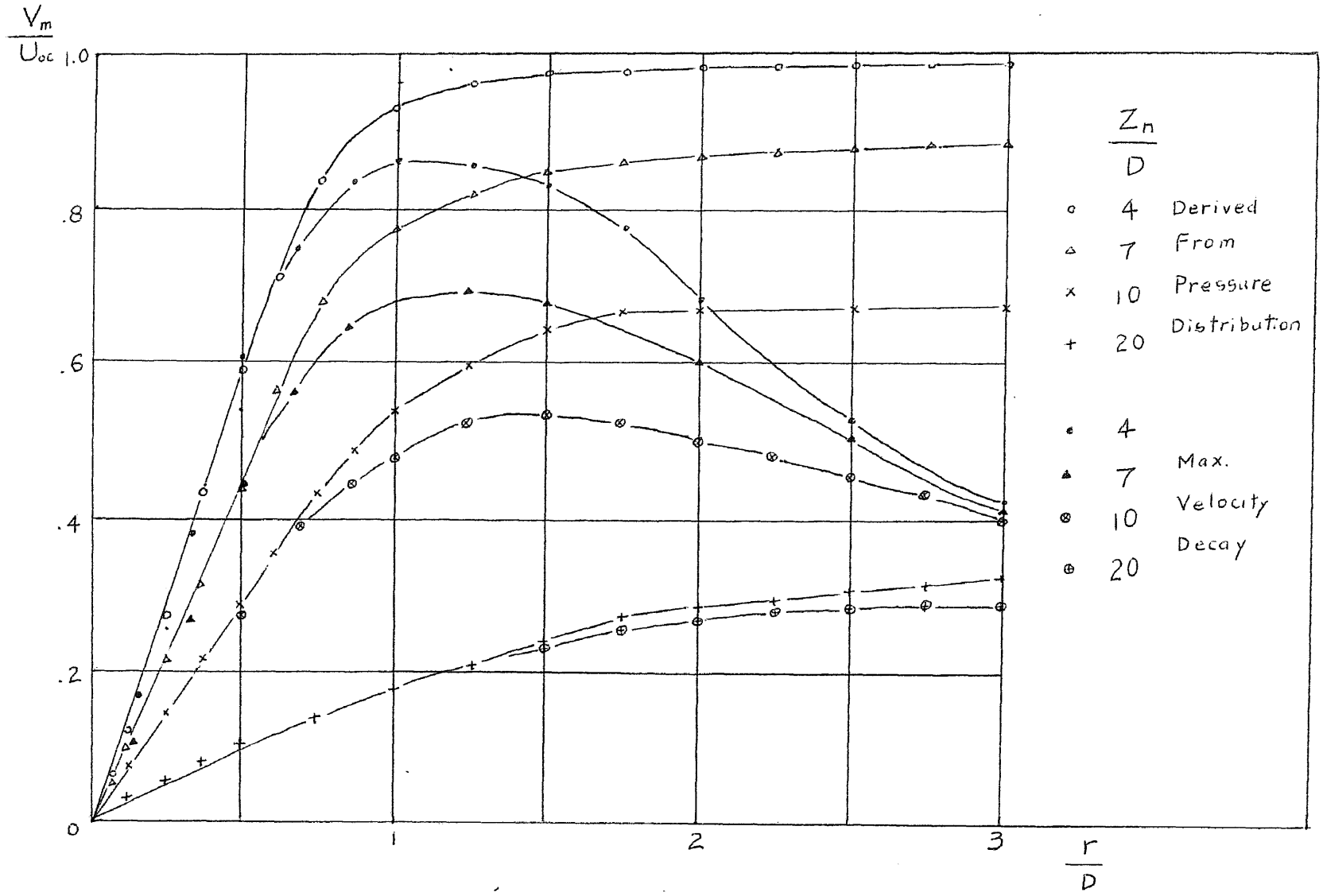

Maximum Velocity Decay along the Flat Plate with Varied Z_n/D

Fig. 4.26.

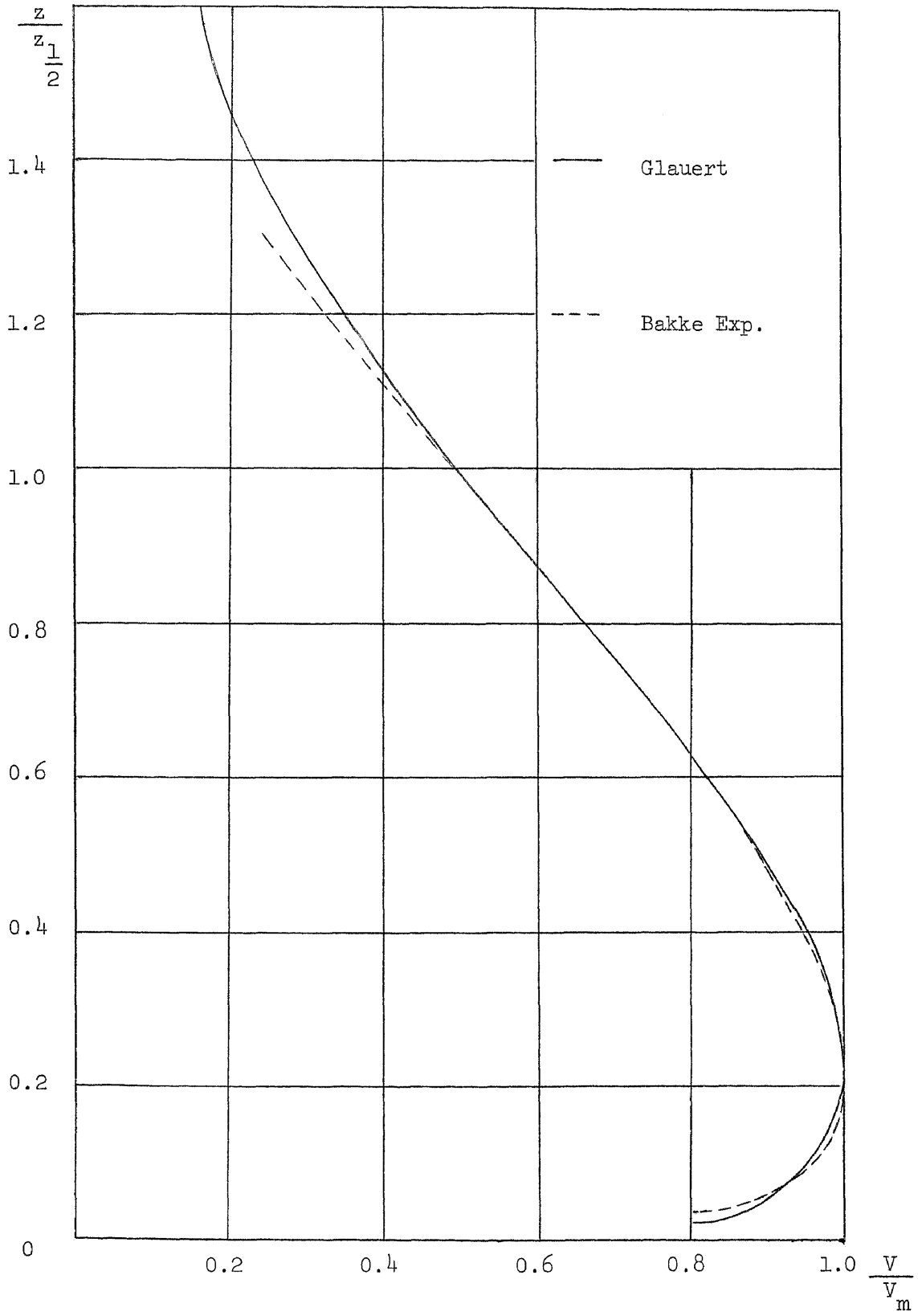

Velocity Profile of Wall Jet by Glauert and Bakke

Fig. 4.27

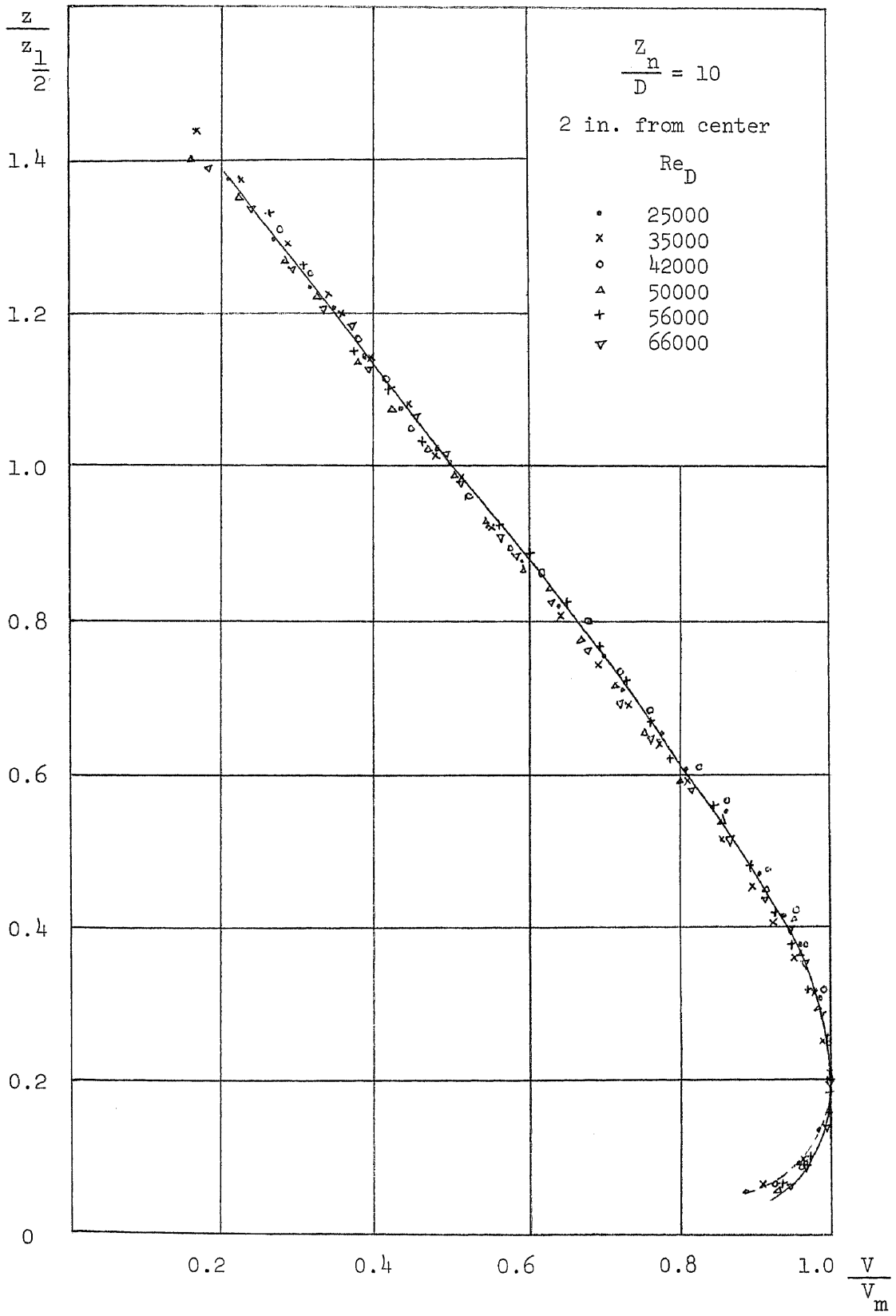

Velocity Profile of Wall Jet

Fig. 4.28

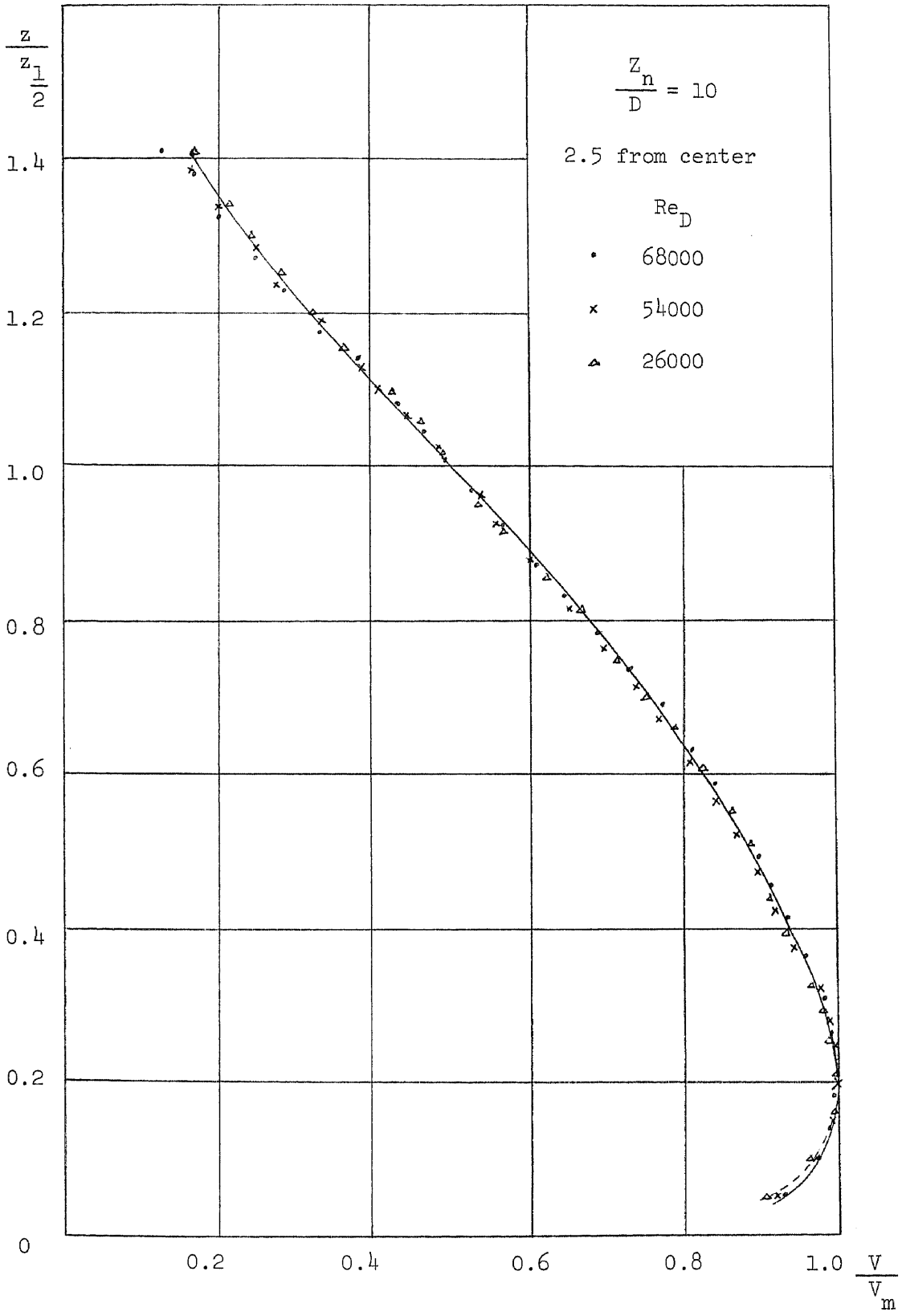

Velocity Profile of Wall Jet

Fig. 4.29

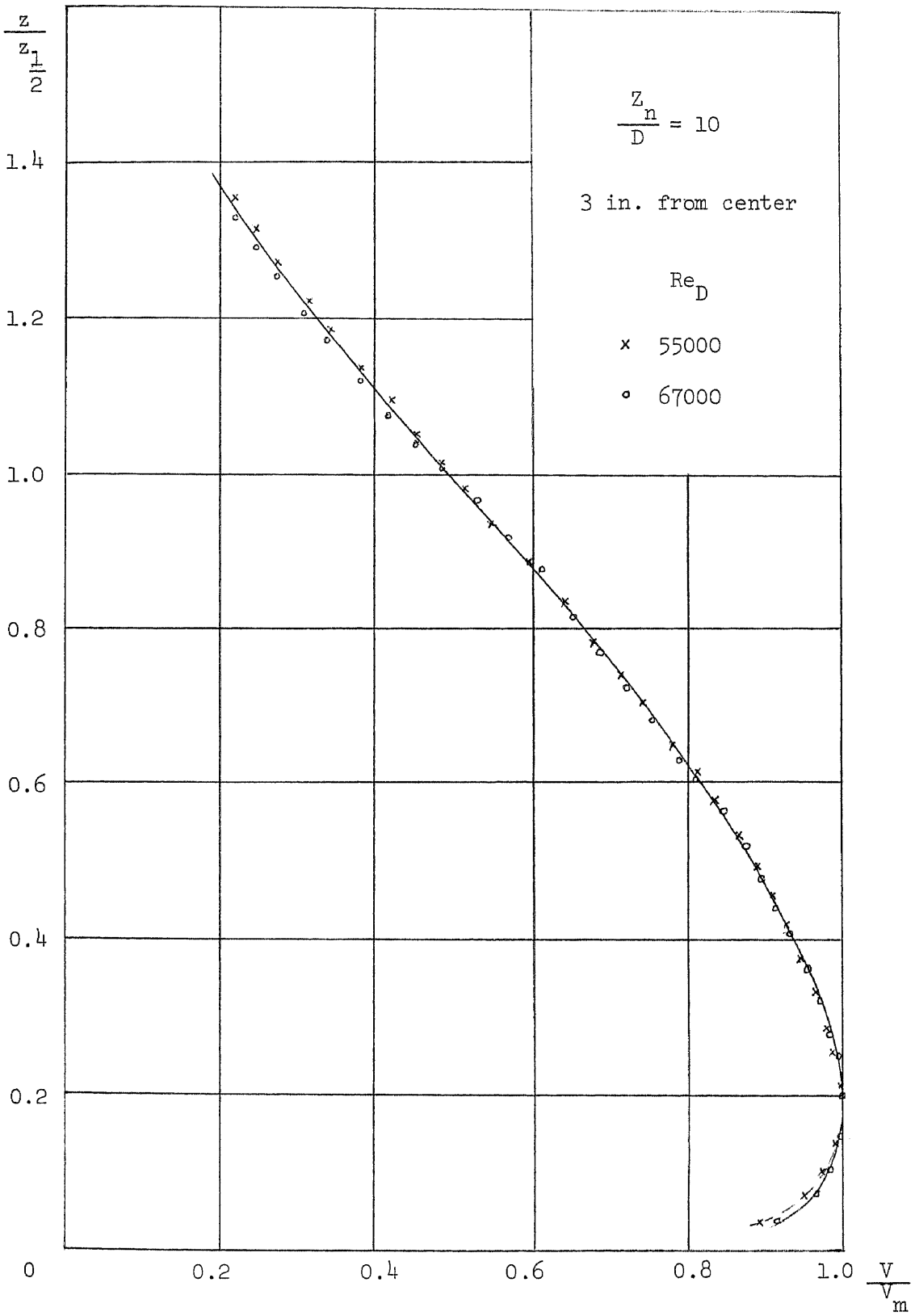

Velocity Profile of Wall Jet

Fig. 4.30

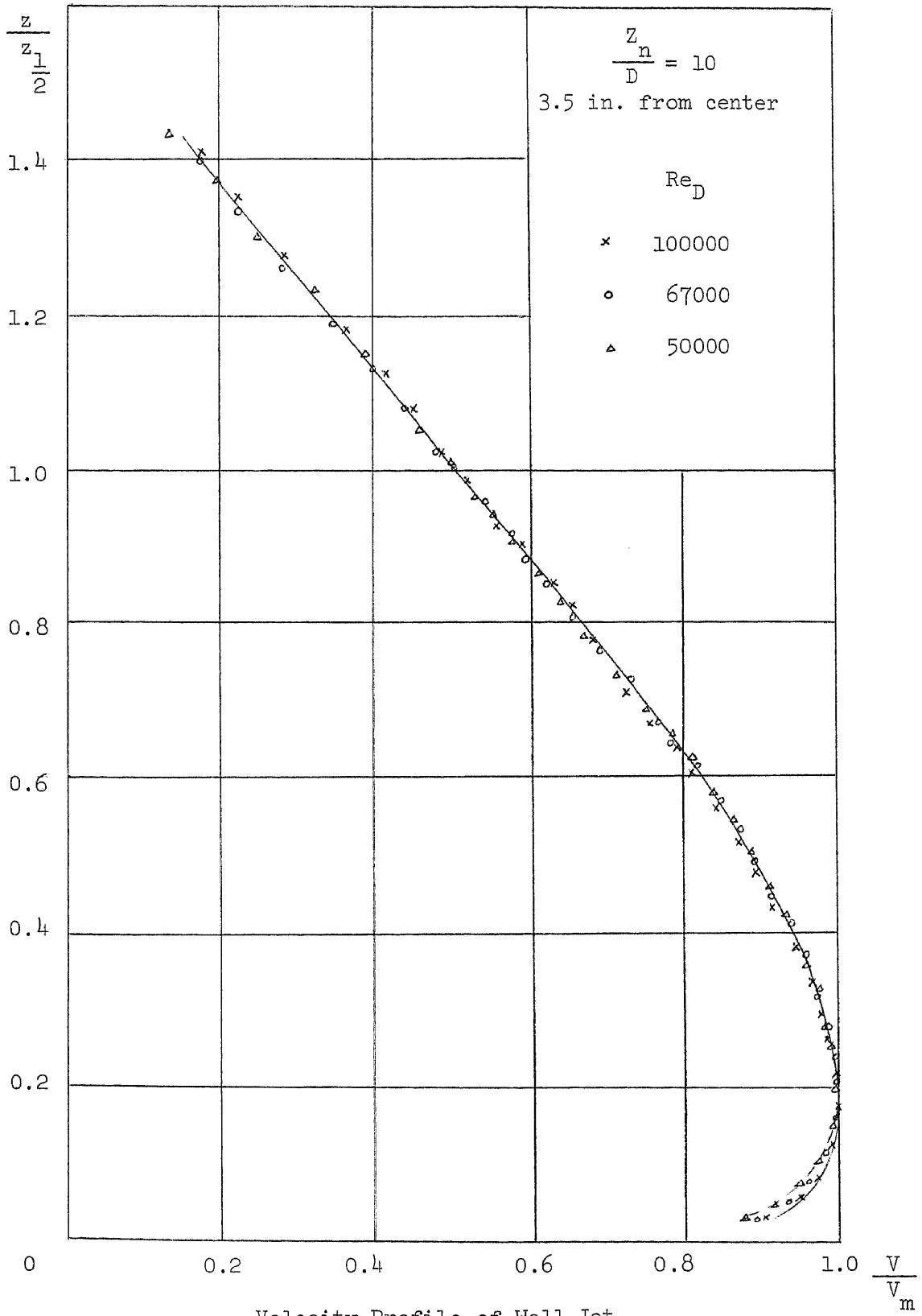

Velocity Profile of Wall Jet

Fig. 4.31

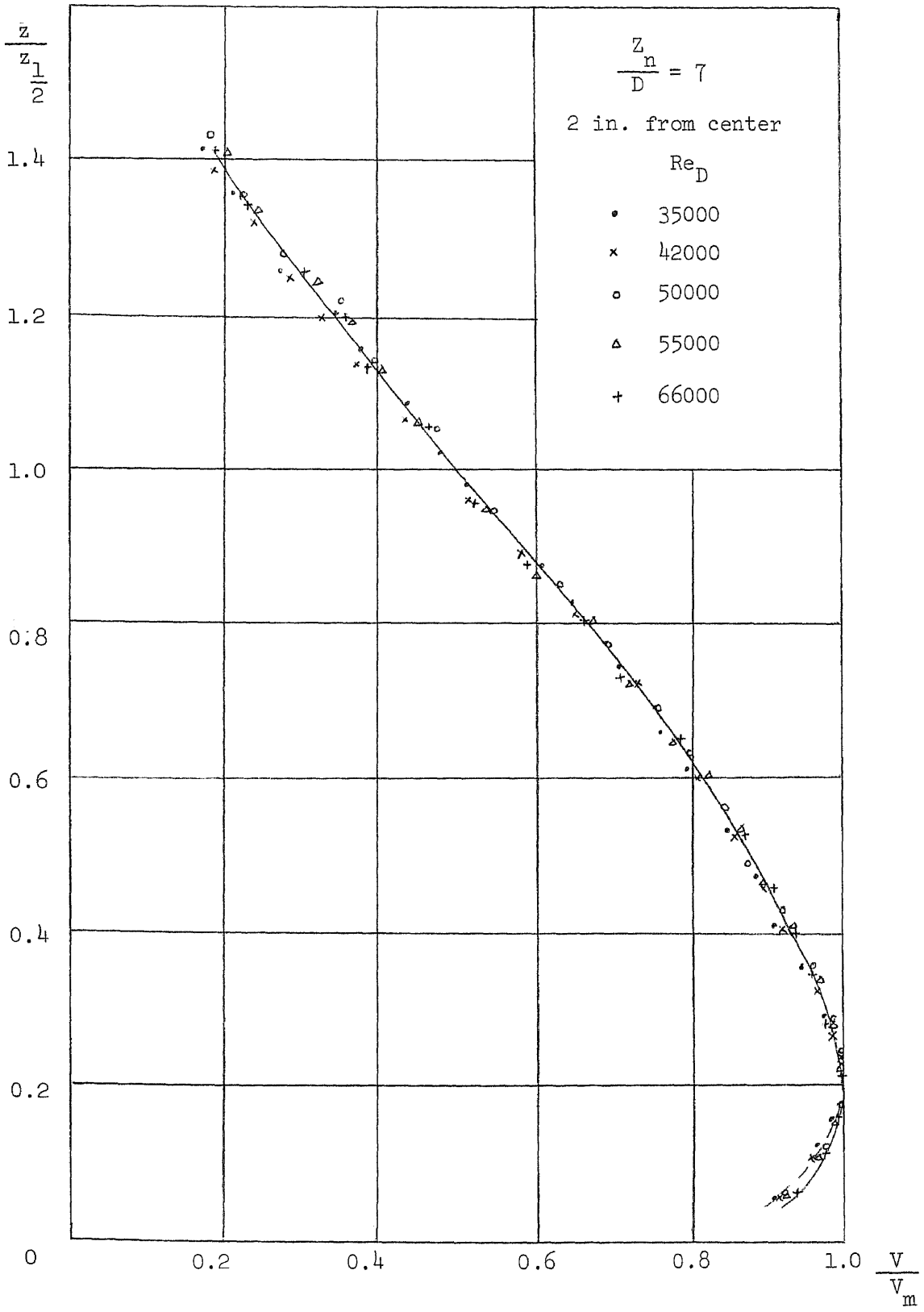

Velocity Profile of Wall Jet

Fig. 4.32

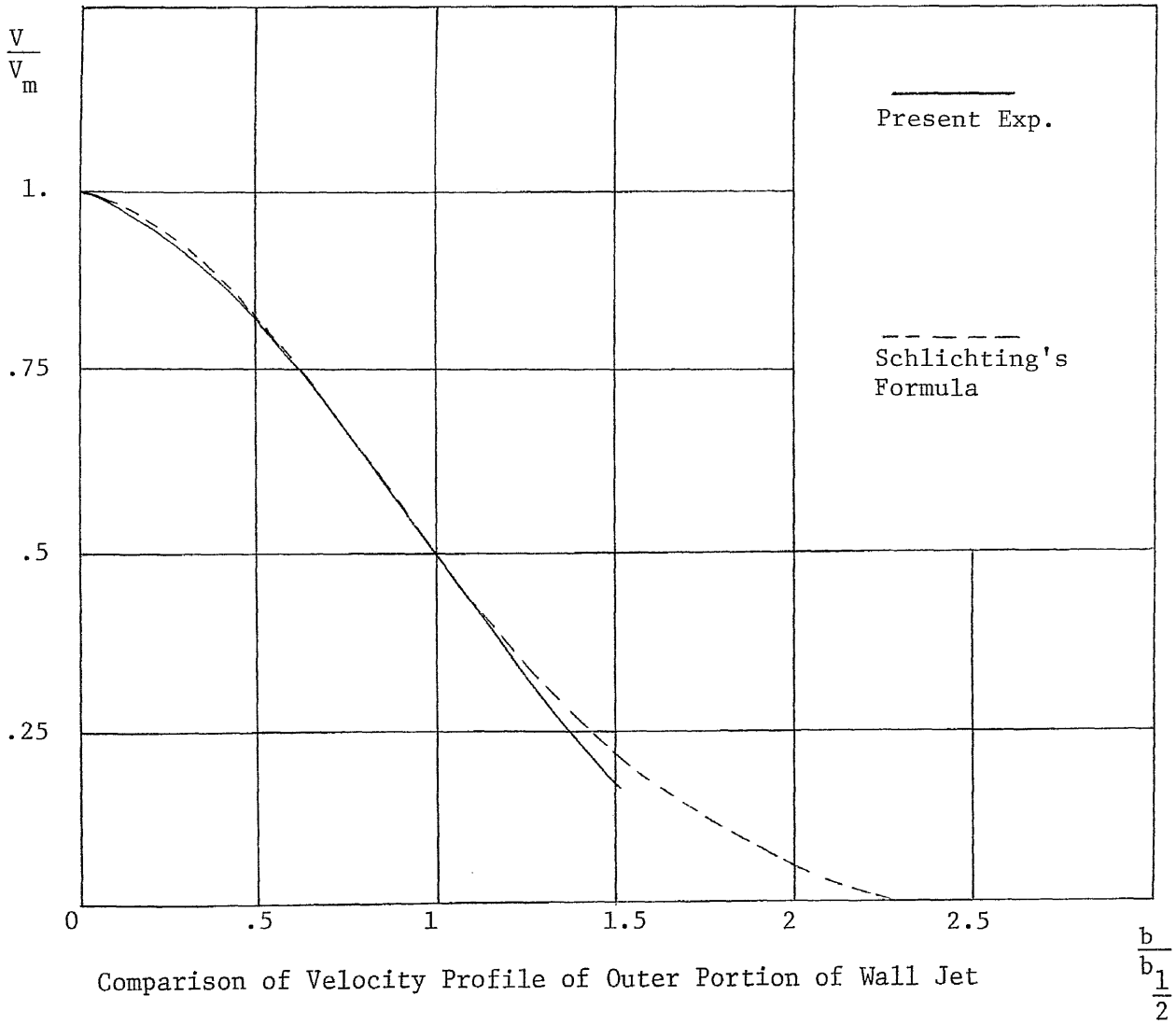

Comparison of Velocity Profile of Outer Portion of Wall Jet

Fig. 4.33

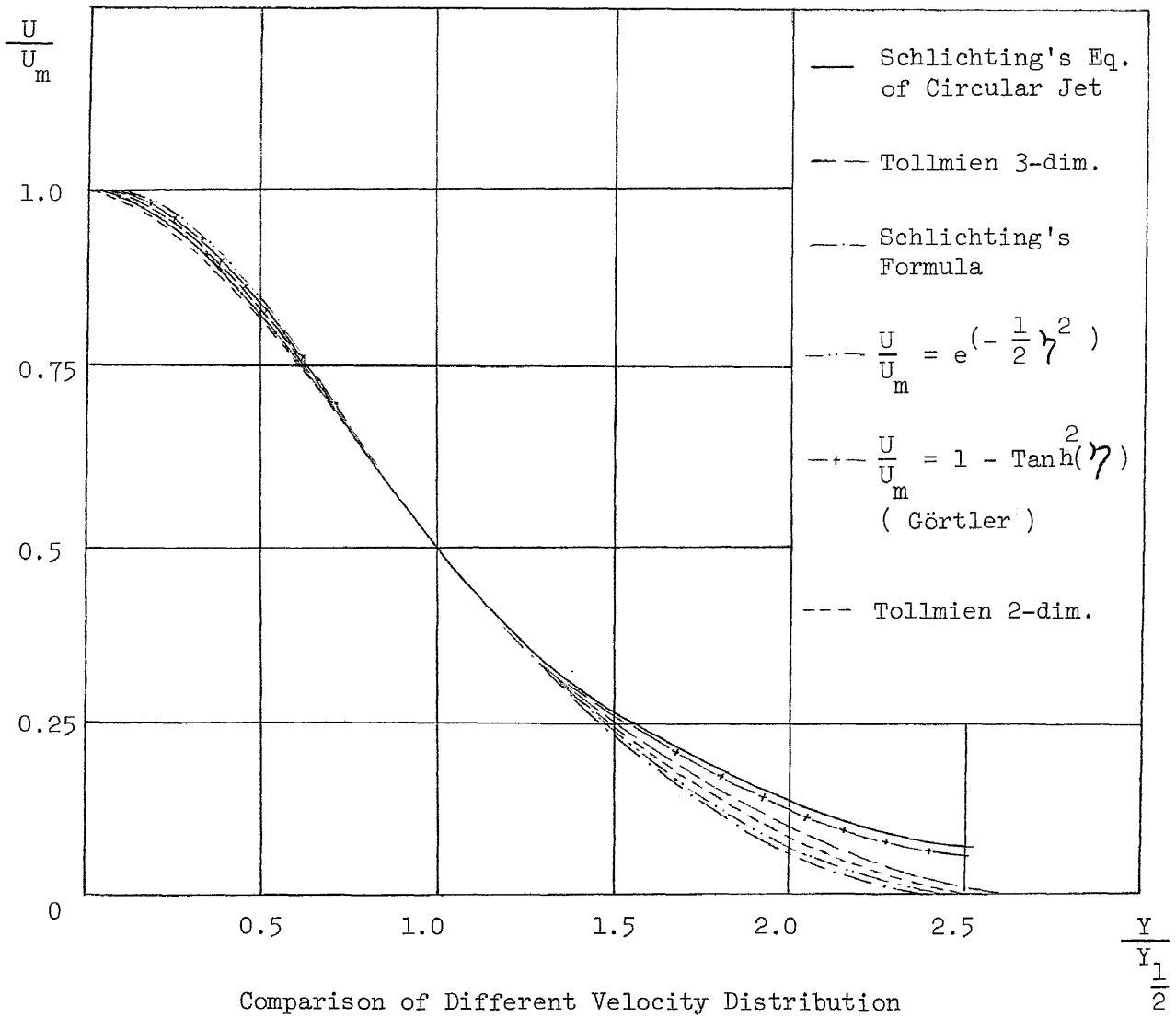

Comparison of Different Velocity Distribution

Fig. 4.34

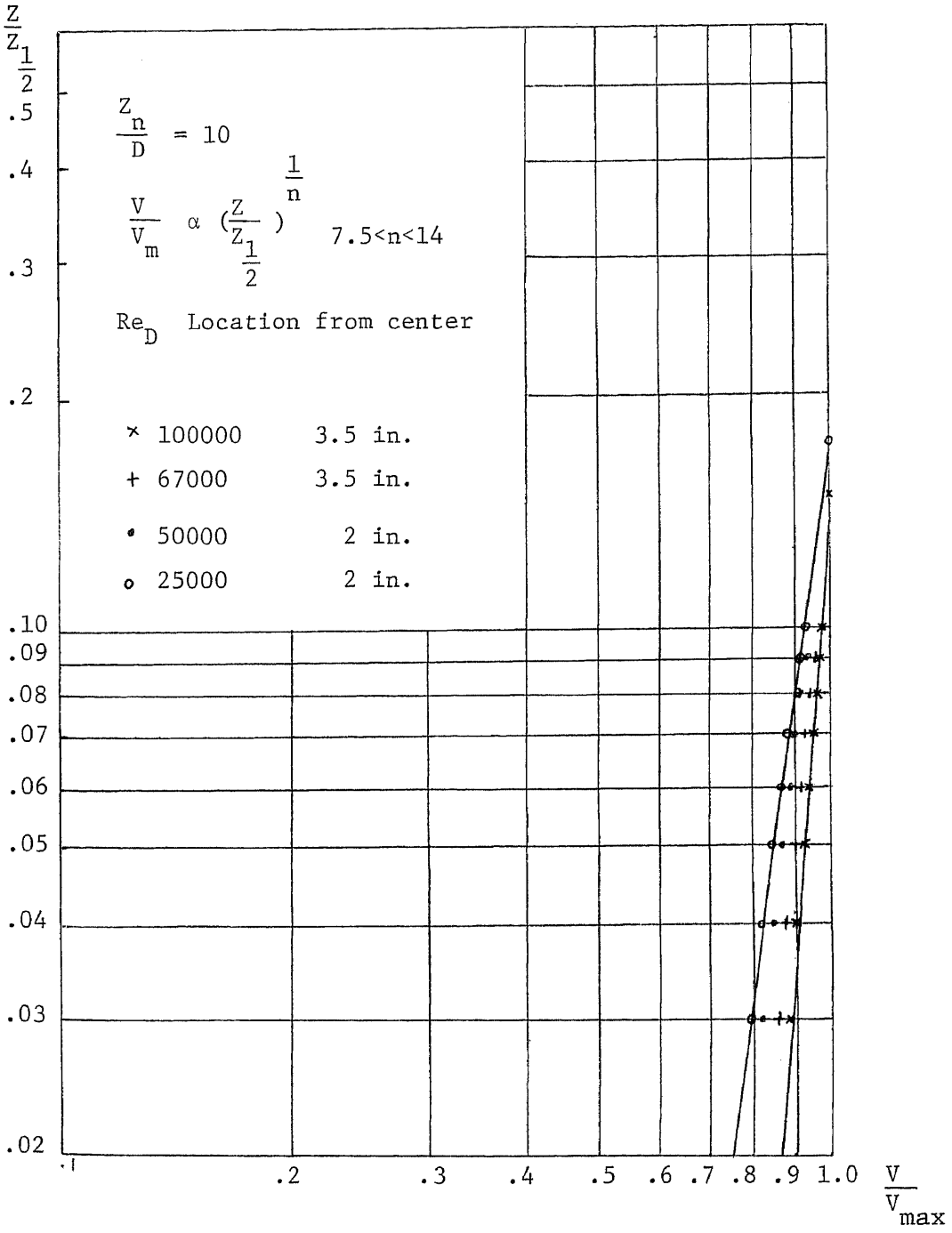

Dimensionless Velocity Distribution along the Flat Plate with Varied Re_D

Fig. 4.35

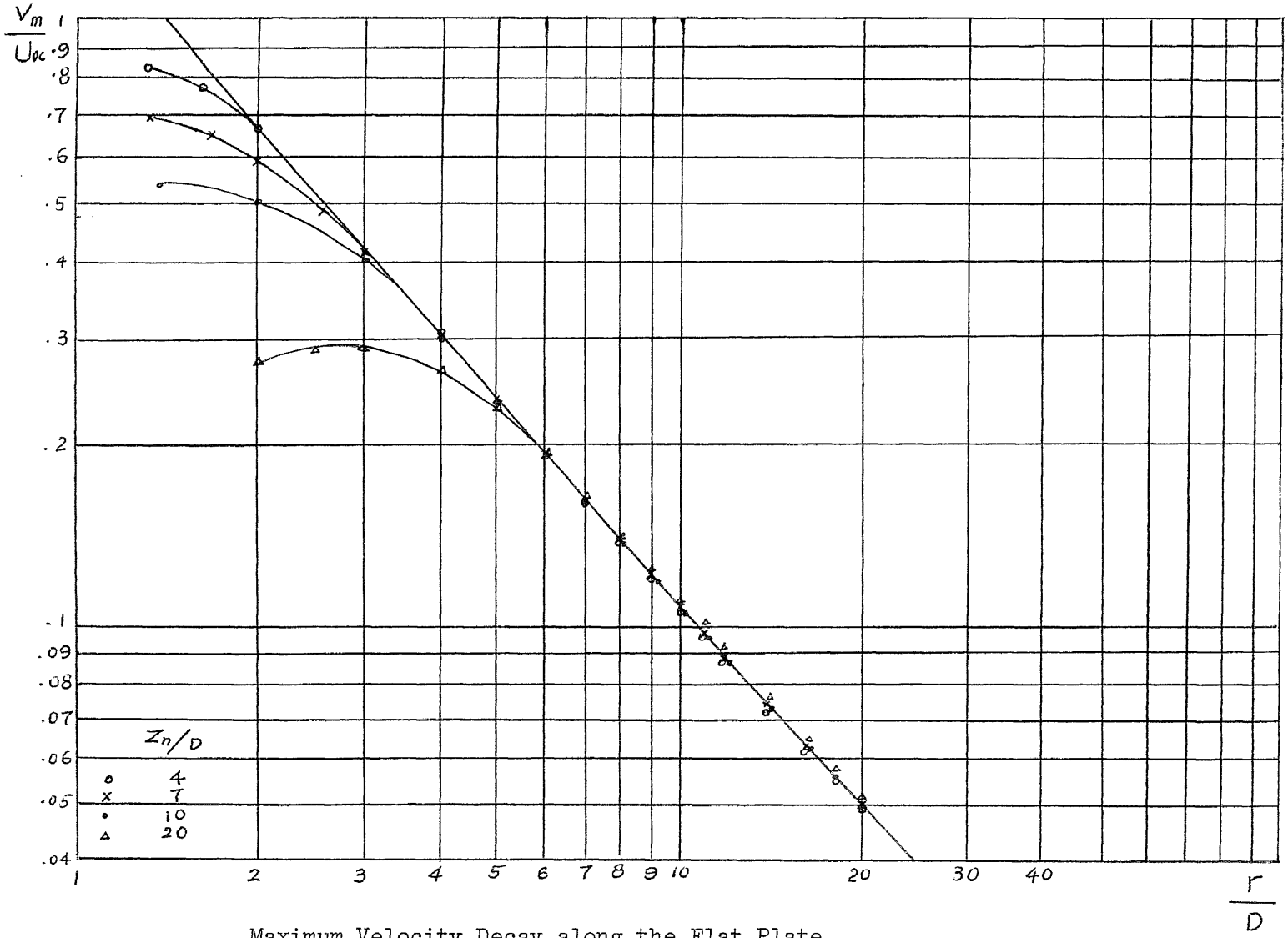

Maximum Velocity Decay along the Flat Plate

Fig. 4.36

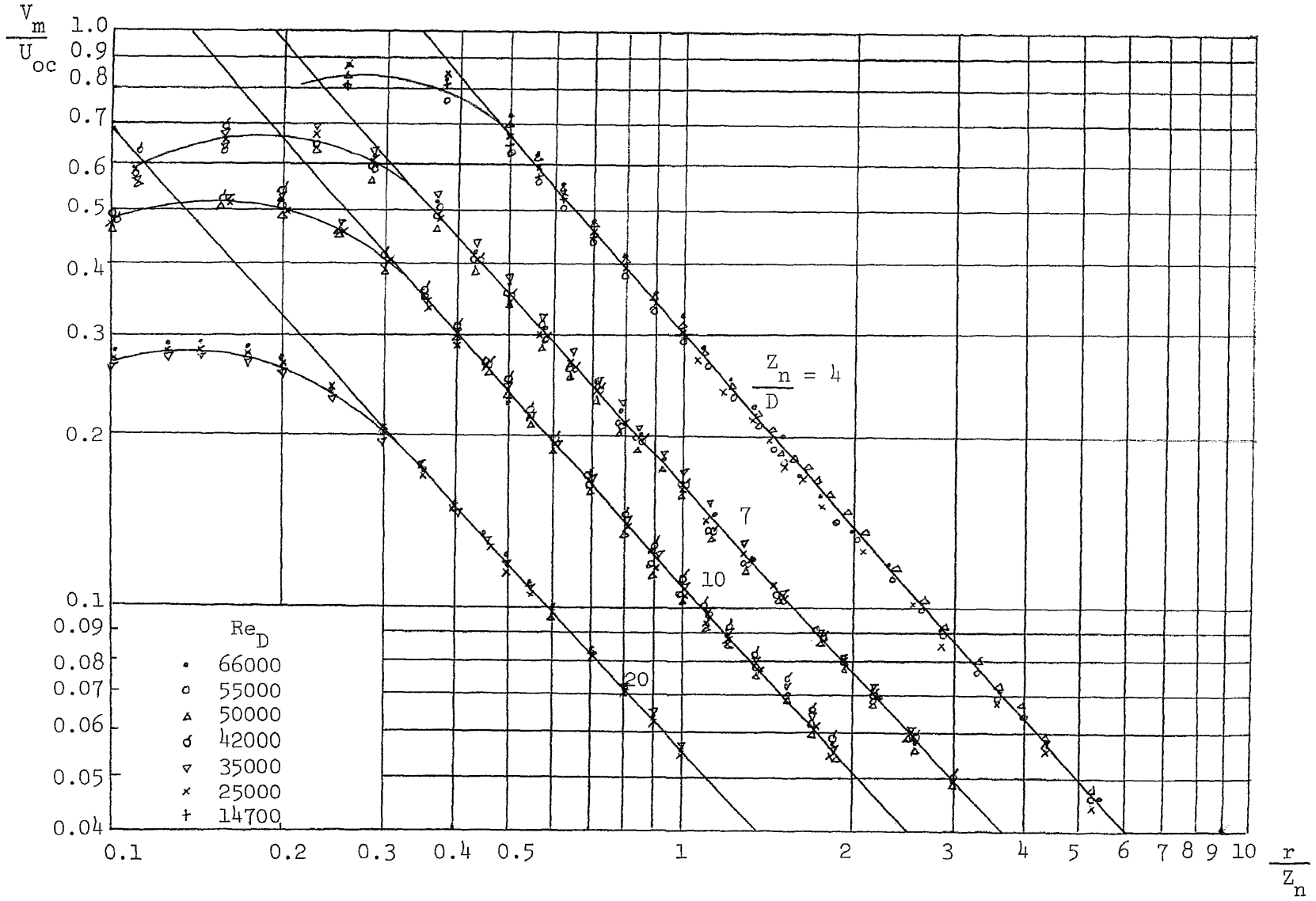

Maximum Velocity Decay along the Flat Plate with Varied Z_n / D

Fig. 4.37

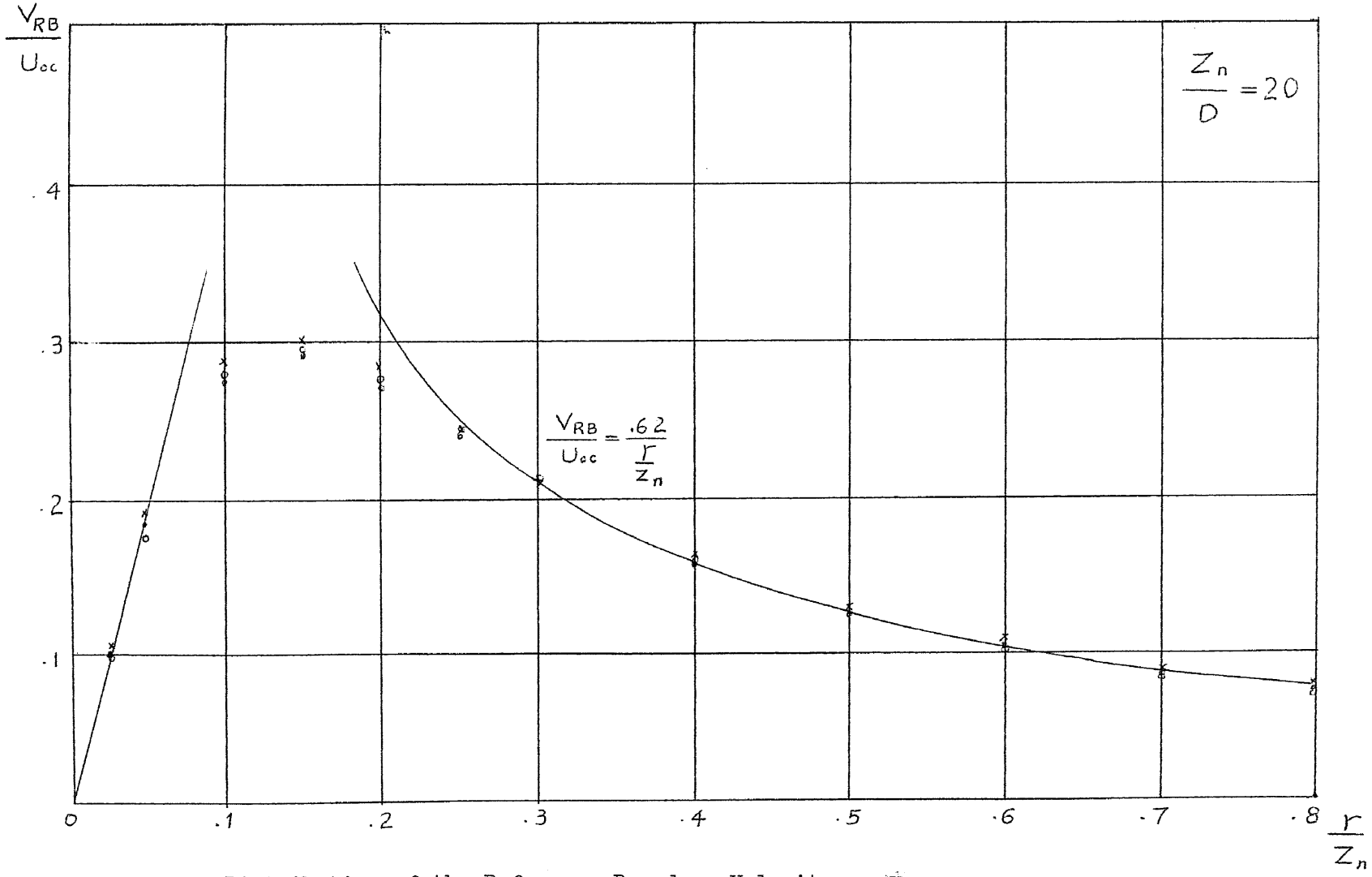

Distribution of the Reference Boundary Velocity--- V_{RB}

Fig. 4.38

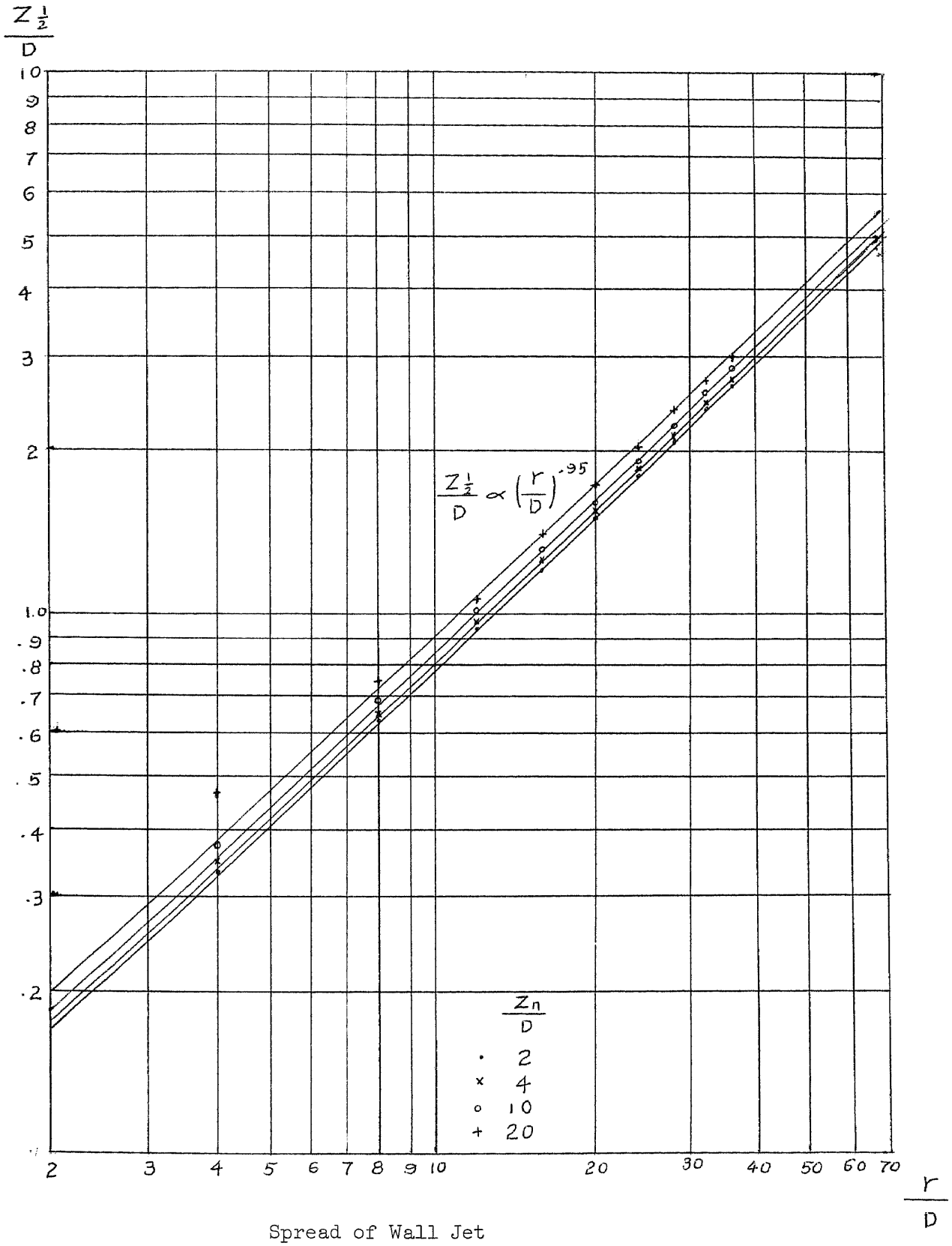

Spread of Wall Jet

Fig. 4.39

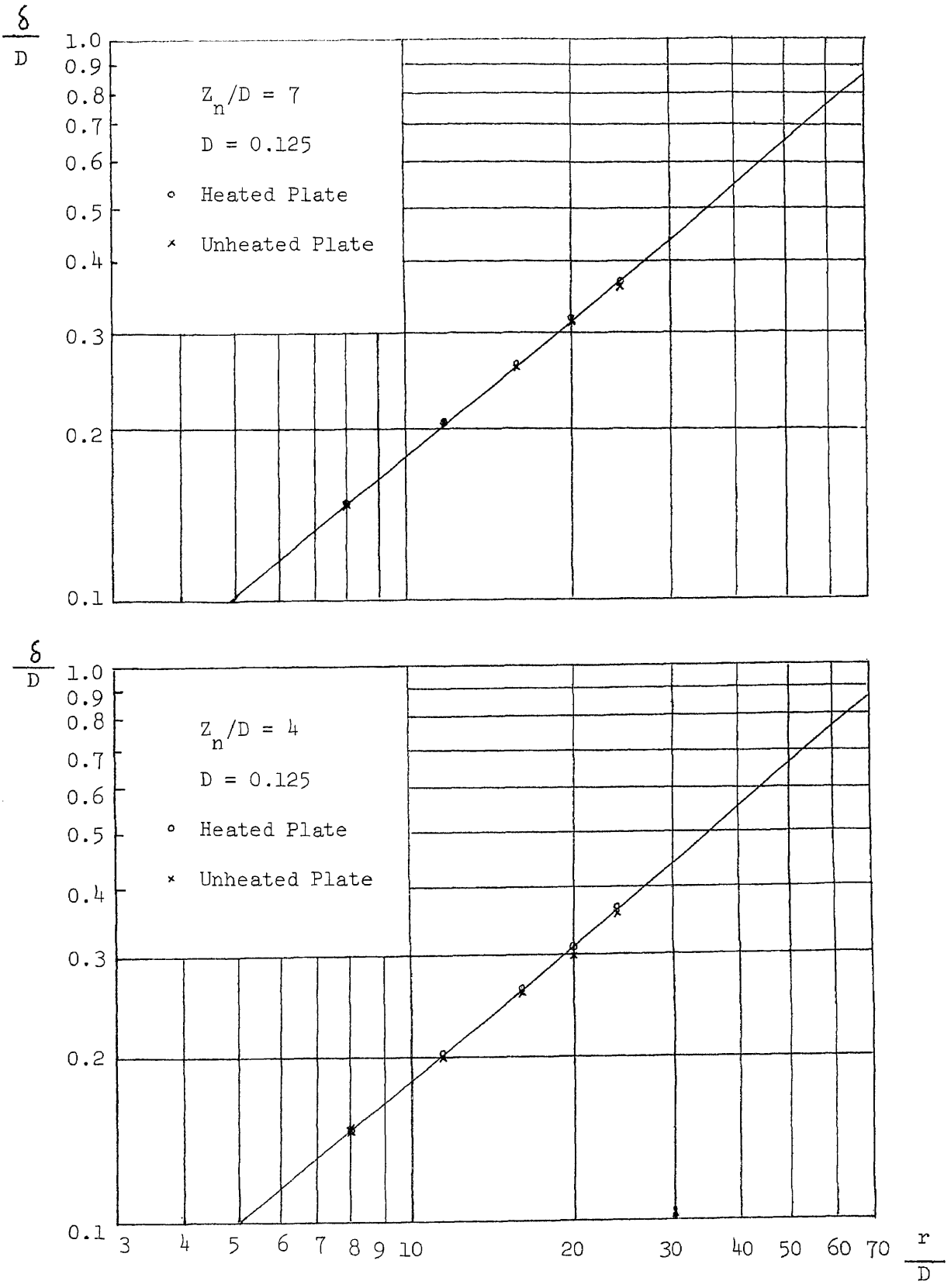

Comparison of the Boundary Layer Thickness for the Plates Heated and Not Heated

Fig. 4.40

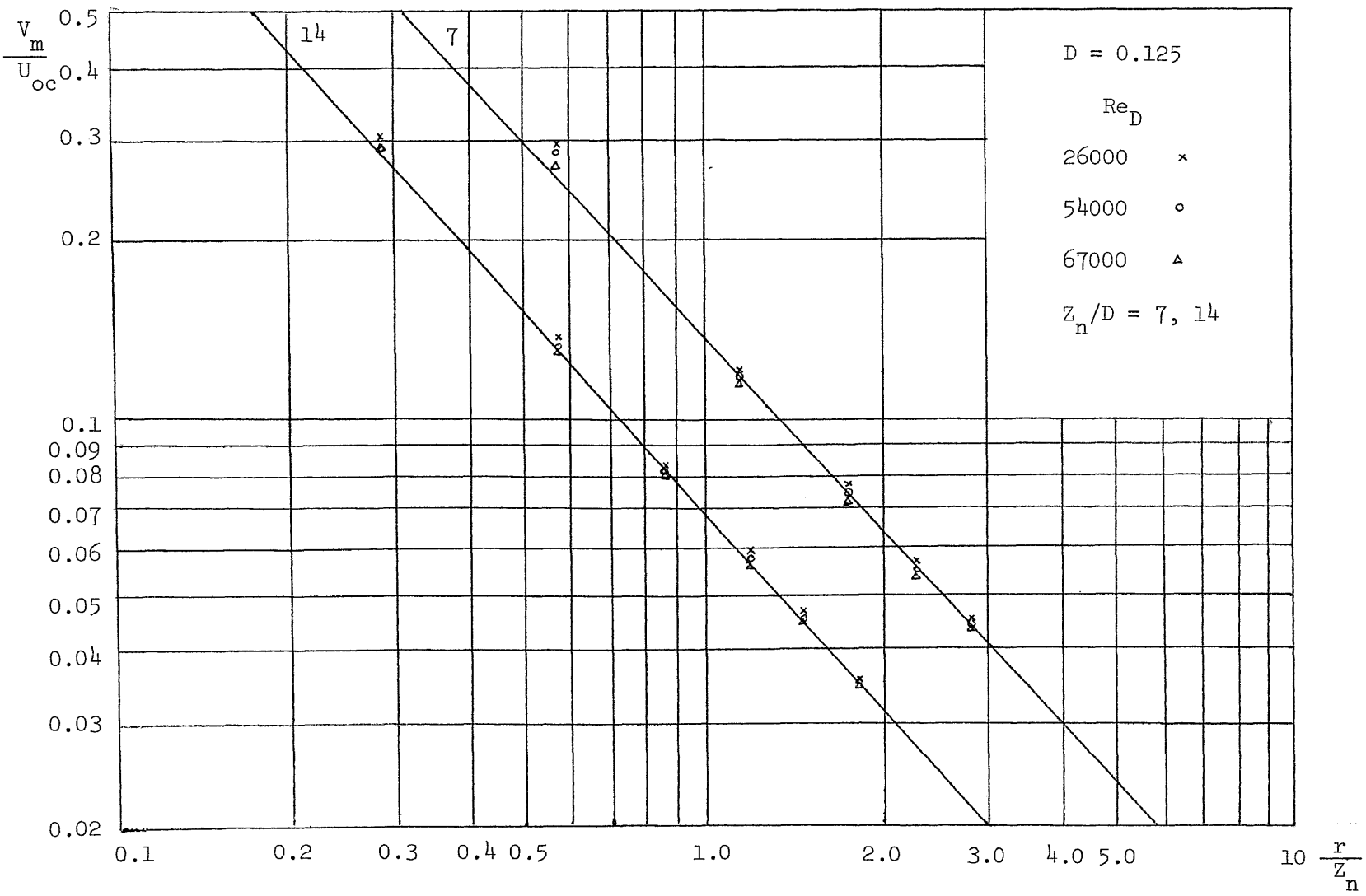

Maximum Velocity Decay of Wall Jet along the Plate Not Heated

Fig. 4.41

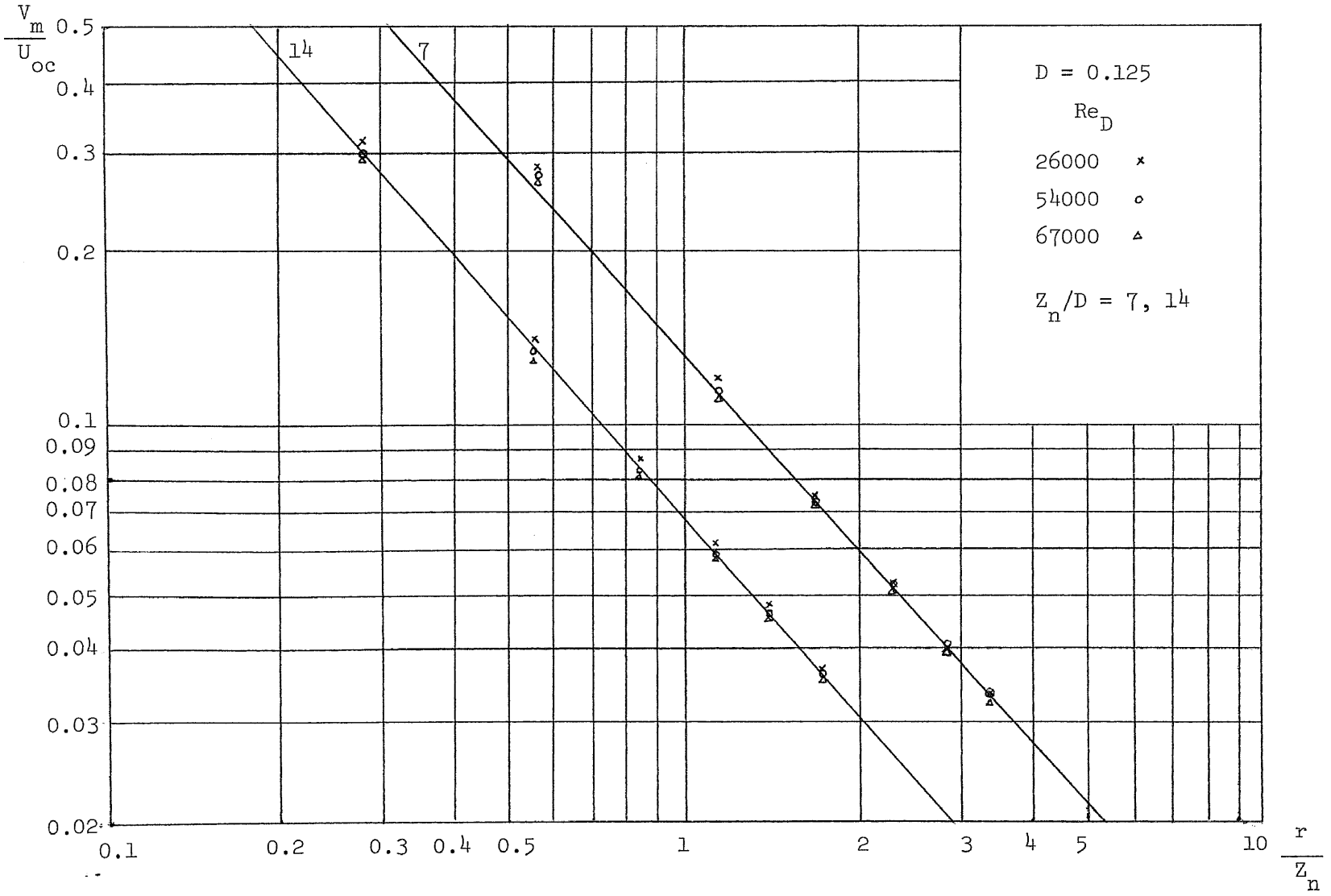

Maximum Velocity Decay of Wall Jet along the Heated Plate

Fig. 4.42

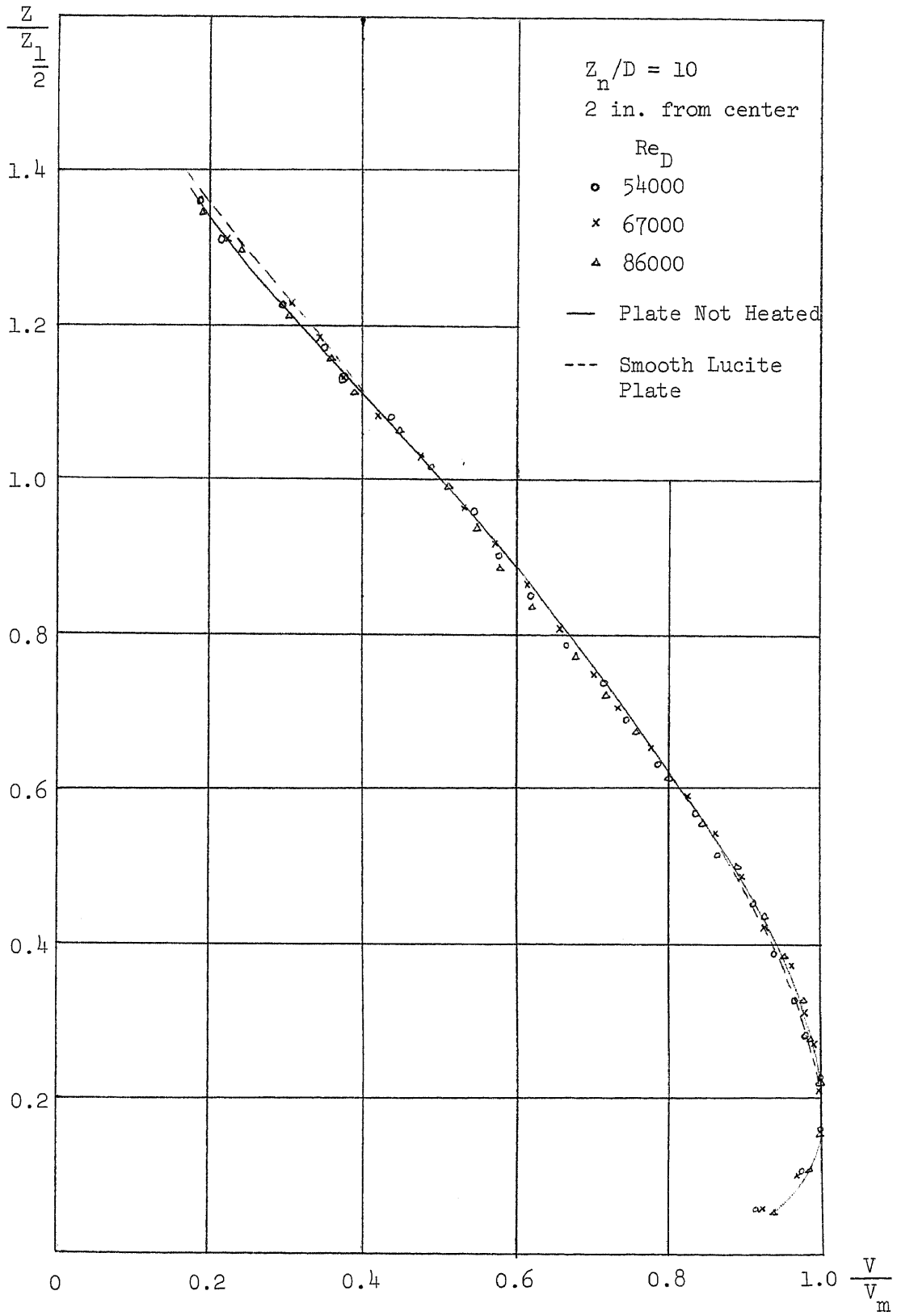

Velocity Profile of Wall Jet along the Plate Not Heated

Fig. 4.43

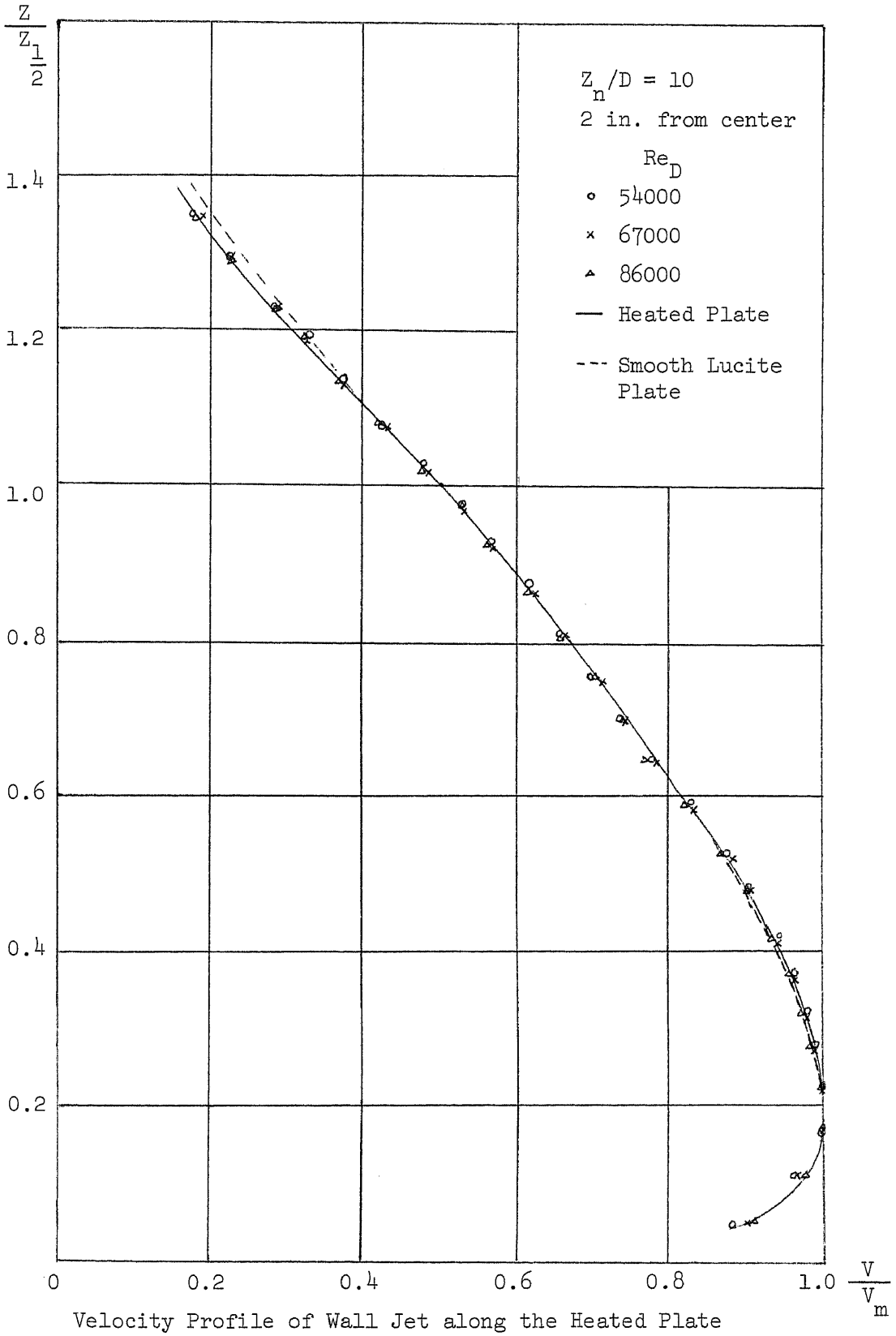

Velocity Profile of Wall Jet along the Heated Plate

Fig. 4.44

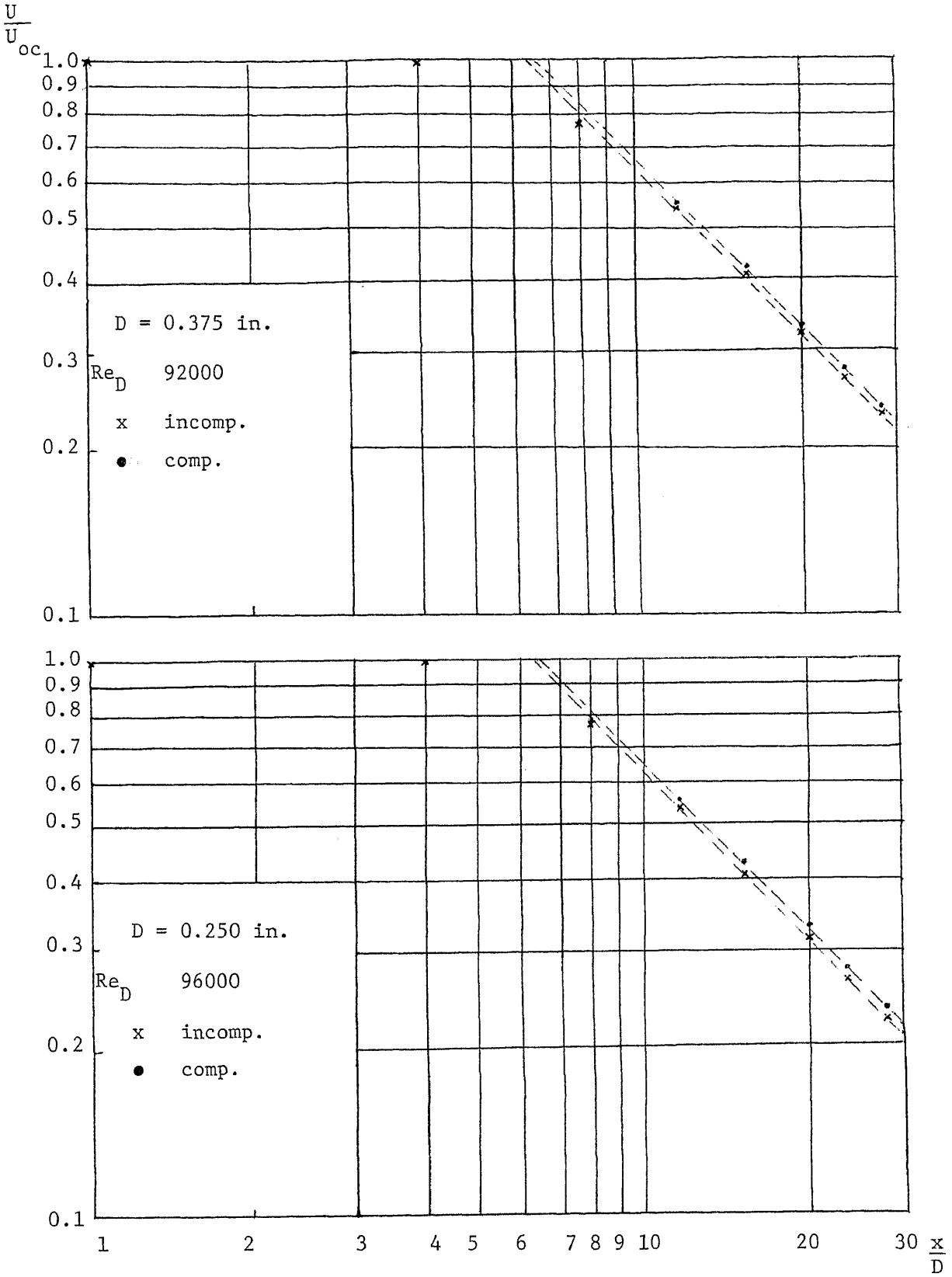

Comparison of Velocity Decays of Compressible and Incompressible Flow of Air

Fig. 4.45 & 4.46

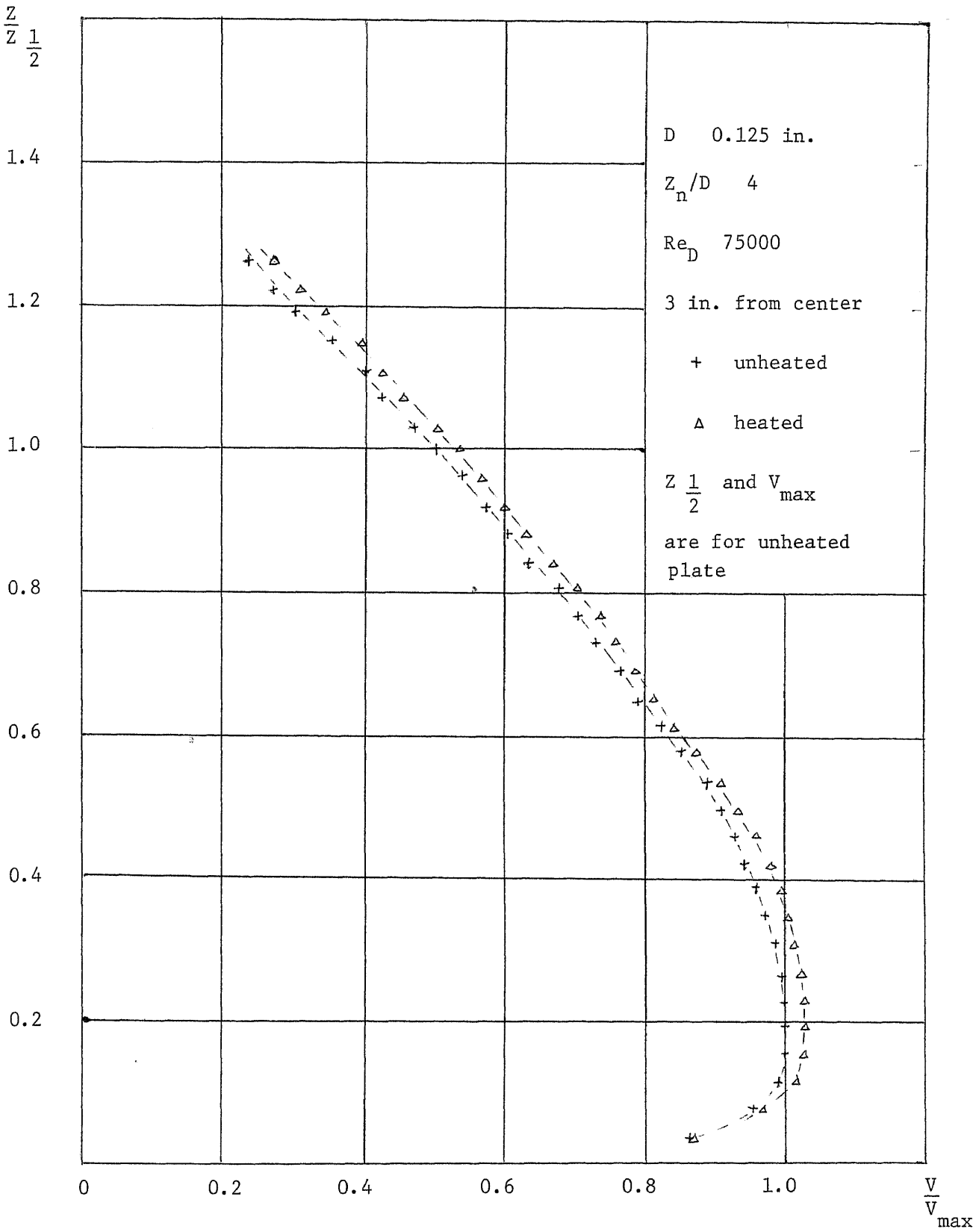
Z/Z 1/2
1.4
1.2
1.0
0.8
0.6
0.4
0.2
0
0.2
0.4
0.6
0.8
1.0
V/V max
D 0.125 in.
Z_n/D 4
Re_D 75000
3 in. from center
+ unheated
Δ heated
Z 1/2 and V_max
are for unheated
plate

Fig. 4.47

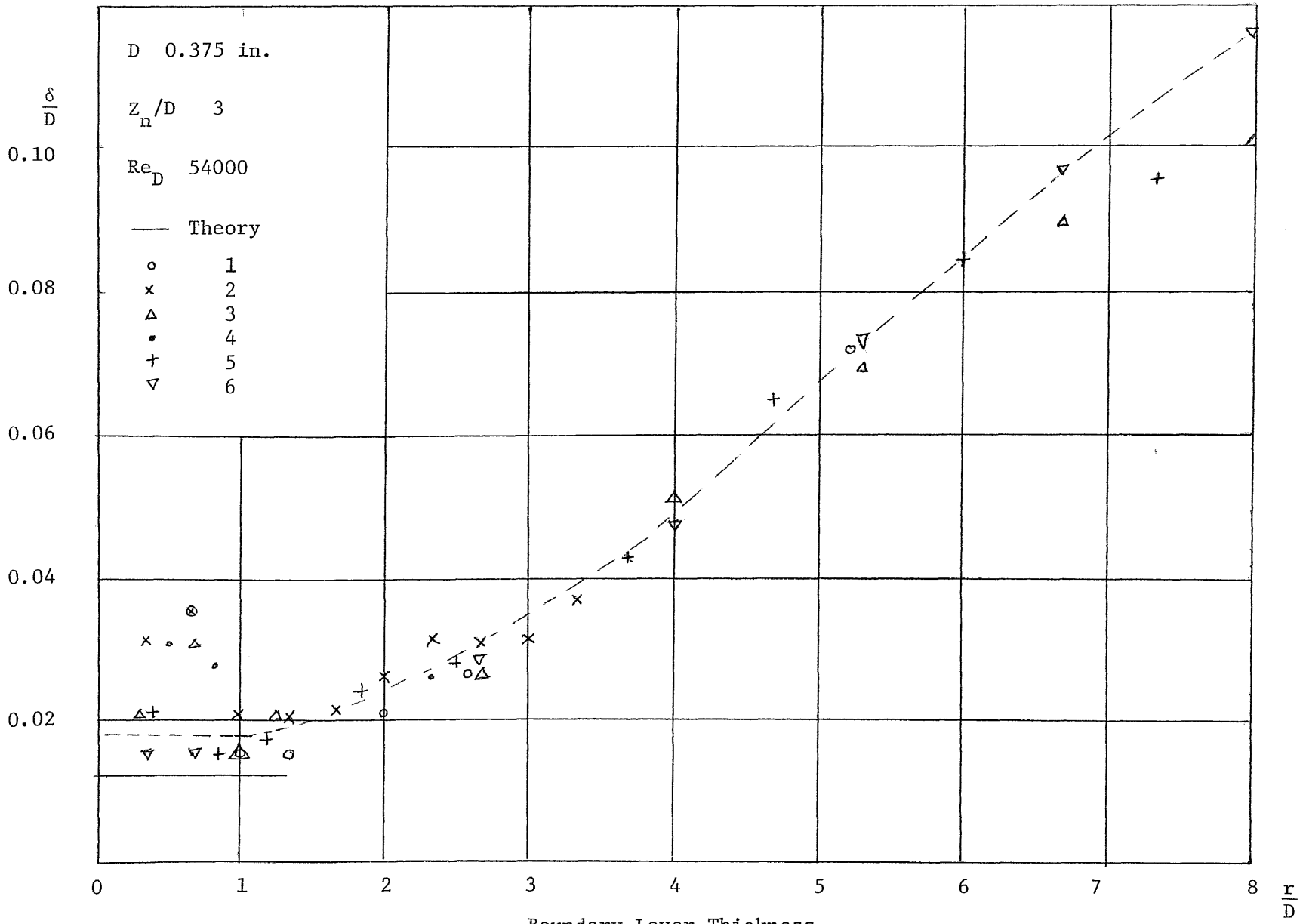

Boundary Layer Thickness

Fig. 4.48

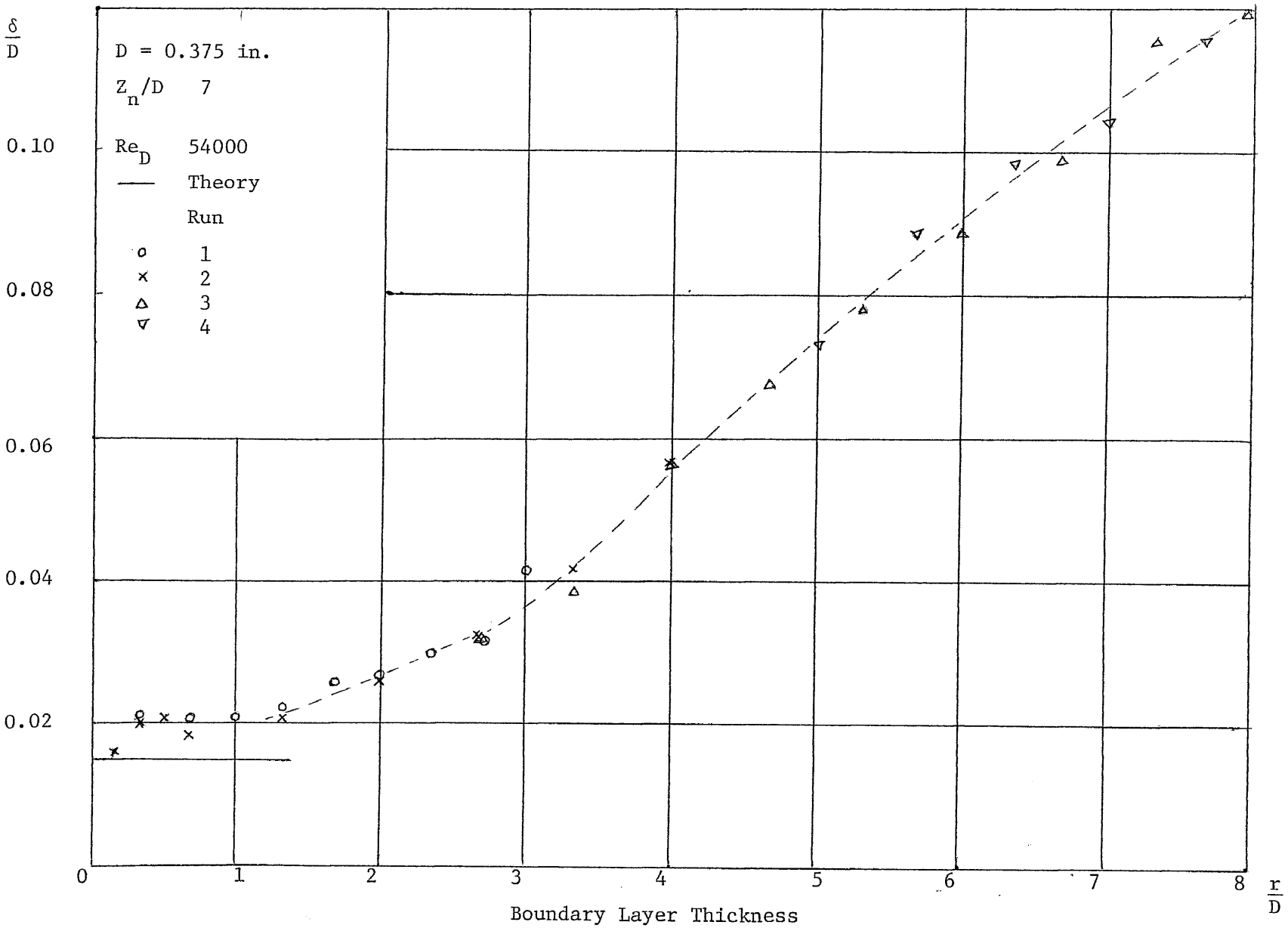

Boundary Layer Thickness

Fig. 4.49

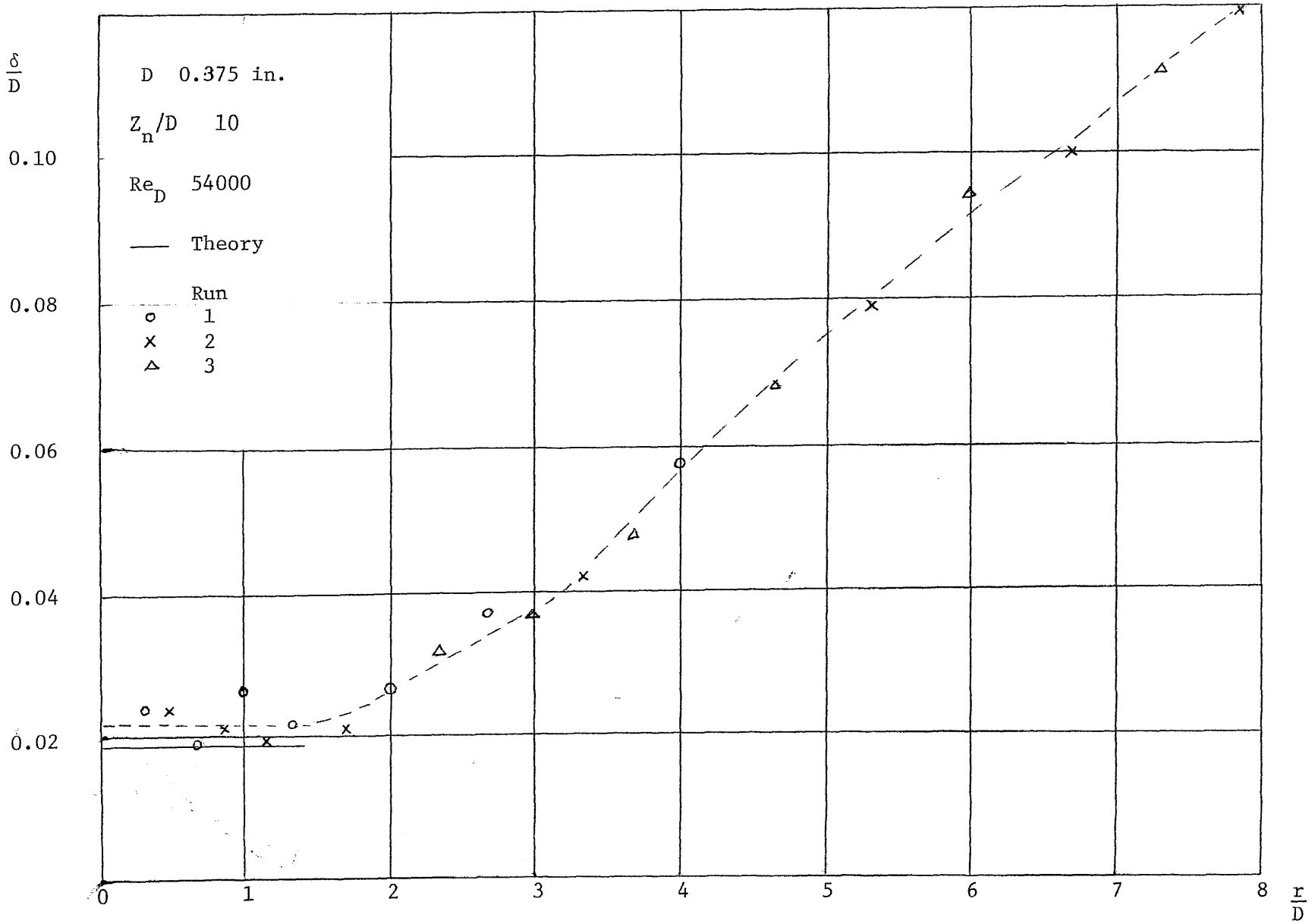

Boundary Layer Thickness

Fig. 4.50

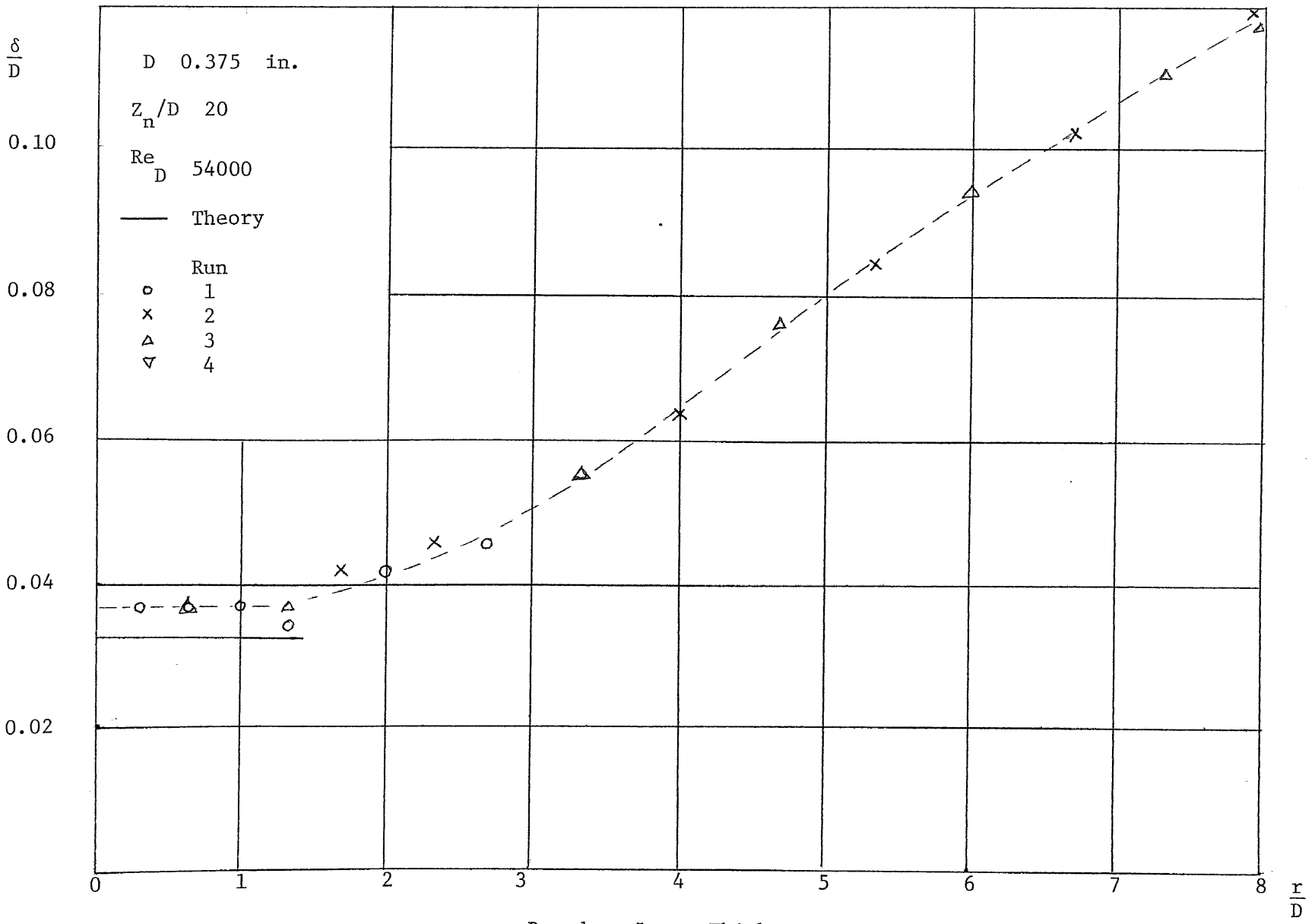

Boundary Layer Thickness

Fig. 4.51

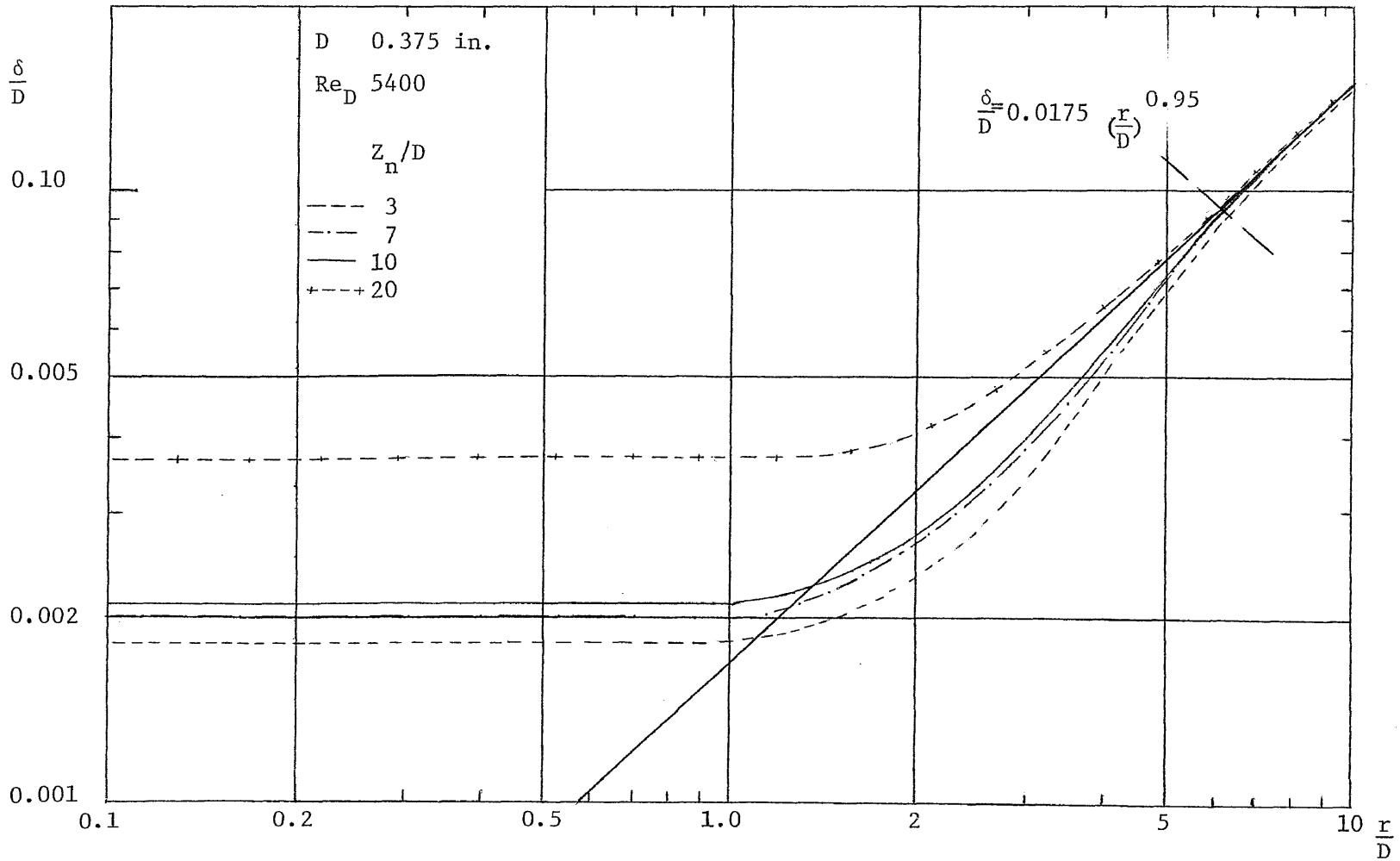

Boundary Layer Thickness for Different Z_n/D

Fig. 4.52